

แรงกระทำของสื่อนามิต่ออาคารที่มีช่องเปิดบนชายฝั่ง

นายณัฐวุฒิ ธนศรีสถิตย์

วิทยานิพนธ์นี้เป็นส่วนหนึ่งของการศึกษาตามหลักสูตรปริญญาวิศวกรรมศาสตรดุษฎีบัณฑิต

สาขาวิชาวิศวกรรมโยธา ภาควิชาวิศวกรรมโยธา

คณะวิศวกรรมศาสตร์ จุฬาลงกรณ์มหาวิทยาลัย

ปีการศึกษา 2554

ลิขสิทธิ์ของจุฬาลงกรณ์มหาวิทยาลัย

บทคัดย่อและแฟ้มข้อมูลฉบับเต็มของวิทยานิพนธ์ตั้งแต่ปีการศึกษา 2554 ที่ให้บริการในคลังปัญญาจุฬาฯ (CUIR)

เป็นแฟ้มข้อมูลของนิสิตเจ้าของวิทยานิพนธ์ที่ส่งผ่านทางบัณฑิตวิทยาลัย

The abstract and full text of theses from the academic year 2011 in Chulalongkorn University Intellectual Repository (CUIR)

are the thesis authors' files submitted through the Graduate School.

TSUNAMI LOADING ON ONSHORE BUILDINGS WITH OPENINGS

Mr. Nuttawut Thanasisathit

A Dissertation Submitted in Partial Fulfillment of the Requirements
for the Degree of Doctor of Philosophy Program in Civil Engineering

Department of Civil Engineering

Faculty of Engineering

Chulalongkorn University

Academic Year 2011

Copyright of Chulalongkorn University

Thesis Title	TSUNAMI LOADING ON ONSHORE BUILDINGS WITH OPENINGS
By	Mr. Nuttawut Thanasisathit
Field of Study	Civil Engineering
Thesis Advisor	Professor Panitan Lukkunaprasit, Ph.D.
Thesis Co-advisor	Assistant Professor Anat Ruangrassamee, Ph.D.

Accepted by the Faculty of Engineering, Chulalongkorn University in Partial Fulfillment of the Requirements for the Doctoral Degree

..... Dean of the Faculty of Engineering
(Associate Professor Boonsom Lerthirunwong, Dr.Ing.)

THESIS COMMITTEE

..... Chairman
(Professor Thaksin Thepchatri, Ph.D.)

..... Thesis Advisor
(Professor Panitan Lukkunaprasit, Ph.D.)

..... Thesis Co-advisor
(Assistant Professor Anat Ruangrassamee, Ph.D.)

..... Examiner
(Associate Professor Tospol Pinkaew, D.Eng.)

..... Examiner
(Assistant Professor Chatpan Chintanapakdee, Ph.D.)

..... External Examiner
(Professor Chaiyuth Chinnarasri, D.Eng.)

ณัฐวุฒิ ธนศรีสถิตย์ : แรงกระทำของสึนามิต่ออาคารที่มีช่องเปิดบนชายฝั่ง.

(TSUNAMI LOADING ON ONSHORE BUILDINGS WITH OPENINGS)

อ.ที่ปรึกษาวิทยานิพนธ์หลัก: ศ.ดร. ปณิธาน ลักคุณะประสิทธิ์,

อ.ที่ปรึกษาวิทยานิพนธ์ร่วม: ผศ.ดร.อาณัติ เรืองรัศมี, 93 หน้า.

จากการสำรวจอาคารที่พังเสียหาย เนื่องจากเหตุการณ์สึนามิในมหาสมุทรอินเดียในปี 2004 พบว่ามีอาคารหลายชั้นจำนวนมากที่เป็นโครงสร้างคอนกรีตเสริมเหล็ก รอดพ้นจากการพังทลายจากสึนามิที่กระทำและมีความเสียหายเกิดขึ้นเพียงเล็กน้อย โดยเฉพาะอาคารที่มีช่องเปิดจะมีความเสียหายน้อยกว่าอาคารที่มีผนังทึบ ดังนั้น จึงได้ทำการทดสอบแบบจำลองในห้องปฏิบัติการชลศาสตร์ เพื่อศึกษาแรงกระทำต่อแบบจำลองที่มีช่องเปิด นอกจากนี้ ได้มีการปรับปรุงมาตรฐาน FEMA P646 เพื่อสามารถนำไปใช้กับอาคารที่มีช่องเปิดได้

ในการทดสอบในห้องปฏิบัติการ ได้ใช้แบบจำลองมาตราส่วน 1:100 โดยมีรูปตัดตามขวางคือ สี่เหลี่ยมจัตุรัส สี่เหลี่ยมผืนผ้า และแปดเหลี่ยม และพิจารณาลักษณะช่องเปิด 3 ลักษณะสำหรับรูปสี่เหลี่ยมจัตุรัสได้แก่ ช่องเปิด 25%, 50% และไม่มีช่องเปิด แบบจำลองถูกแรงกระทำจากคลื่นคล้ายโซลิตารี ซึ่งถูกสร้างขึ้นโดยการปล่อยน้ำทันทีจากถังน้ำ จากผลการทดสอบพบว่า แรงที่กระทำลดลงประมาณ 15-25% และ 35-50% สำหรับช่องเปิด 25% และ 50% ตามลำดับ โดยเปรียบเทียบกับแรงที่กระทำกับแบบจำลองที่ไม่มีช่องเปิด ส่วนความดันที่เกิดขึ้นพบว่า ความดันที่ผิวหน้าแบบจำลองมีขนาดใกล้เคียงกันตลอดความกว้างที่ระดับความสูงจากพื้นเดียวกัน และถือได้ว่ามีความดันเท่ากันในทางปฏิบัติ แม้ว่าแบบจำลองจะมีช่องเปิดหรือไม่มีก็ตาม จากผลการทดสอบนี้ สามารถนำมาปรับปรุงมาตรฐาน FEMA P646 เพื่อนำไปใช้ในการคำนวณแรงสึนามิต่ออาคารที่มีช่องเปิดได้ จากเดิมที่มาตรฐานนี้ไม่มีข้อเสนอในการคำนวณแรงสึนามิต่ออาคารที่มีช่องเปิด การคำนวณกระทำโดยการคำนวณแรงตามมาตรฐาน FEMA P646 ของเดิม แล้วทำการปรับแรงตามอัตราส่วนของพื้นที่ประสิทธิผลต่อพื้นที่เต็ม วิธีการนี้ได้รับการตรวจสอบความถูกต้องกับผลการทดสอบแบบจำลองที่กล่าวข้างต้นในห้องปฏิบัติการชลศาสตร์ รวมทั้งแบบจำลองของอาคารที่เสียหายในเหตุการณ์สึนามิปี 2004 ซึ่งมีพื้นที่เปิดมาก ผลการตรวจสอบพบว่า วิธีการที่เสนอให้ค่าแรงกระทำที่เป็นขอบเขตบนพอประมาณเมื่อเทียบกับผลการทดสอบ

ภาควิชา ...วิศวกรรมโยธา..... ลายมือชื่อนิสิต

สาขาวิชา ...วิศวกรรมโยธา..... ลายมือชื่อ อ.ที่ปรึกษาวิทยานิพนธ์หลัก

ปีการศึกษา ...2554..... ลายมือชื่อ อ.ที่ปรึกษาวิทยานิพนธ์ร่วม

4871852921 : MAJOR CIVIL ENGINEERING

KEYWORDS: TSUNAMI / BUILDING / EXPERIMENT / HYDRODYNAMIC FORCES /
FIELD LOAD TEST / FEMA P646

NUTTAWUT THANASISATHIT: TSUNAMI LOADING ON ONSHORE
BUILDINGS WITH OPENINGS. ADVISOR: PROF. PANITAN LUKKUNAPRASIT,
Ph.D., CO-ADVISOR: ASST. PROF. ANAT RUANGRASSAMEE, Ph.D., 93 pp.

From the field survey of the damaged buildings in the 2004 Indian Ocean tsunami, a substantial number of multi-story reinforced concrete buildings were found to survive with minor structural damage, especially those with openings exhibited better performance than the ones with solid walls. Experiments were therefore carried out in a hydraulic wave flume to investigate tsunami force on models with different configurations of openings. Furthermore, FEMA P646 has been adapted to estimate the hydrodynamic forces on buildings with openings.

One-to-one hundred-scale models of square, rectangular and octagonal shapes were tested in a wave flume. Three configurations of openings were investigated for the square models, viz., 0%, 25% and 50%. The models were subjected to solitary - like waves, which were generated by a sudden release of water from the water tank. The experimental results show that there is a reduction in the forces acting on the whole building in the order of 15% to 25% and 35% to 50% for the 25% and 50% opening configurations, respectively. Although the models have different opening configurations, the pressures on the front panel do not vary significantly across the width at the same level and they can be regarded as the same for practical purposes. Based on this observation, FEMA P646 which does not provide any recommendation for buildings with openings, has been adapted for estimating tsunami loading on buildings with openings. The FEMA P646 specified loading is computed and then modified by the effective area to gross area ratio. The adapted FEMA P646 loading is verified by comparison with the measured forces from experiments which include the simple models mentioned above, and a model of a damaged building in the 2004 event, which has a large open exposure. The proposed method provides, in general, a reasonable upper bound to the experimental results.

Department ...Civil Engineering.....Student's Signature

Field of Study ...Civil Engineering.....Advisor's Signature

Academic Year ...2011..... Co-advisor's Signature

ACKNOWLEDGEMENTS

I highly appreciate my advisor, Prof. Panitan Lukkunaprasit for his experienced suggestions, kindness, support and patience while I did research. I wish to express to him all my gratitude. I would also like to thank Asst. Prof. Anat Ruangrassamee and Prof. Harry Yeh for their valuable suggestions and comments.

I am grateful for the financial support granted by Thailand Research Fund (TRF) for the Royal Golden Jubilee Ph.D. Program scholarship. With this fund, I had an opportunity to conduct research at Oregon State University for 11 months, under the supervision of Prof. Harry Yeh, an expert in this research area. I am deeply grateful for his guidance and support.

For experimental study in wave flume, I would like to acknowledge financial support from the Department of Public Works and Town & Country Planning, Ministry of Interior. I also wish to thank Asian Institute of Technology for providing the use of facilities at the hydraulic laboratory; and all personnel involved: Dr. Somboon Shaingchin, Dr. Tze Liang Lau, Dr. Tayagorn Charuchaimontri, and Mr. Surakai Banchuen are also deeply appreciated.

For full scale testing, the members of Center of Excellence on Earthquake Engineering and Vibration, Chulalongkorn University had assisted the test since the beginning. Their assistances are highly appreciated.

Finally, special thanks go to my family for their support throughout my life.

CONTENTS

	Page
Abstract in Thai.....	iv
Abstract in English.....	v
Acknowledgements	vi
Contents.....	vii
List of Tables.....	x
List of Figures	xi
Abbreviations and Notations.....	xv
Chapter 1 Introduction.....	1
1.1 Recent Deadly Tsunamis.....	1
1.1.1 2004 Indian Ocean tsunami.....	1
1.1.2 2011 Tohoku earthquake	2
1.2 Research Background and Motivations.....	3
1.3 Research Objectives	5
1.4 Scopes of Research	5
1.5 Outline of Dissertation.....	6
Chapter 2 Literature Review	7
2.1 Existing Design Guidelines	7
2.1.1 Hydrostatic forces.....	8
2.1.2 Hydrodynamic forces (Drag forces)	8
2.1.3 Buoyant forces.....	11
2.1.4 Surge forces	11
2.1.5 Debris impact forces	12
2.2 Experimental and Analytical Studies.....	14
Chapter 3 Experimental Study.....	20
3.1 Experimental Procedure	20
3.2 Relationship of Model and Prototype Scale	20
3.3 Experimental Setup.....	21
3.4 The Building Models	25

	Page
3.5 Instrumentation and Calibration.....	29
3.5.1 Flow depth	29
3.5.2 Velocity	31
3.5.3 Force.....	32
3.5.4 Pressure.....	34
3.6 Test Program	35
3.7 Results and Discussions.....	37
3.7.1 Characteristics of flow propagation on slope profile	37
3.7.2 Time history of flow depth and flow velocity	37
3.7.3 Characteristics of flow past model.....	41
3.7.4 Time history of force on models with and without openings	45
3.7.5 Effect of openings.....	45
3.7.6 Time histories of pressure on upstream front panel.....	48
3.7.7 Vertical pressure profile	49
3.7.8 Time histories of pressure variation across the frontal face at the same level.....	51
3.7.9 Time histories of pressure on the back panel	55
3.7.10 Time histories of pressure inside the model with opening	56
3.7.11 Effect of shapes	58
3.7.12 Confirmation of experimental results with Fujima et al. (2009).....	60
Chapter 4 Experimental Verification of FEMA P646	62
4.1 Hydrodynamic Forces in FEMA P646	62
4.2 Estimation of Runup Height from Flow Depth and Velocity.....	64
4.3 Comparison of Experimental Results with FEMA P646	67
4.3.1 Building without openings	68
4.3.2 Buildings with openings.....	69
Chapter 5 The Adapted FEMA P646 and Its Verification with Experiments and Field Load Test.....	70
5.1 Detail of Case Study Building	70
5.2 Field Load Test	72

	Page
5.3 Wave Flume Experiment	75
5.3.1 Experimental setup	75
5.3.2 Experimental results	76
5.4 Adapted FEMA P646	79
5.5 Comparison of Field Tested Load with Computed Load from Adapted FEMA P646	82
Chapter 6 Conclusions and Recommendations	84
6.1 Conclusions	84
6.2 Recommendations for Future Studies	85
References	86
Appendices	89
Appendix A Similitude Ratio for Froude Similarity	90
Appendix B Example Computations of Force using Adapted FEMA P646 on WMB ..	92
Curriculum Vitae	93

LIST OF TABLES

	page
Table 1-1. Ten deadliest tsunami disasters	2
Table 1-2. Casualties caused by the 2004 Indian Ocean tsunami in Thailand (as of September 5, 2005).....	3
Table 2-1 Comparison of drag coefficient	9
Table 2-2 Drag coefficient for larger obstruction (FEMA, 2000)	9
Table 3-1. Relationship of model and prototype scale	21
Table 3-2. Detail and photograph of building model	25
Table 3-3. Test program	36
Table 3-4. Maximum forces (N) on square model for Khaolak slope profile.....	48
Table 3-5. Maximum forces (N) on square model for Kamala slope profile.....	48
Table 3-6. Maximum forces (N) on model without openings for Kamala slope profile.....	59
Table 5-1. Experimental results of maximum drag forces (after first peak) and estimated maximum runup heights	78

LIST OF FIGURES

	Page
Figure 2-1. Effect of impulsive force on bore condition (Ramsden, 1996).....	15
Figure 3-1. Wave flume	22
Figure 3-2. Wave tank.....	23
Figure 3-3. Wave buffer	23
Figure 3-4. Slope profile at Khaolak, Phang-Nga	24
Figure 3-5. Slope profile at Kamala, Phuket.....	24
Figure 3-6. Plan of each shape (unit: mm).....	26
Figure 3-7. Three Configurations of openings for square shape (unit: mm)	27
Figure 3-8. Three Configurations of openings for rectangular shape (unit: mm)	28
Figure 3-9. DHI wave meter (wave gauge) and DHI synthesizer.....	29
Figure 3-10. Typical calibration curve of flow depth for onshore wave gauge	30
Figure 3-11. Typical calibration curve of flow depth for offshore wave gauge	30
Figure 3-12. Instruments to measure velocity	31
Figure 3-13. Typical calibration curve of velocity	32
Figure 3-14. Instruments to measure force	33
Figure 3-15. Calibration of load cell.....	33
Figure 3-16. Typical calibration curve of shear force.....	33
Figure 3-17. Pressure gauge	34
Figure 3-18. Typical calibration curve of pressure head	35
Figure 3-19. Locations and designation of pressure gauges	36
Figure 3-20. Characteristics of wave profile	38
Figure 3-21. Typical time history of flow depth (black line) and flow velocity (gray line) for Khaolak slope profile	39
Figure 3-22. Typical time history of flow depth (black line) and flow velocity (gray line) for Kamala slope profile	40
Figure 3-23. Sequence of the wave attack on the building model in the side view with nominal wave height of 60 mm.....	42
Figure 3-24. Sequence of the wave attack on the square model at upstream side	

with nominal wave height of 60 mm..... 43

Figure 3-25. Sequence of the wave attack on the square model at downstream side with nominal wave height of 60 mm..... 44

Figure 3-26. Typical time history of force for Khaolak slope profile with 0% opening (solid line), 25% openings (gray line) and 50% openings (dotted line)..... 46

Figure 3-27. Typical time history of force for Kamala slope profile with 0% opening (solid line), 25% openings (gray line) and 50% openings (dotted line)..... 47

Figure 3-28. Typical time histories of normalized pressures and forces for square shape model without openings and nominal wave height 80 mm..... 49

Figure 3-29. Variation of normalized pressure with height at the instant of maximum force - Kamala slope and square shape..... 51

Figure 3-30. Time history of pressure in case: KS1F-1C2-1C3-1C4_00_90_01 (Khaolak slope, Square shape, No opening, Nominal wave height 80 mm) 52

Figure 3-31. Time history of pressure in case: KS2F-2C2-2C3-2C4_00_90_03 (Khaolak slope, Square shape, No opening, Nominal wave height 80 mm) 52

Figure 3-32. Time history of pressure in case: KS2F-2C5-1F-1C5_25_90_03 (Khaolak slope, Square shape, 25% opening, Nominal wave height 80 mm) 53

Figure 3-33. Time history of pressure in case: KS2F-2C5-1F-1C5_50_90_05 (Khaolak slope, Square shape, 50% opening, Nominal wave height 80 mm) 53

Figure 3-34. Time history of average pressure at level 1 with different configuration of openings on the square shape and nominal wave height 80 mm at the Khaolak slope..... 54

Figure 3-35. Time history of average pressure at level 2 with different configuration of openings on the square shape and nominal wave height 80 mm at the Khaolak slope..... 54

Figure 3-36. Time history of pressure on the front and back of model (Khaolak

	Page
slope, Square shape, No opening, Nominal wave height 80 mm)	55
Figure 3-37. Time history of pressure inside of model (Kamala slope, Square shape, 25% opening, Nominal wave height 40 mm)	57
Figure 3-38. Time history of pressure inside of model (Kamala slope, Square shape, 25% opening, Nominal wave height 80 mm)	57
Figure 3-39. Comparison of measured resultant force with calculated force from pressure	58
Figure 3-40. Comparison of measured maximum forces with different shapes.....	59
Figure 3-41. Comparison of measured maximum forces with results in literature (Fujima et al., 2009)	61
Figure 4-1. Horizontal force-time histories in dimensionless quantity on the square column with various bore conditions (Arnason, 2005).....	63
Figure 4-2. Example of curve fitting on the measured depths and velocities by using the formula of Peregrine and Williams (2001)	66
Figure 4-3. Relationship of maximum runup height and maximum flow depth	67
Figure 4-4. Comparison of measured maximum forces with predicted forces based on momentum flux and runup for model without openings	68
Figure 5-1. Photograph of case study building (front view)	71
Figure 5-2. Case study building plan and elevation (unit: mm)	71
Figure 5-3. The inside view of the building shows the remaining structure and major brick wall (BW).....	72
Figure 5-4. Schematic diagram of the re-loading curve in the push-over of the damaged building	73
Figure 5-5. Overview of test setup in field load test (front view).	73
Figure 5-6. Overview of test setup in field load test (side view).....	74
Figure 5-7. Major brick wall with cracks before and after testing	74
Figure 5-8. Model of WMB in wave flume	75
Figure 5-9. Model dimensions of WMB in wave flume	75
Figure 5-10. Sequences of the wave attack on WMB model at upstream side with nominal wave height 60 mm.....	77

	Page
Figure 5-11. Typical time history of force for WMB model	78
Figure 5-12. Effective area of model with opening	80
Figure 5-13. Simplification of vertical pressure profile	81
Figure 5-14. Measured maximum force in wave flume experiments versus computed forces from Adapted FEMA P646.....	81
Figure 5-15. Frontal area of building submerged in flow	82
Figure 5-16. Comparison of computed forces from adapted FEMA P646 and FEMA 55 with measured force from field load test.....	83

ABBREVIATIONS AND NOTATIONS

Abbreviations

3D	Three-Dimensional
BW	Major brick wall
WMB	The weather monitoring building of the Meteorological Department station

Notations

A	Gross area
A_{eff}	Effective area
B	Breadth of the structure in the plane normal to the flow direction
B_{eff}	Effective width
C_D	Drag coefficient
C_m	Added mass coefficient
d	Flow depth
D	Distance from the shoreline to structure
F	Force dimension
F_b	Buoyant force
F_d	Hydrodynamic force or Drag force
F'_d	Drag force for the model with openings
F_i	Debris impact force
F_{imp}	Impulsive force
F_m	Maximum force
Fr	Froude number
F_r	Force scale
F_s	Surge force
F_{sta}	Hydrostatic force
g	Gravitational acceleration
h	Flow depth at the location of interest when there is no flow obstruction

h_{im}	Maximum inundation depth at the point of interest in the absence of obstacles
h_{in}	Maximum inundation height on building
h_m	Maximum flow depth at the location of interest when there is no flow obstruction
h_{max}	Maximum flow depth at the location of structure
h_0	Nominal wave height
h_R	Distance above the base of the structure to the center of force
h_s	Height of surge front
h_w	Maximum water height at the location of structure
hu^2	Momentum flux
k	Effective stiffness of debris
L	Length dimension
L_r	Length scale
m	Mass of the debris
M_r	Mass scale
P	Pressure
R	Maximum runup height
t	Time
T	Time dimension
T_r	Time scale
u	Flow velocity
u_{im}	Maximum flow velocity at the point of interest in the absence of obstacles
u_m	Maximum flow velocity
u_{max}	Maximum flow velocity carrying the debris at the site
u_r	Velocity scale
V	Displaced volume of water
Z	Distance of pressure gauge to base
z	Ground elevation of the location of interest from the initial shoreline

Δt Duration of impact

Greek letters

α Bottom slope (radian)

β Horizontal wave pressure index

ρ Fluid density

ρ_s Fluid density including sediment

CHAPTER 1

INTRODUCTION

Tsunamis are generated by abrupt vertical displacements of the seafloor caused by natural hazards, such as submarine earthquakes, volcanic eruptions, underwater explosions and landslides. The term tsunami comes from the Japanese words meaning harbor wave. The tsunami has a very long wavelength (several hundreds of kilometers long), small wave height (one meter or so) and high speed (in order to 800 kilometers per hour depending on the depth of the ocean) in deep ocean. The small wave height makes tsunamis almost unnoticeable in deep sea. When tsunami propagates from deep ocean to shore, the flow height increases while the flow velocity decreases. Tsunamis can have tremendous inundation height and force. They cause severe damage to structures and loss of lives.

1.1 Recent Deadly Tsunamis

Tsunamis are rare events and they occur worldwide. Table 1-1 shows the deadliest tsunami disasters in modern history. From historic tsunami events, submarine earthquakes often create tsunamis that can cause huge damage and loss of life.

1.1.1 2004 Indian Ocean tsunami

The unprecedented devastation of the 2004 Indian Ocean tsunami was generated by a submarine earthquake of a moment magnitude of 9.1 off the west coast of northern Sumatra, on Sunday December 26, 2004 at 00:58:53 UTC (07:58:53 a.m. local time). The tsunami resulted in inundation of coastal communities with waves up to 30 m (at some locations) spreading throughout the Indian Ocean. It caused catastrophic destruction in countries around the Indian Ocean basin even as far as the east coast of Africa, killing more than 230,000 people and displaced over 1.5 million people (FEMA, 2008). It was one of the deadliest natural disasters in history. Indonesia, Sri Lanka, India, and Thailand were hardest hit.

1.1.2 2011 Tohoku earthquake

The 2011 Tohoku earthquake was generated by a submarine earthquake with a moment magnitude of 9.0 off the coast of Japan, on Friday March 11, 2011 at 05:46:23 UTC (02:46:23 p.m. local time). The height of the tsunami was estimated to be 10 m high along the northeastern coast of Japan and the maximum runup height is 38.9 m. More than 25,000 deaths and missing have been reported. The earthquake and tsunami caused widespread devastation and severe damage to buildings and infrastructure including the Fukushima Daiichi nuclear power plant of significance is the nuclear power plant crisis which results from failure of back up generators and cooling system for the fuel rods and spent fuel.

Table 1-1. Ten deadliest tsunami disasters

Rank	Death toll	Event	Date
1	230,210	2004 Indian Ocean Tsunami, Indonesia	26 Dec 2004
2	123,000	1908 Messina earthquake/tsunami, Italy	1908
3	100,000	1755 Lisbon earthquake/tsunami/fire, Portugal	1755
4	36,000	1883 eruption of Krakatoa, Indonesia	1883
5	30,000	1707 Hoei earthquake, Japan	1707
6	25,674	1868 Arica earthquake/tsunami, Chile	1868
7	22,070	1896 Meiji-Sanriku earthquake, Japan	1896
8	15,273	2011 Tohoku earthquake and tsunami, Japan	11 Mar 2011
9	15,030	1792 Mount Unzen eruption in southwest Kyushu, Japan	1792
10	12,000	1771 Great Yaeyama Tsunami, Japan	1771

From: http://en.wikipedia.org/wiki/List_of_natural_disasters, August, 2011

1.2 Research Background and Motivations

Before the 2004 Indian Ocean tsunami, there was no recorded tsunami disaster in Thailand. People were unaware of tsunami disaster; therefore, there was no tsunami early warning system in place and people were not prepared for disaster caused by tsunamis. That is the main reason for the great loss of human life and economy, even though the affected provinces along the Andaman sea coastline of Thailand are 500 km or more from the earthquake epicenter, and it took 2 hours before the tsunami propagated from the source to Thailand.

Tsunamis of about 5 to 12 m in inundation depth (up to 20 m at a few locations according to some reports) struck the coastlines of six provinces facing the Andaman Sea, resulted in more than 8,000 deaths and missing, and severe damage to buildings in the affected areas in Thailand. Table 1-2 summarizes casualties reported by the Department of Disaster Prevention and Mitigation, Ministry of Interior, Thailand.

Table 1-2. Casualties caused by the 2004 Indian Ocean tsunami in Thailand (as of September 5, 2005).

Province of Thailand	Dead				Injured			Missing		
	Thai	Foreigner	Unidentified	Total	Thai	Foreigner	Total	Thai	Foreigner	Total
Phuket	151	111	17	279	591	520	1111	245	363	608
Phangnga	1389	2114	722	4225	4344	1253	5597	1352	303	1655
Krabi	357	203	161	721	808	568	1376	314	230	544
Ranong	153	6	-	159	215	31	246	9	-	9
Trang	3	2	-	5	92	20	112	1	-	1
Satun	6	-	-	6	15	-	15	-	-	-
Total	2059	2436	900	5395	6065	2392	8457	1921	896	2817

From: <http://www.disaster.go.th>, September, 2005

Considerable efforts have been focused on the development of tsunami warning systems, tsunami hazard maps, and stimulation of public awareness to improve evacuation efficiency. Along with these measures, evacuation of people to high ground (or terrain) should be considered. However, this may not be possible in some areas. For example, in flat terrains as in Ban Bang Niang, Khaolak and Ban Nam Kem, inundation penetrated more than 1 km inland, making it difficult for people especially the elderly, women and small children to escape to safety. A possible alternative would be to evacuate people near the shore to the upper floors of tsunami resistant buildings. In this research, we will focus on buildings located onshore for safe vertical evacuation.

Ruangrassamee et al. (2006) and Lukkunaprasit and Ruangrassamee (2008) reported damage to buildings caused by the 2004 tsunami. Based on the observation from the field reconnaissance, Lukkunaprasit and Ruangrassamee (2008) suggested that the design for tsunami resistant buildings was practically feasible for moderate tsunamis. A number of multi-story reinforced concrete buildings were found to survive with minor structural damage even though they were not designed for tsunami or earthquake loading. This indicates that it is possible to design tsunami resistant buildings to serve as tsunami shelters, or to reduce damage of buildings for life safety, minimizing of economic loss, and rapid restoration.

In most of the existing design codes, tsunami loadings considered are hydrostatic forces, buoyant forces, hydrodynamic forces, impact forces, surge forces, and wave breaking forces. Since tsunami resistant buildings are usually located onshore away from shoreline, they are not affected by wave breaking forces because tsunamis break offshore. Impact force is another important one, and it depends on several parameters such as mass and effective stiffness of floating debris (e.g. floating driftwood, lumber, boats, containers, etc.), and the drifting current. This is entirely a separate issue to be addressed specifically. Therefore, both wave breaking and debris impact forces are not considered in this research.

Tsunami induced loading depends on flow velocity, flow depth, size and shape of buildings, among others. The mechanics underlying these forces is complex. Therefore, testing of physical models in a wave flume is a necessity. Moreover, analytical models have often to be calibrated by experimental studies.

1.3 Research Objectives

The main objective of this research is to investigate tsunami loading on buildings in a moderate tsunami zone. To achieve this main objective, the following specific objectives have to be fulfilled:

- a) To study hydrodynamic forces due to tsunami loading on onshore buildings based on experimental investigations in a wave flume.
- b) To assess the effect of openings in building structures in reducing tsunami induced forces.
- c) To calibrate tsunami loading considering performance of a damaged building by field load test.

1.4 Scopes of Research

This research covers a broad range of interest areas. Due to the time and resource constraints, the research is confined to the following scopes:

- a) Focus is on the horizontal hydrodynamic force as the main tsunami loading. Other force components (such as wave breaking force, debris impact force, etc.) are not considered.
- b) Experimental investigation in a wave flume is the main concern of this study. Simplified slope profiles are represented at Khaolak and Kamala beaches as the typical beach profiles in the study region.
- c) Only dry bed conditions are considered.
- d) Model shapes are made simple in plan, i.e., square, rectangular and octagonal shapes. Three types of openings with the same configurations at the front and back panels of the models are considered for the square shapes, viz. 0%, 25% and 50%.
- e) Maximum flow depth of tsunami investigated is limited to about 8 cm in model scale (about 8 m in prototype scale).

1.5 Outline of Dissertation

This dissertation consists of six chapters. After the introduction in Chapter 1, Chapter 2 reviews the literature of the existing design guidelines and experimental studies in a wave flume. In Chapter 3, the test setup and experimental results are presented. Chapter 4 presents the experimental verification of FEMA P646 (FEMA, 2008). Chapter 5 extends the applicability of FEMA P646. A simple approach is proposed to adapt it for buildings with openings. The approach is verified with experimental results of a physical model of a damaged building in the 2004 Indian Ocean tsunami, and a field load test. Conclusion of this study and recommendation of future study are finally given in Chapter 6.

CHAPTER 2

LITERATURE REVIEW

In this chapter, previous studies of tsunami loading including the existing design guidelines and experimental studies in wave flumes are reviewed. The selected literature focuses on hydrodynamic forces and surge forces. Based on this useful information in this chapter, the suitable approach will be applied in research methodology to achieve the research objectives.

2.1 Existing Design Guidelines

The following existing design guidelines computation of tsunami loading have been reviewed:

- a) CCH - The City and County of Honolulu building code (CCH, 2000) (Chapter 16, Article 11), issued by the department of planning and permitting of Honolulu, Hawaii. It provides specific guidance due to tsunamis in Section 16-11.5(f).
- b) FEMA 55 - Coastal Construction Manual (FEMA, 2000), Chapter 11 proposed by the Federal Emergency Management Agency.
- c) TSTRB - Tsunami loads and structural design of tsunami refuge buildings (Okada et al., 2005) proposed by the Building Centre for Japan.
- d) FEMA P646 - Guidelines for design of structures for vertical evacuation from tsunamis (FEMA, 2008), Chapter 6 proposed by the US Department of Homeland Security's Federal Emergency Management Agency.

Tsunami loading consists of (1) hydrostatic forces, (2) hydrodynamic forces or drag forces, (3) buoyant forces, (4) Surge forces and (5) Debris impact forces. These are briefly presented in the following sections.

2.1.1 Hydrostatic forces

Hydrostatic forces are forces resulting from the water mass exerting on a structure in a static condition. These forces are important for long structures such as seawalls and dikes.

The hydrostatic force is generally determined by equation 2-1 and its resultant applies horizontally at level given in equation 2-2.

$$F_{sta} = \frac{1}{2} \rho g h_w^2 \quad (2-1)$$

$$h_R = \frac{h_w}{3} \quad (2-2)$$

where F_{sta} is the hydrostatic force per unit width of the structure,

ρ is the water density,

g is the gravitational acceleration,

h_w is the maximum water height at the location of structure,

h_R is the distance above the base of the structure to the center of force.

Note that FEMA 55 uses the design still water depth for h_w .

It should be noted, however, that CCH (2000) accounts for the velocity head and includes it in hydrostatic formula as shown below:

$$F_{sta} = \frac{1}{2} \rho g \left(h_w + \frac{u^2}{2g} \right)^2 \quad (2-3)$$

$$h_R = \frac{1}{3} \left(h_w + \frac{u^2}{2g} \right) \quad (2-4)$$

where u is the flow velocity at the location of structure.

Hydrostatic forces are usually less important for structures of finite size as the water can quickly flow around them and fill up on all sides of the structures.

2.1.2 Hydrodynamic forces (Drag forces)

Hydrodynamic forces or usually known as drag forces exist when water flows around a structure (or structural component). They arise as a result of pressure exerted on the upstream face, drag along the sides, and suction on the downstream face.

Hydrodynamic forces are a function of flow velocity, shape of the object, and mass density of water, and can be computed using equation 2-5.

$$F_d = \frac{1}{2} \rho C_d h u^2 B \quad (2-5)$$

where F_d is the hydrodynamic force,

ρ is the water density,

C_d is the drag coefficient as given in Table 2-1,

h is the flow depth,

u is the flow velocity at the location of structure,

B is the breadth of the structure in the plane normal to the flow direction.

Table 2-1 Comparison of drag coefficient

Types of Structure	CCH	FEMA 55	FEMA P646
Round Piles	1.0	1.2	N/A
Square or Rectangular Piles	2.0	2.0	2.0
Wall Sections	1.5	see Table 2-2	N/A

Table 2-2 Drag coefficient for larger obstruction (FEMA, 2000)

Ratio of Width to Water Height	Drag Coefficient
1 – 12	1.25
13 – 20	1.30
21 – 32	1.40
33 – 40	1.50
41 – 80	1.75
81 – 120	1.80
> 120	2.00

Several standards specify the same equation to compute hydrodynamic force but the drag coefficient and flow velocity may be slightly different. Table 2-1 shows drag

coefficients for several types of structures. The resultant force is applied approximately at the center of mass of the wetted front surface of the structures.

The flow velocity is one of the most important parameters in computing tsunami-related forces. FEMA 55 mentions that water velocity is highly uncertain and a high value should be assumed in an extreme event like tsunami. The recommended value is given in equation 2-6.

$$u = 2\sqrt{gh_w} \quad (2-6)$$

CCH recommends that the velocity be approximated from the water height at the structure with the time taken as 1 sec. Thus,

$$\begin{aligned} u &= \frac{h_w}{t} \\ &= h_w \end{aligned} \quad (2-7)$$

FEMA P646 combines the flow depth and flow velocity to represent the maximum momentum flux, hu^2 which can be related to the maximum runup height. The detail is described in section 4.1.

Note that the hydrodynamic force specified by FEMA 55 is computed using both the maximum flow depth and maximum flow velocity in Eq. 2-5. In reality, the maximum flow depth and maximum flow velocity do not occur at the same time (Yeh, 2007). This fact has been recognized in FEMA P646 (Yeh, 2007).

For FEMA P646, the possibility of a tsunami bore impinging on a structure is accounted for as an impulsive force with a magnitude of 1.5 times the hydrodynamic force, i.e.,

$$F_{imp} = 1.5F_d \quad (2-8)$$

where F_{imp} is the impulsive force,

F_d is the hydrodynamic force.

2.1.3 Buoyant forces

Buoyant forces or vertical hydrostatic forces on a structure or structural member exist when the structure or structural member are subjected to partial or total submergence. These forces are a concern for the design of basement, empty above the surface of the ground and below ground tanks. Buoyant forces must be resisted by the weight of the structure or structural member and any opposing forces resisting floatation (such as anchorage forces but not the forces due to dead or live loads that may not be in existence all the time). Several standards provide the same expression for buoyant force that it is given by equation 2-9. Buoyant forces act vertically through the center of mass of the displaced volume.

$$F_b = \rho g V \quad (2-9)$$

where F_b is the Buoyant force,

ρ is the water density,

g is the gravitational acceleration,

V is the displaced volume of water.

2.1.4 Surge forces

Surge forces are caused by the leading edge of tsunami impinging on a structure located on a dry bed. CCH specifies the surge force per unit width on a structure as given by equation 2-10.

$$F_s = 4.5 \rho g h_s^2 \quad (2-10)$$

where F_s is the surge force per unit width of a structure,

ρ is the water density,

g is the gravitational acceleration,

h_s is the height of surge front.

Note that this equation is applicable for structures with heights equal to or greater than $3h_s$, and the surge force is 9 times the hydrostatic force. The resultant force acts at a distance h_s above the base of the structure. Structures whose heights are less than $3h_s$ require surge forces to be calculated by using appropriate combination of hydrostatic and hydrodynamic force equations for the given situation. It is interesting to note that, if we take $C_d = 2$ and $u = 2\sqrt{gh_w}$, the combination of hydrodynamic and hydrostatic forces yields:

$$\begin{aligned} F_s &= F_{sta} + F_d \\ &= \frac{1}{2}\rho gh_w^2 + \frac{1}{2}\rho C_d h u^2 \\ &= \frac{1}{2}\rho gh_w^2 + \frac{1}{2}\rho(2)h_w(2\sqrt{gh_w})^2 \end{aligned} \quad (2-11)$$

Thus,

$$F_s = 4.5\rho gh_w^2 \quad (2-12)$$

which is the same formula as equation 2-10.

It is interesting to observe that TSTRB has proposed the same equation for the tsunami force, which is adapted from the empirical result given by Asakura et al. (2002).

2.1.5 Debris impact forces

The debris impact forces are caused by debris (e.g. timbers, small boats, etc.) which is transported by the wave and attacks on structures. These forces act locally at the point of contact, and hence they are generally assumed to act at the surface level at the building location. These forces can be estimated using the impulse-momentum concept.

Both FEMA 55 and CCH recommend the same equation for computing debris impact forces but the flow velocity and duration of time may be slightly different. The debris impact forces are shown in equation 2-13.

$$F_i = m \frac{u}{\Delta t} \quad (2-13)$$

where F_i is the debris impact force,
 m is the mass of the debris,
 u is the flow velocity,
 Δt is the duration of impact.

For FEMA P646, the debris impact force is estimated from equation 2-14. This formula is obtained by solving the equation of motion of a one degree of freedom system simulating the building under an impulsive loading. The effective stiffness and mass coefficients are recommended in FEMA P646, which are based on laboratory experiments. Thus,

$$F_i = C_m u_{max} \sqrt{km} \quad (2-14)$$

where F_i is the debris impact force,
 C_m is the added mass coefficient,
 u_{max} is the maximum flow velocity carrying the debris at the site,
 k is the effective stiffness of debris,
 m is the mass of debris.

2.2 Experimental and Analytical Studies

Tsunami loading on structures has been studied by several researchers using wave flume experiments and formulae developed from experiments. The experimental studies over the few past decades were mostly concentrated on wall type structures. Investigation on three-dimensional (3D) structures were conducted rather recently.

Fukui et al. (1963) conducted experiments using a dike model and two types of hydraulic flumes:

- a) Small-scale tests were carried out in a flume 0.6 m wide, 21 m long, and 0.6 m high with the waves generated by a flap gate.
- b) Large-scale tests were 2.0 m wide, 70 m long, and 2.0 m high with the waves generated almost the same way as the small-scale tests.

Based on the test data, they developed a relationship between the maximum pressure and velocity and suggested that the maximum pressure be proportional to velocity to the power of four.

Cross (1967) investigated the forces produced by waves striking a vertical wall on a dry bed. The wave was generated by the dam-break method and the profile was measured using modified parallel-wire resistance wave gauges. The pressure distribution against the wall was measured and the results were applied to predict the total force from the surge striking a vertical wall. A simple theory was developed based on the linear momentum equation with the assumptions that the tip moved as a rigid body and convective accelerations were negligible. The forces predicted theoretically from the measured surge shapes were found to be in close agreement with the measured forces.

Ramsden and Raichlen (1990) conducted experiments in a hydraulic laboratory using a 1.10 m wide, 40 m long, and 0.61 m high flume with a bed slope of 1:50. The waves were generated by a piston and the waves were broken before impact on a vertical wall, which was submerged in 5 mm deep water. They found that the maximum runup varied from 2 to 2.6 times the velocity head computed using the celerity of the

incident bore. The maximum measured force occurred after the maximum runup for all conditions of this study. The maximum measured forces varied from $\frac{5.5}{2}\rho gh^2$ to $\frac{7}{2}\rho gh^2$ and flow velocity was almost $1.8\sqrt{gh}$ based on the height of the incident bore. It was also found that Cross's theory predicted the maximum measured force with reasonable agreement.

Ramsden (1996) experimentally investigated the influence of solitary waves, bores and surges striking a vertical wall. Two wave tanks, namely a horizontal tank and a tilted one were used. The solitary waves were generated with a computer-controlled hydraulically actuated piston. A pneumatic gate was used to create bores and surges by releasing a volume of water in a reservoir with certain depth. Force transducers and pressure transducers were installed to measure the wave forces. A laser-induced fluorescence system was developed to record two-dimensional profiles of the incident wave. The experimental results due to solitary waves and undular bores agreed with the solitary wave theory. Empirical equations were also proposed based on the experiments. Another important finding is that an initial impulsive force was generated in the case of a bore but not in the dry-bed surge as shown in Figure 2-1. The initial impulsive force is also accounted for in FEMA P646 (2008).

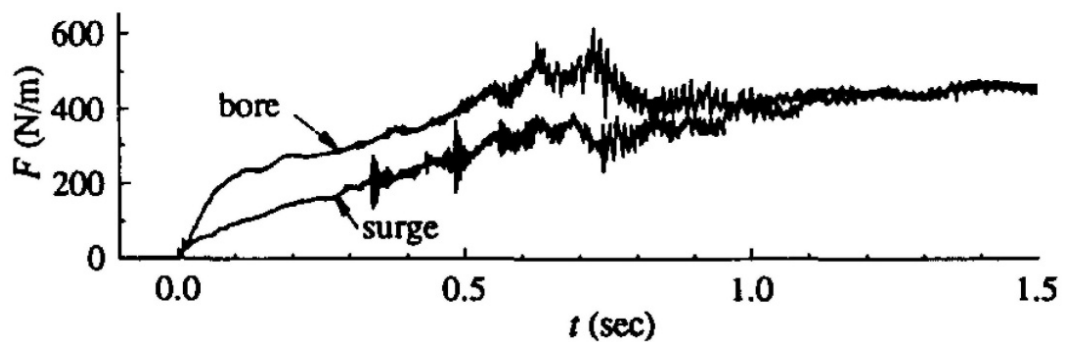


Figure 2-1. Effect of impulsive force on bore condition (Ramsden, 1996)

Hamzah et al. (2000) conducted experiments in a hydraulic laboratory using a 1 m wide, 50 m long, and 1.5 m high flume with a bed slope of 0.035 degree. The water height in the experiments was 0.8 m. A piston was utilized to generate the waves. The waves were broken before impact on a vertical wall, which was submerged in 0.10 m deep water. Pressure gauges were installed to measure the wave pressure and vertical distribution of the pressure was determined. The results were compared with theoretical calculations. In their investigation, two types of pressure peaks were observed. The first peak was caused by the impulsive pressure which could be easily observed in experiment. The second peak, somewhat smaller than the first one, could be obtained from numerical simulation, and was found to agree well with experimental results.

Asakura et al. (2002) conducted experiments using three types of hydraulic flumes:

- a) 2-D flume 2 m wide, 62 m long, 2 m high and the bed slopes of 1:200, 1:100, 1:50, 1:30 with the waves generated by a piston-type wave maker.
- b) 2-D flume 0.7 m wide, 60 m long, 1.5 m high and the bed slopes of 1:200, 1:100, 1:50, 1:30 with the waves generated by a pump-type wave maker capable of producing very long period waves.
- c) 3-D wave basin 20 m wide, 58 m long, 1.5 m high and the bed slope of 1:200 with the waves generated by a pump-type wave maker.

For all three cases, the structures were located onshore. Capacity-type wave gauge, laser doppler velocimeter, force sensor in six-components, and condenser-type wave pressure gauges were installed to measure runup, velocity, force, and pressure, respectively. Two types of tsunami waves, namely wave with fission and wave without fission, were observed. When the tsunami wave was without fission, the vertical distribution of the dimensionless maximum wave pressure could be expressed by a linear relationship. When the tsunami wave was wave with fission, the distribution could be expressed by a bilinear relationship. These expressions were referred to in the guidelines - tsunami loads and structural design of tsunami refuge buildings (Okada et al., 2005).

Arnason (2005) and Arnason et al. (2009) conducted experiments in a 16.6 m long wave flume with cross section of 0.6 m x 0.45 m. The flow was generated by lifting the gate like a dam break. Three shapes of models were studied. It was observed that there was an overshoot in hydrodynamic forces for the case of a square column and small flow depth. For the circular shape, it was found that the drag coefficient was larger than that recommended in standards.

Yeh (2006) and Yeh (2007) reviewed existing design guidelines and proposed a rational methodology for determining drag forces on land structures located on a uniformly sloping beach. Based on an analytic model of a fully nonlinear shallow-water wave theory, a formula for determining the maximum momentum flux, $(hu^2)_{max}$ is proposed. This formula can be expressed by

$$\frac{(hu^2)_{max}}{gR^2} = 0.125 - 0.235 \frac{z}{R} + 0.11 \left(\frac{z}{R}\right)^2 \quad (2-15)$$

where g is the gravitational acceleration,

R is the maximum runup height,

z is the ground elevation at the location of building from the initial shoreline.

Fujima et al. (2009) conducted experiments in a wave basin 11 m long, 7 m wide and 1.5 m deep. Two models with different widths (parallel to the shoreline) were investigated, i.e. 0.1 m and 0.2 m. The width (perpendicular to the shoreline) and height of model were 0.1 m. The distance from the shoreline to structure was set as 0.20, 0.50, 0.80 and 1.50 m. The paddle stroke of the wave generator was varied from 0.10 to 0.20 m at 0.05 m increments. They proposed suitable forms for estimation of tsunami loading. The hydrostatic form was appropriate for buildings located near the shoreline and hydrodynamic form was appropriate for buildings far from the shoreline. Thus, For average estimation:

$$F_m = \begin{cases} \frac{1.5}{2} \rho B h_{im} u_{im}^2 & ; \left(\frac{h_{im}}{D} < 0.05\right) \\ 1.8 \rho g h_{im}^2 B & ; \left(\frac{h_{im}}{D} > 0.05\right) \end{cases} \quad (2-16)$$

For safety estimation:

$$F_m = \begin{cases} 1.3\rho B h_{im} u_{im}^2 & ; \left(\frac{h_{im}}{D} < 0.05\right) \\ 3.3\rho g h_{im}^2 B & ; \left(\frac{h_{im}}{D} > 0.05\right) \end{cases} \quad (2-17)$$

where F_m is the maximum force,

ρ is the fluid density,

B is the breadth of the structure in the plane normal to the flow direction,

h_{im} is the maximum inundation depth at the point of interest in the absence of obstacles,

u_{im} is the maximum flow velocity at the point of interest in the absence of obstacles,

D is the distance from the shoreline to structure.

Lukkunaprasit et al. (2009b) investigated tsunami forces acting on a 150 mm cube in a 40 m long wave flume with 1m x 1m cross section. The flow was generated by an abrupt release of water from an elevated tank. In computation, they predicted the maximum runup height from the time history of measured flow depth and flow velocity using Peregrine and Williams' formulas (Peregrine and Williams, 2001). It is confirmed that the drag force as per FEMA P646 gives an upper bound for the experimental results. Tsunami loading on buildings with openings were also studied by Lukkunaprasit et al. (2008)

Lukkunaprasit et al. (2010) investigated the tsunami loading on a damaged building in the 2004 Indian Ocean tsunami. The field load test was conducted to assess the tsunami loading in that event. They found that the tsunami force based on the velocity specified by FEMA 55 (FEMA, 2000) guidelines was excessively large. A back calculation was made based on field load test. They recommended that the velocity of $1.20\sqrt{gh}$ to $1.36\sqrt{gh}$ be appropriate for use in FEMA 55 for Thai coasts.

From the literature review, it is evident that different research findings suggest different values of tsunami loading. Moreover, there are few studies of tsunami loading on buildings with openings. Therefore, it is of research significance to investigate the tsunami loading on such structures.

CHAPTER 3

EXPERIMENTAL STUDY

The details of the experiment setup, slope profiles, shapes of models, instrumentation, calibration and results are presented in this chapter.

3.1 Experimental Procedure

Tsunami loadings were investigated in a wave flume on scaled models by changing the parameter of slope profile, shape of model, percentage of openings, and flow depth. Measurements included flow depth, flow velocity, force and pressure.

The steps in the test procedure included selection of building prototype and model scaling that were appropriate for the size of wave flume; design of the experimental setup, construction of building models and testing in the wave flume. Instruments were carefully calibrated and installed. Experiments were performed in two steps: first in the absence of the model (to obtain flow depth and velocity) and then testing with the model present (to obtain force and pressure). Video and digital cameras were used to capture the wave motion around on the model. The data from all the instruments were collected by data loggers. The data were processed and discussed.

3.2 Relationship of Model and Prototype Scale

In experiments, the behavior of the model should be similar to the behavior of the prototype (full scale). This means that the dimensions, kinematics and dynamics have to be scaled. For physical model tests in long-waves, it is usually assumed that the dominant physical forces are the gravitational force and the inertial force (Hughes, 2005). The similitude criterion for these forces is the Froude criterion. Thus, the Froude number, defined as the square root of the ratio of the inertial to gravity force, must be of the same value for the model and prototype. The Froude number is given by

$$Fr = \sqrt{\frac{\text{inertial force}}{\text{gravity force}}} = \sqrt{\frac{\rho L^2 u^2}{\rho L^3 g}} = \frac{u}{\sqrt{gL}} \quad (3-1)$$

where Fr is Froude number, ρ is the fluid density, L is the length dimension, u is the flow velocity and g is the gravitational acceleration. The relations between the model and the prototype quantities are summarized in Table 3-1. Details of derivation for some of the important parameters are described in Appendix A.

Table 3-1. Relationship of model and prototype scale

Quantity	Dimension	Scale
Length	L	L_r
Area	L^2	L_r^2
Volume	L^3	L_r^3
Flow	$\frac{L^3}{T}$	$L_r^{\frac{5}{2}}$
Time	T	$L_r^{\frac{1}{2}}$
Velocity	$\frac{L}{T}$	$L_r^{\frac{1}{2}}$
Force	F	L_r^3
Pressure	$\frac{F}{L^2}$	L_r

where L is the length dimension, T is the time dimension, F is the force dimension and L_r is the Length scale.

3.3 Experimental Setup

The experiments were carried out in a wave flume at the Hydraulic Laboratory, Asian Institute of Technology, Thailand. The flume had a length of 40 m with a square cross section of 1 m x 1 m as shown in Figure 3-1. The flume walls were made of thick glass panes and the rigid beds were painted steel plates supported by structural steel sections. Solitary-like waves were generated by quickly opening the control gate at the lower end of the water tank, thereby releasing water from the tank. Because of the sudden release of water, the generated flow was highly turbulent. Figure 3-2 shows the

water tank that stored water at one end of the flume. It was a large water tank having capacity of 10 cubic meters. At the side wall near the bottom of the tank is connected a release gate measuring 1.0 m by 0.50 m. The turbulent flow under release of the gate passed through the wave buffer (Figure 3-3) which contained rocks of different sizes to filter and smooth the generated tsunami. The volume of water in the tank determined the strength of the generated wave.



Figure 3-1. Wave flume



Figure 3-2. Wave tank



Figure 3-3. Wave buffer

Figure 3-4 and Figure 3-5 illustrate the slope profiles representing two beaches in Thailand, viz., Khaolak (Phang-Nga) and Kamala (Phuket), respectively. At Khaolak, the compound slope beach consisted of two slopes – 1:575, 1:44 – and a flat terrain. At Kamala, the corresponding slopes were 1:115 and 1:15.6, respectively. Note that a very steep slope was utilized to effect formation of solitary-like wave offshore. The mild beach offshore slopes were obtained from bathymetric maps and field measurement for onshore beaches. The rather steep slope just before the flat terrain represents the embankment on the beach.

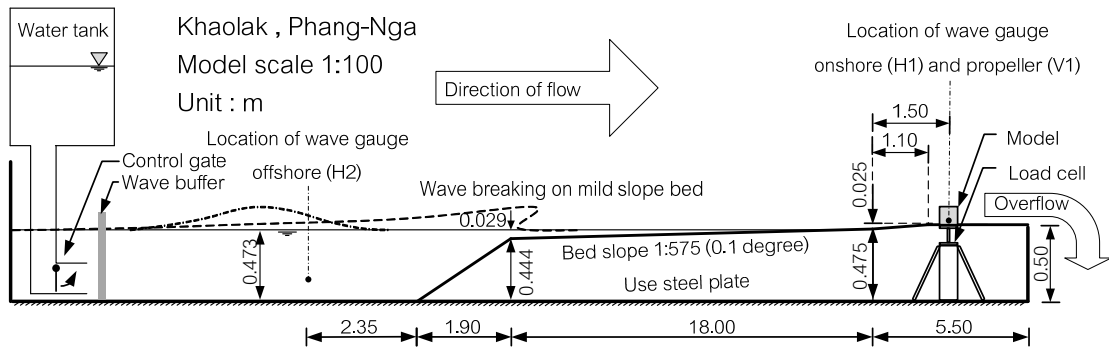


Figure 3-4. Slope profile at Khaolak, Phang-Nga

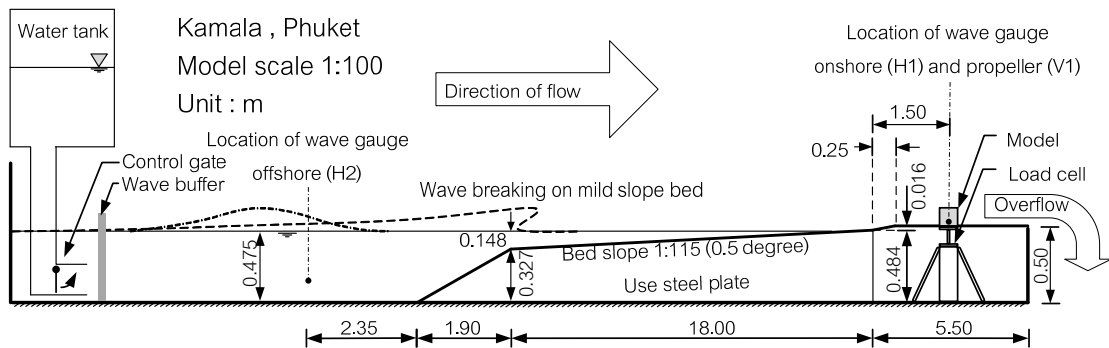


Figure 3-5. Slope profile at Kamala, Phuket

At the downstream end of the flume, the model was installed on the load cell that was fixed to the structural frame of the flume. The generated tsunamis passed the model and flowed directly out to the drain channel located at the downstream end of the flume.

Experiments were first performed in the absence of the model to obtain the time histories of flow gate depth and velocity. Subsequently, the model was installed in the wave flume and experiments rerun to obtain the time histories of forces and pressures on the model. In all cases, experiments were repeated at least three times to account for random nature of flow and uncertainties.

3.4 The Building Models

This building prototypes of this study are reinforced concrete buildings, which are widely constructed on beaches in Thailand. The target buildings are 5 storeyed houses: 15 m x 15 m x 15 m for the square shape and 24 m x 15 m x 15 m for the rectangular shape.

The models were made of 3mm thick acrylic plates. There were three types of building models to be tested. Table 3-2 shows details and photographs of all building models. These are models with square, rectangular and octagonal shapes in plan, the dimensions of which are shown in Figure 3-6. The last type is meant to represent a cylindrical shape for simplicity to avoid the difficulty of installing pressure sensors on a curved surface.

Table 3-2. Detail and photograph of building model

Shape	Dimension W x L x H (mm x mm x mm)	Opening area ratio (%)	Scale model	Photograph
Square	150 x 150 x 150	0, 25, 50	1:100	
Rectangular	240 x 150 x 150	0, 25, 50	1:100	
Octagonal	150 x 150 x 150	0	1:100	

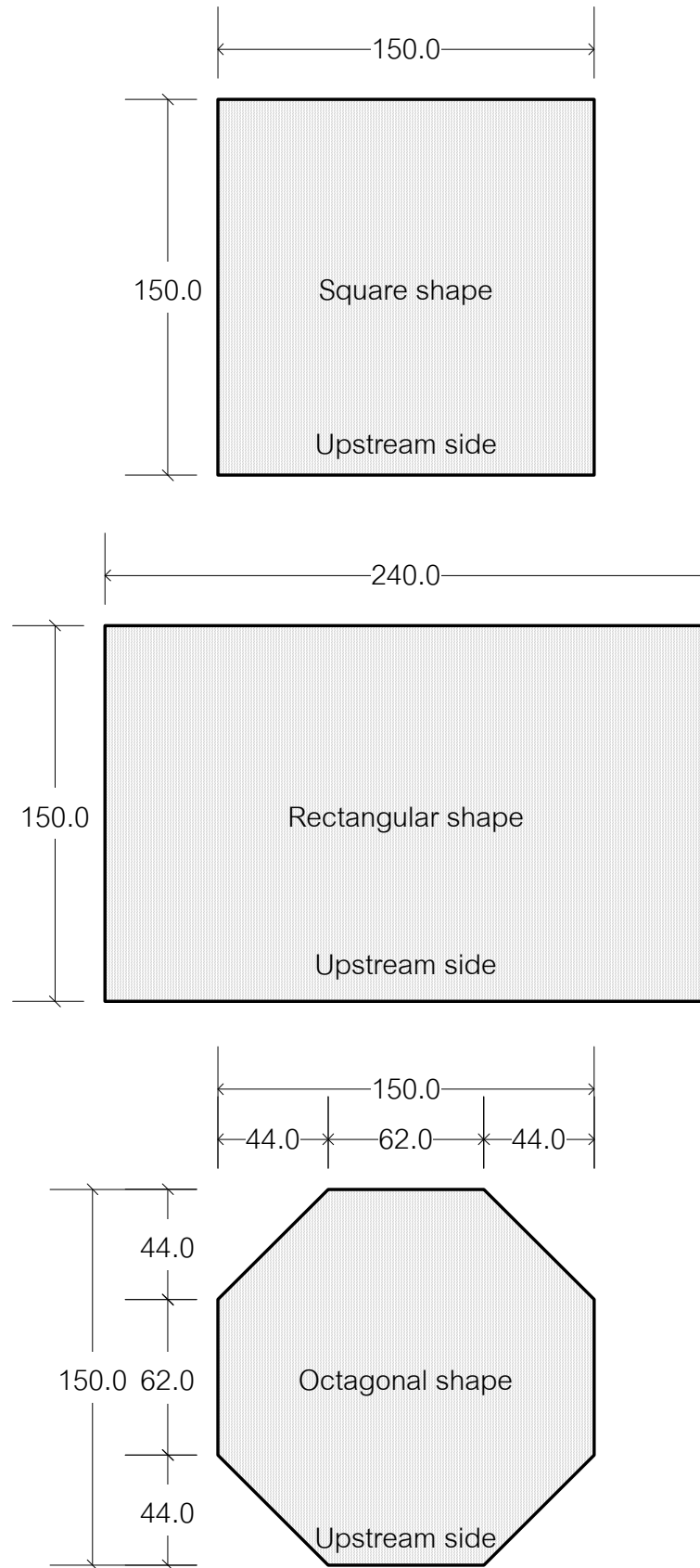


Figure 3-6. Plan of each shape (unit: mm)

Three configurations of openings at the front and back panels of the models were considered, viz. 0%, 25% and 50% as shown in Figure 3-7 and Figure 3-8 for the square and rectangular shapes, respectively.

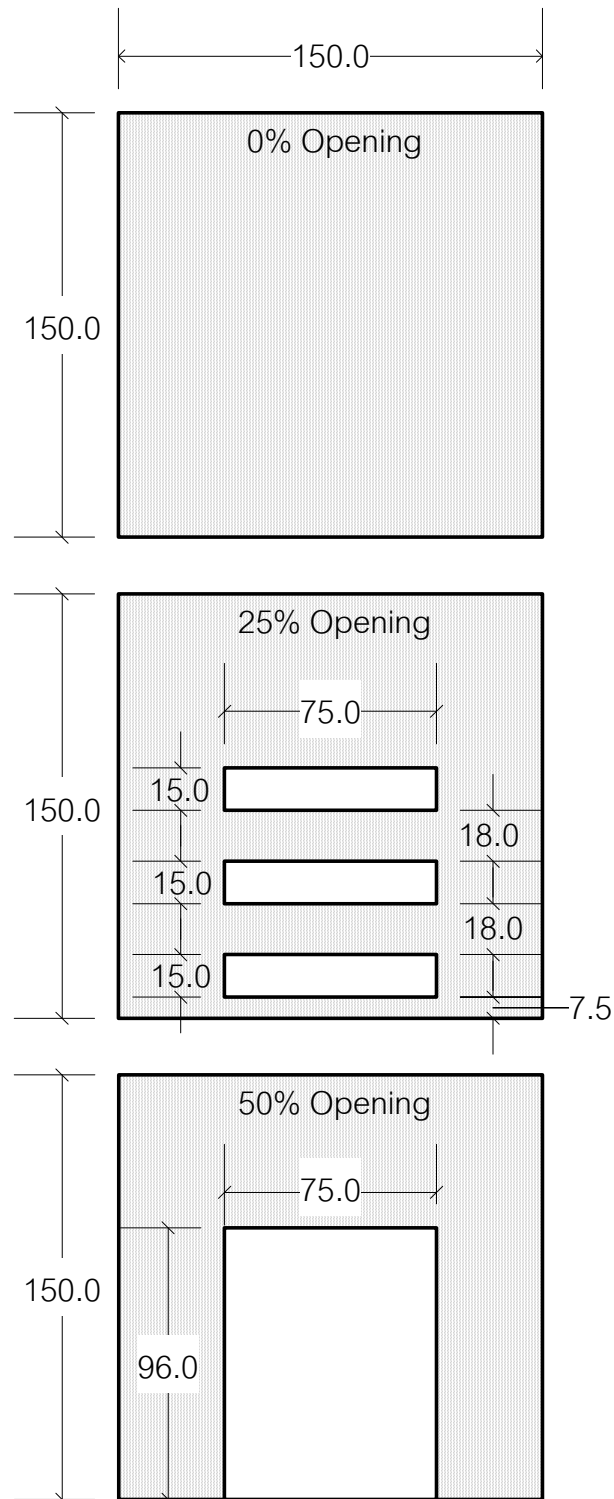


Figure 3-7. Three Configurations of openings for square shape (unit: mm)

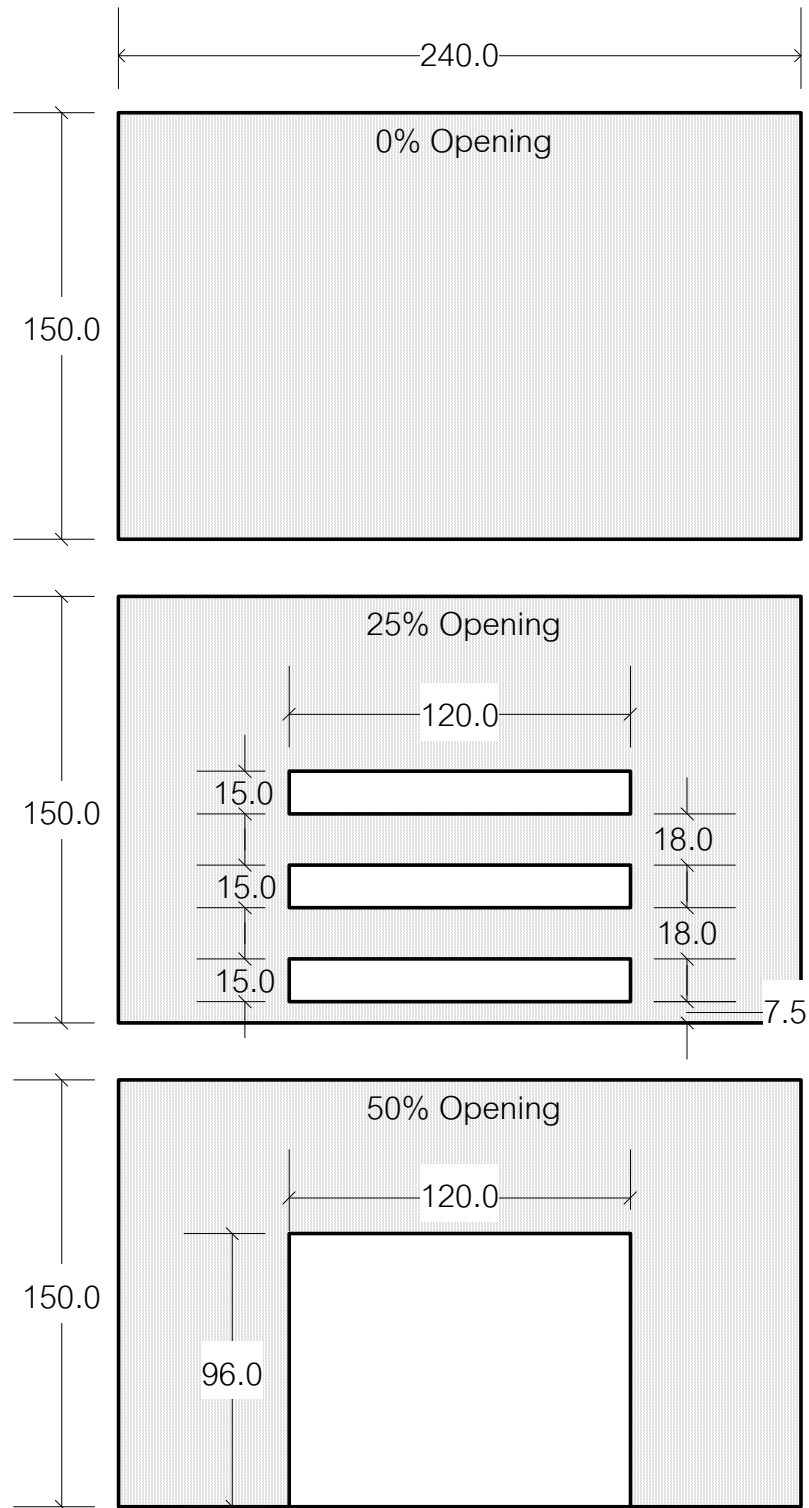


Figure 3-8. Three Configurations of openings for rectangular shape (unit: mm)

3.5 Instrumentation and Calibration

Measurements of the physical quantities, i.e. flow depth, velocity, force, and pressure were made by using appropriate instrumentations as described below.

3.5.1 Flow depth

The DHI wave meter and synthesizer as shown in Figure 3-9 measure the flow depth at onshore (H1) and offshore (H2) locations as illustrated in Figure 3-4. DHI wave meter is an electrical capacitance wave gauge with accuracy of $\pm 5\%$ and 50Hz sensitive frequency. DHI synthesizer, which is used to transform the signal, is connected to a computer acquisition system for storing the output data. It should be emphasized that the wave gauge at the onshore location was installed in the compartment beneath the channel bed filled with water so that part of it was fully submerged.

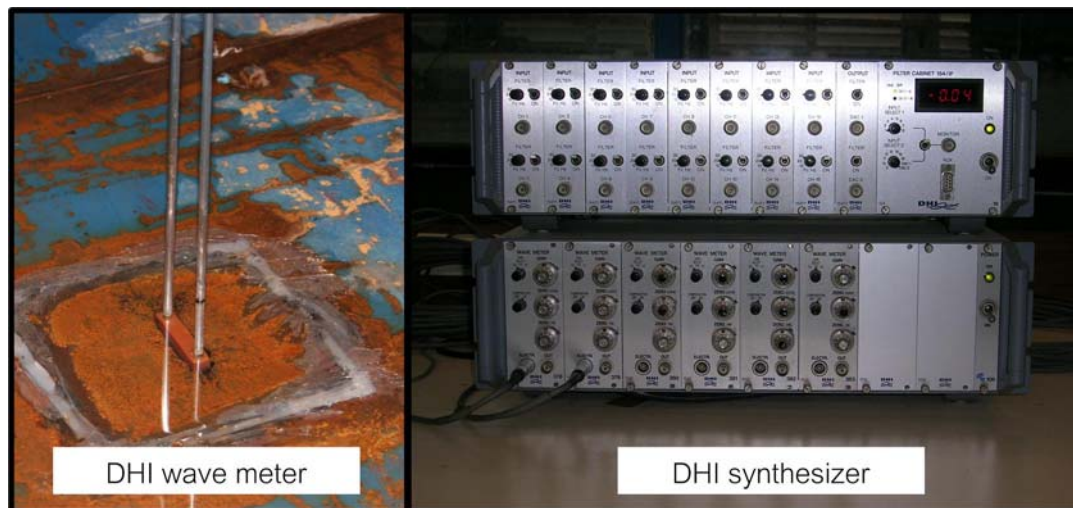


Figure 3-9. DHI wave meter (wave gauge) and DHI synthesizer

The wave gauges were calibrated by taking measurements in standing water of varying known depths. Figure 3-10 and Figure 3-11 show typical calibration curves for flow depth. The calibrated flow depth ranges from 0 to 0.10 m for the onshore wave gauge and 0 to 0.40 m for the offshore one. The linear calibration equations are obtained by means of least square regression and shown in the calibration curves.

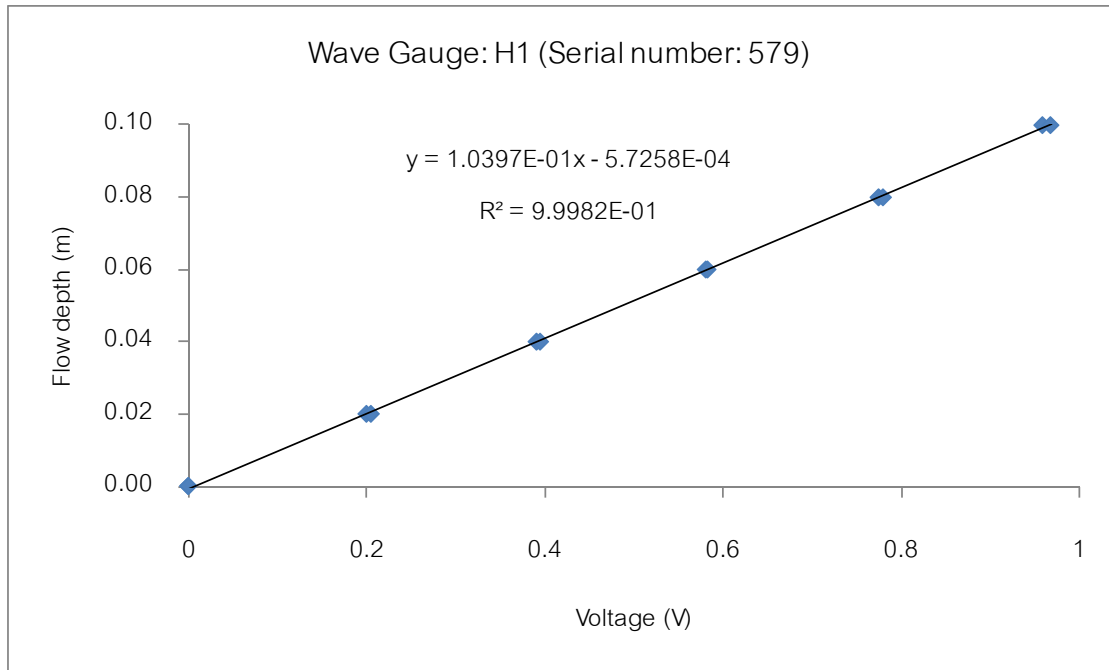


Figure 3-10. Typical calibration curve of flow depth for onshore wave gauge

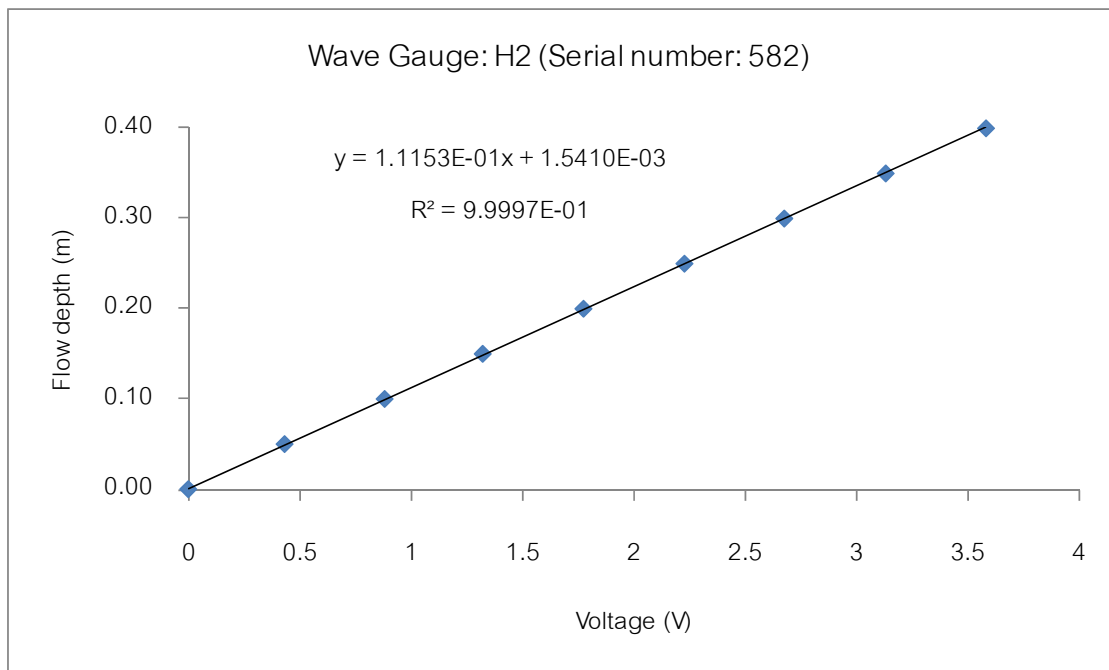


Figure 3-11. Typical calibration curve of flow depth for offshore wave gauge

3.5.2 Velocity

The propeller velocity flow meter measures the velocity of the waves in the flume for various wave heights. The current meter probe consists of a 11.6 mm rotor with five PVC blades. It can measure velocities in the range of 0.6-3.0 m/sec, which covers the range of velocity in the experiment. The current meter is set with the rotor center 12 mm from the bottom of the channel at the location of the model but without the existence of the model. The Nixon StreamFlo Digital Indicator transforms the recorded rotation of the propeller to digital signals. The data logger, Kyowa EDS-400A Compact Recorder, records the output signal. Figure 3-12 shows the instruments described.

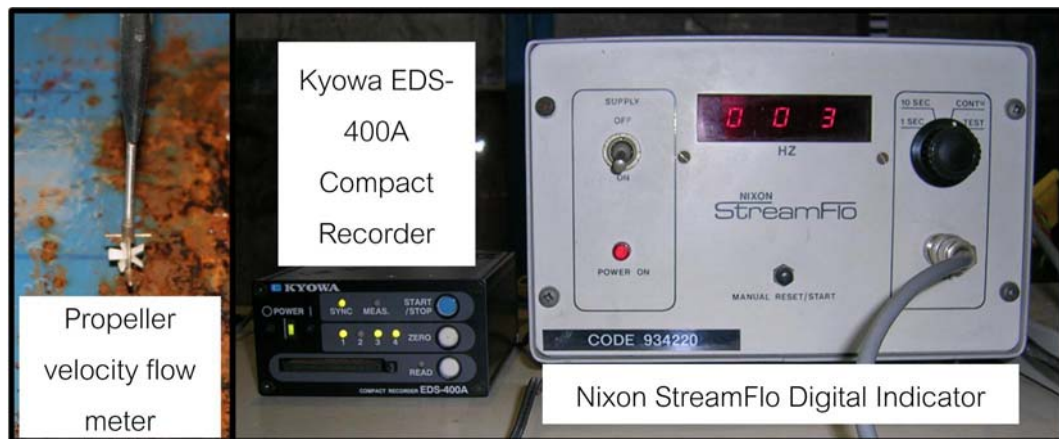


Figure 3-12. Instruments to measure velocity

The propeller velocity flow meter was calibrated by moving the instrument with a constant speed along the channel. The output signal was converted into the period of revolution. Figure 3-13 shows a typical calibration curve of velocity. The power calibration formula was determined by means of least square regression and shown in the calibration curve.

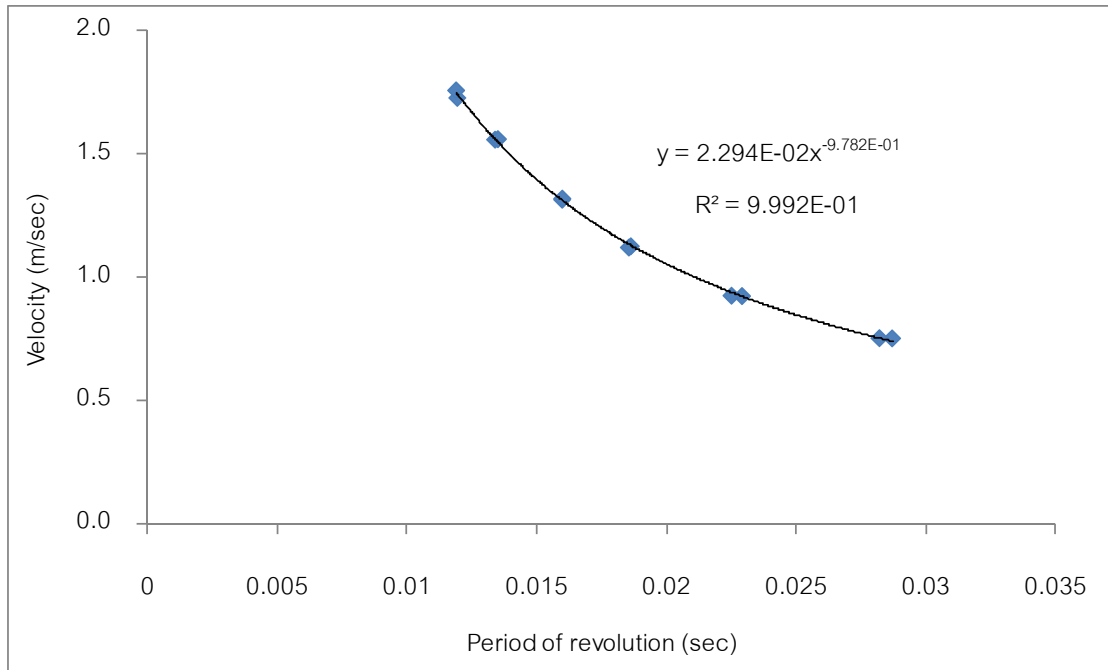


Figure 3-13. Typical calibration curve of velocity

3.5.3 Force

A load cell was used to measure the horizontal shear forces. It was mounted at the base of the model and fastened to a rigid steel support as shown in Figure 3-14.

A load cell is a device that converts the forces acting on the model to electrical signal in the strain gauges attached to the load cell body. Four strain gauges were attached at two levels on opposite sides of the cylindrical tube of load cell to complete the Wheatstone bridge circuit. The output voltage from the Wheatstone bridge circuit was proportional to the forces that acted on the model. Force data were recorded by the data logger, Kyowa PCD-300A Sensor Interface. The sampling frequency for the device was set to 500 Hz, which was sensitive enough to capture the impulsive wave force signals.

The load cell was calibrated by applying standard weights at various heights from the base of the model through a string and pulley system as shown in Figure 3-15. Figure 3-16 shows typical calibration curves for shear force. The linear calibration formulas were obtained using the least square regression.

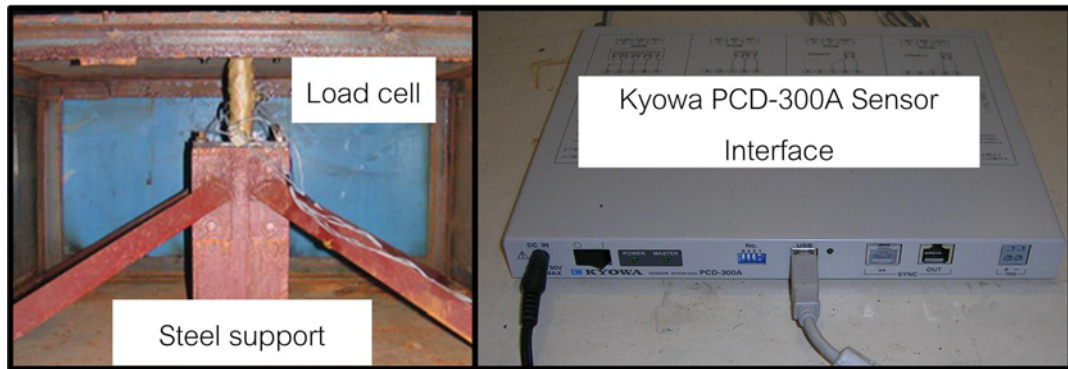


Figure 3-14. Instruments to measure force



Figure 3-15. Calibration of load cell

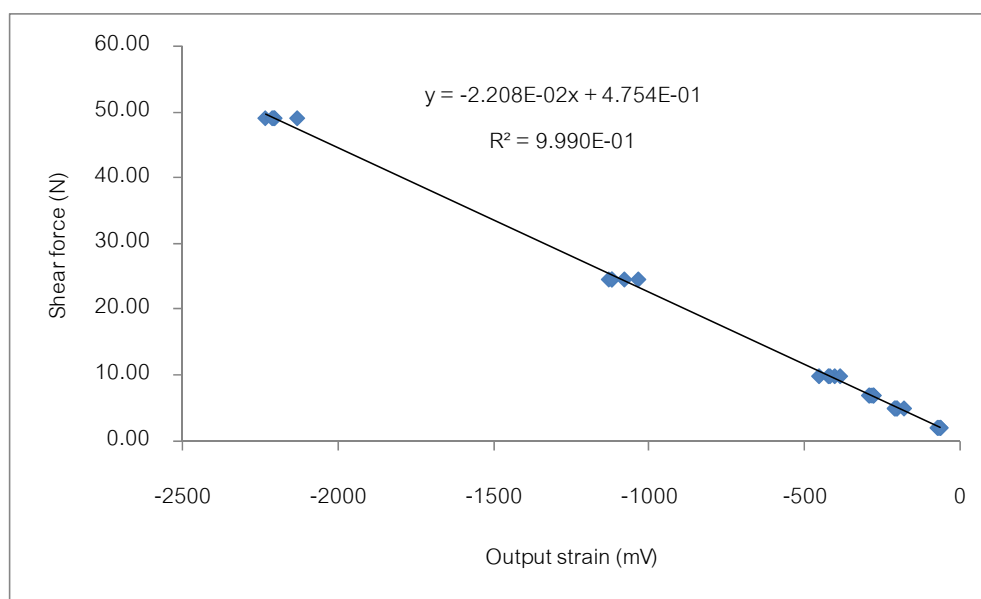


Figure 3-16. Typical calibration curve of shear force

3.5.4 Pressure

Pressure gauges were attached to the face of the model at different positions to measure wave pressure. The commercial pressure gauges used were Sankei waterproof diaphragm type pressure gauges SSK P310-01 and SSK P310-02 with rated capacities of 10 kPa (Pressure head about 1 m) and 20 kPa (Pressure head about 2 m), respectively. Each pressure gauge had a circular frontal surface of 10 mm in diameter as shown in Figure 3-17. Pressure data were recorded by the data logger, EDS-400A Compact Recorder. The sampling frequency for the device was set to 500 Hz so that it was sensitive enough to capture the impulsive wave pressure signals.

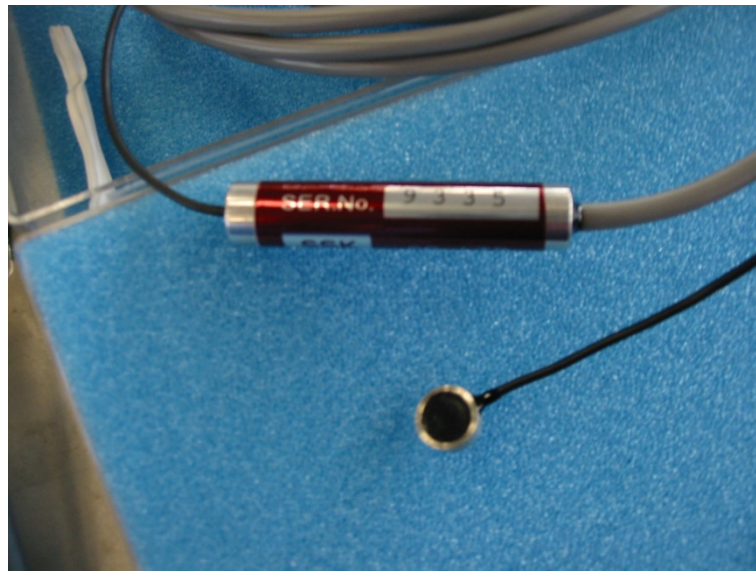


Figure 3-17. Pressure gauge

The pressure gauges were calibrated by taking measurements in standing water of varying known depths. Figure 3-18 shows a typical calibration curve of the pressure head. The linear calibration formulas were obtained using the least square regression.

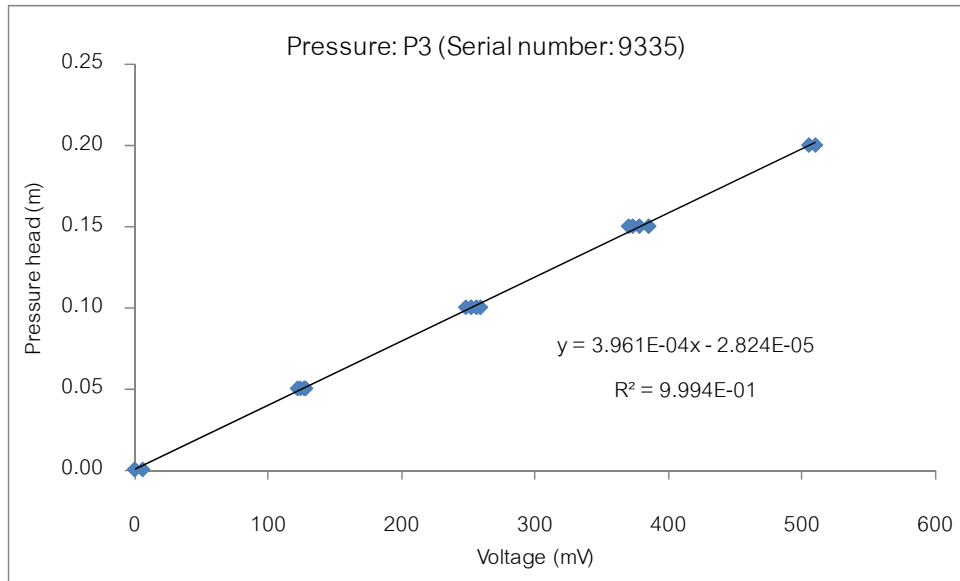


Figure 3-18. Typical calibration curve of pressure head

3.6 Test Program

Table 3-3 presents a general overview of the test program. The programs consisted of a combination of 2 slope profiles with 3 model shapes viz., square, rectangular and octagon shapes. Three configurations of openings were investigated for the square and rectangular shapes, whereas no openings were considered for the octagonal shape. Each configuration was tested under 3 nominal wave heights. The nominal wave height is roughly the maximum flow depth at the location of the model obtained from the flow condition without the presence of the model. Each test condition was repeated three times, in general, to confirm the repeatability of the experiment. The total number of the basic test conditions amounted to 126 cases.

Figure 3-19 shows the location of pressure gauges on the face of the model. For the basic test conditions, the pressure gauges were attached at locations 1F, 2F and 3F. For the special test conditions, the vertical and horizontal distributions of the pressure were investigated by appropriately locating the pressure gauges to suit each case.

Table 3-3. Test program

Slope profile	Shape	Opening (%)	Nominal wave height (mm)
Khaolak, Phang-Nga (K)	Square (S)	00, 25 and 50	30, 60 and 80
Khaolak, Phang-Nga (K)	Rectangular (R)	00, 25 and 50	30, 60 and 80
Khaolak, Phang-Nga (K)	Octagonal (O)	00	30, 60 and 80
Kamala, Phuket (P)	Square (S)	00, 25 and 50	40, 60 and 80
Kamala, Phuket (P)	Rectangular (R)	00, 25 and 50	40, 60 and 80
Kamala, Phuket (P)	Octagonal (O)	00	40, 60 and 80

Remark: Letters in parentheses designate slope profiles or shapes

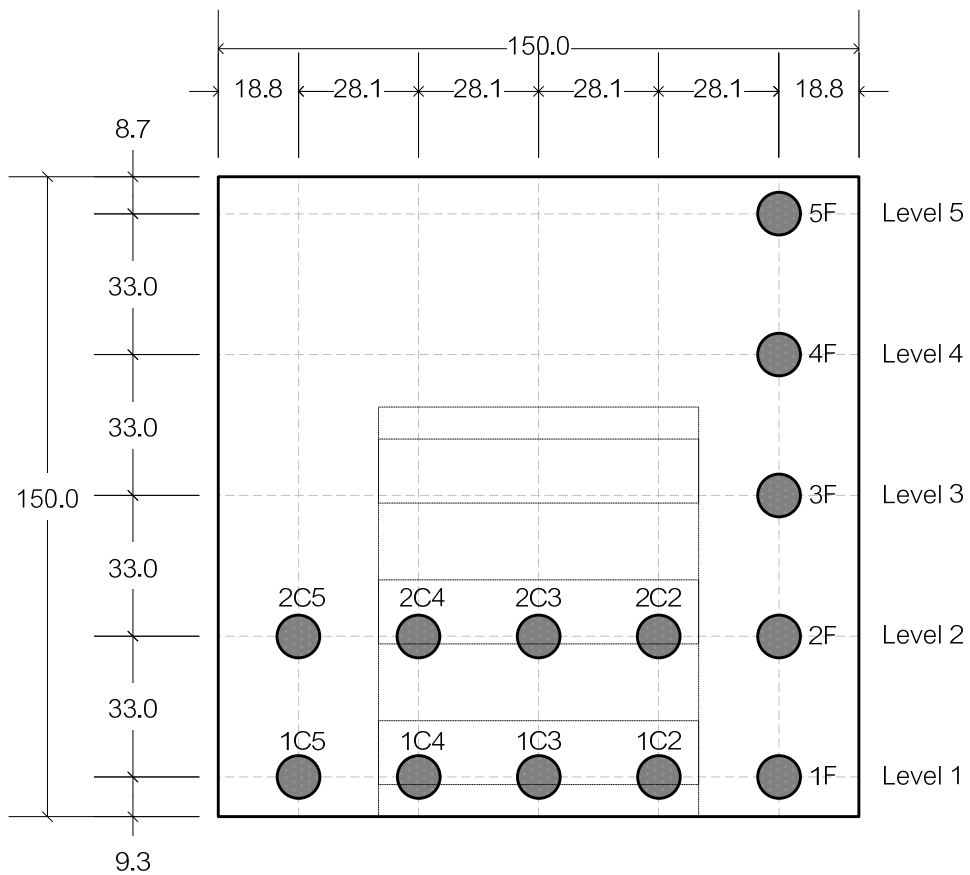


Figure 3-19. Locations and designation of pressure gauges

3.7 Results and Discussions

3.7.1 Characteristics of flow propagation on slope profile

Figure 3-20 shows characteristics of wave profile at offshore. The wave profile is similar to solitary-like waves. Wave breaking always occurs at the offshore end of the mildly sloping beach and a bore-like broken wave is formed prior to arriving at the building model.

3.7.2 Time history of flow depth and flow velocity

Before testing models in the wave flume, experiments were conducted to obtain time histories of the flow depth and flow velocity at the location of model. The time histories of the flow depth and flow velocity with inundation depth for various nominal heights at the location of the model (in the absence of the model) are shown in Figure 3-21 and Figure 3-22 for Khaolak and Kamala slope profiles, respectively. In each figure, the flow depths are shown with black lines while the flow velocities are shown with gray lines. The plots indicate that the flow depth and flow velocity on each case vary with reasonable consistency throughout the time history. This demonstrates the adequate replication in the conduct of tests. For this study, the time is taken as zero when the wave instantly hits the model.

In every case, the maximum flow velocity occurs at the leading front of the wave when the flow depth is very small. Thereafter, the flow velocity is decreased but the flow depth is increased with time to maximum flow depth during the first 1-2 seconds, and then the flow depth becomes reasonably uniform. It is important to observe that the maximum flow velocity does not occur at the same time with the maximum flow depth.

The experiments show that for the same nominal wave height, different flow velocities are obtained for different slope profile. Thus, formulas for calculating tsunami loading should include both flow depth and flow velocity as parameters.

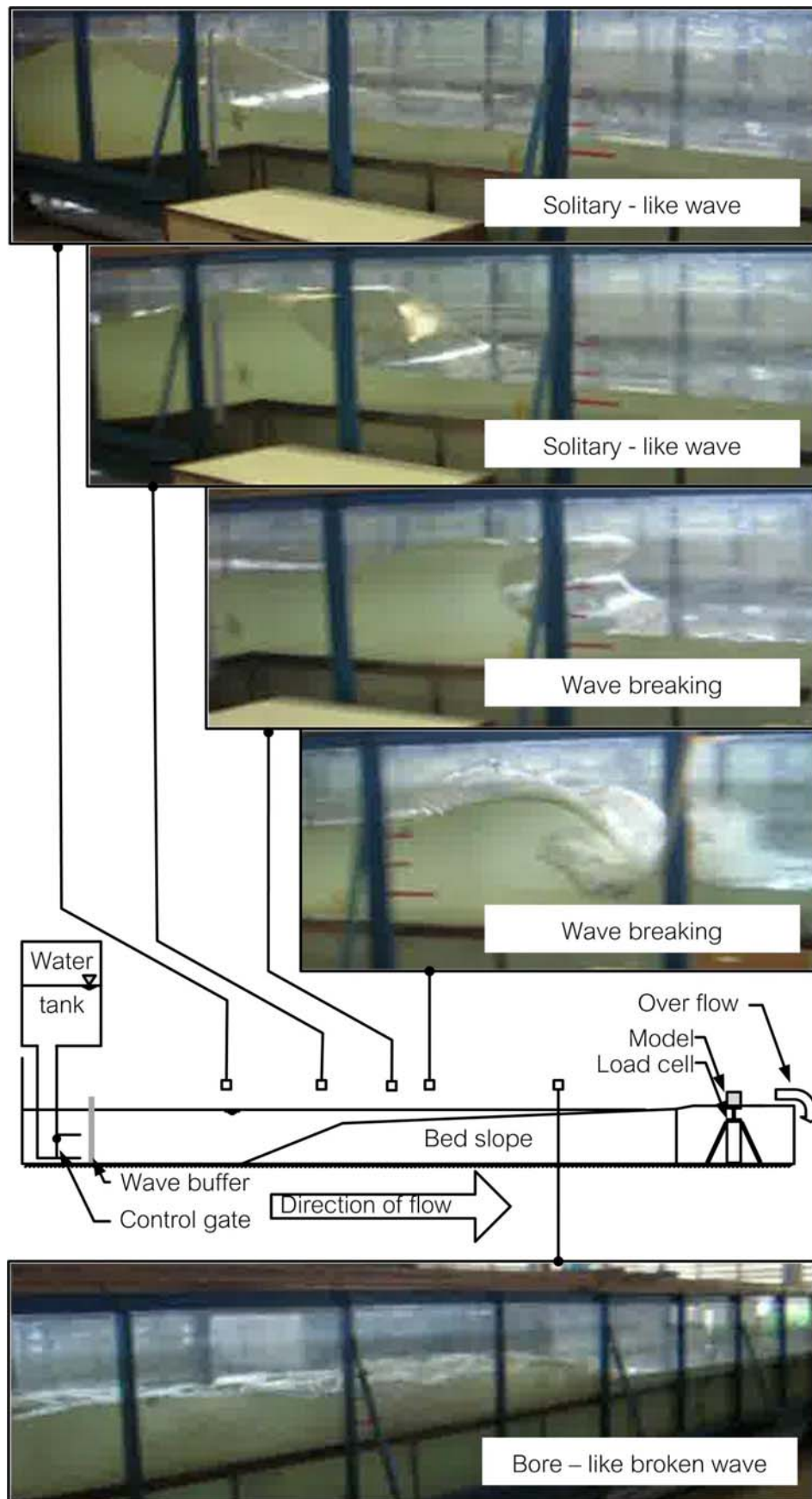
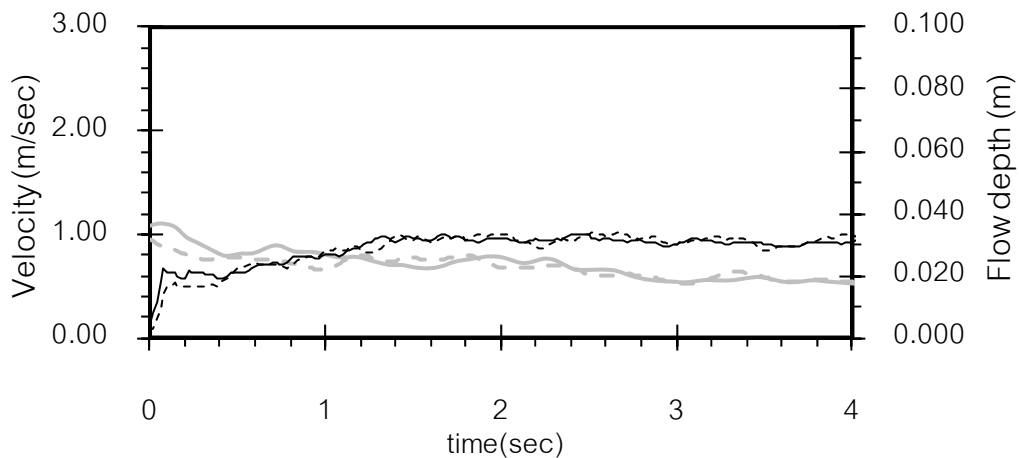
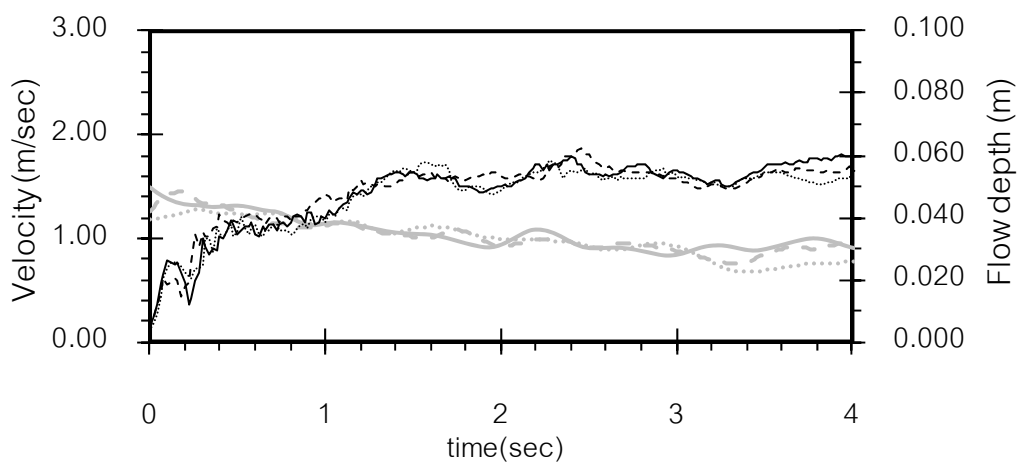


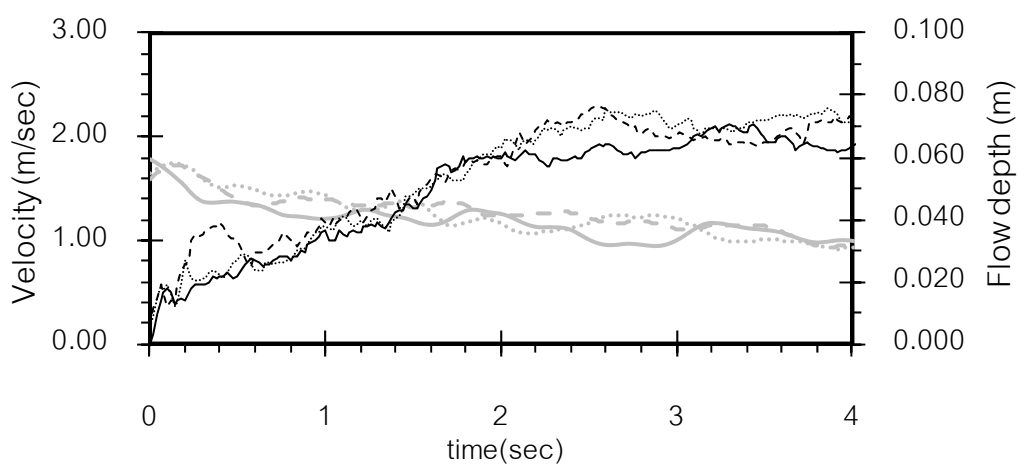
Figure 3-20. Characteristics of wave profile



(a) Nominal wave height 30 mm

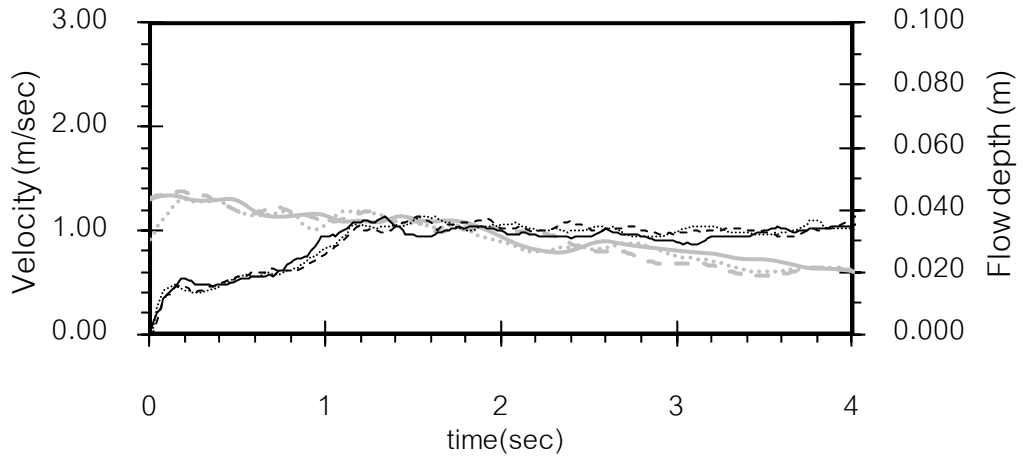


(b) Nominal wave height 60 mm

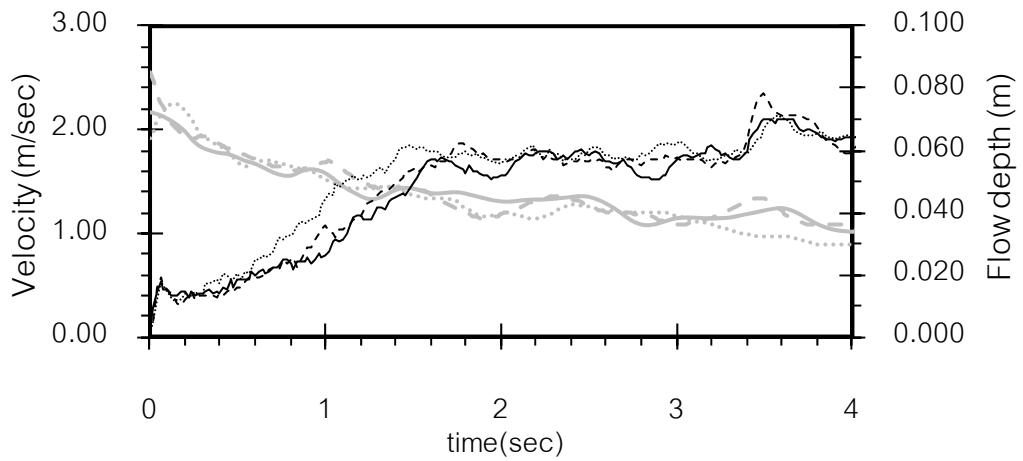


(c) Nominal wave height 80 mm

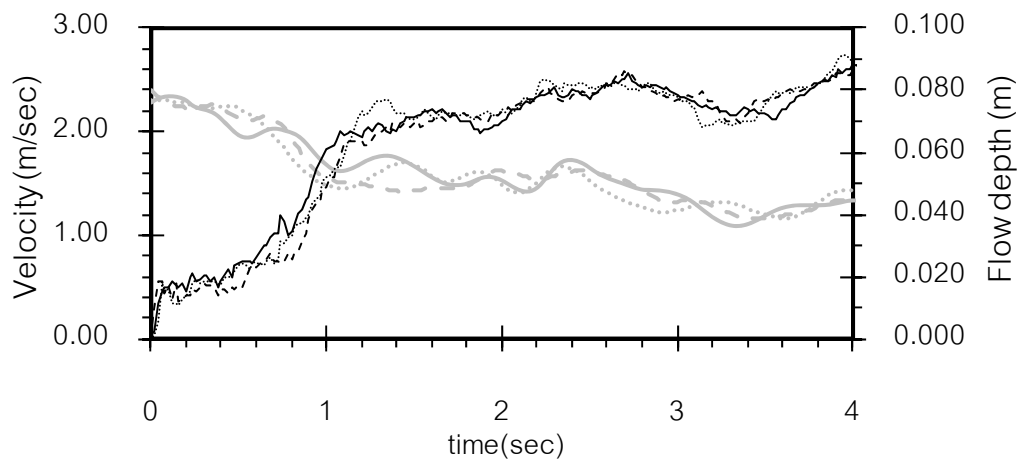
Figure 3-21. Typical time history of flow depth (black line) and flow velocity (gray line) for Khaolak slope profile



(a) Nominal wave height 40 mm



(b) Nominal wave height 60 mm



(c) Nominal wave height 80 mm

Figure 3-22. Typical time history of flow depth (black line) and flow velocity (gray line) for Kamala slope profile

3.7.3 Characteristics of flow past model

The typical characteristics of flow past a model is illustrated in Figure 3-23 to Figure 3-25 for the case of a square section model without openings for Kamala slope profile and a nominal wave height of 60 mm. The images in Figure 3-23 were captured from a video file taken at 25 frames per second. Each capture is marked with the time that has passed since the wave attacks the model. Figure 3-24 and Figure 3-25, which were captured from another digital camera, present the upstream and downstream captures of the flow, respectively. Because of low resolution in the time recording in the camera, it was not possible to identify the exact time of the capture.

When the wave hits the model, the wave splashes up on the upstream side of the model like a wave striking on a wall. Then the flow overtops the model as shown in Figure 3-24 (a) and Figure 3-25 (a). Afterwards, the water falls back; there is a buildup of water on the upstream face of the model due to the flow blockage as shown in Figure 3-24 (c). In Figure 3-25 (e), it is evident that the flow depth on the downstream side is much lower than that on the upstream face.

The above description generally applies to nominal wave heights of 60 and 80 mm with flow overtopping the models, even though the model height is still larger than the maximum flow depth. As indicated in Figure 3-23, the splash on the face of the model reaches a height larger than that of the model. For smaller nominal wave heights (30 and 40 mm), the models are not overtopped.

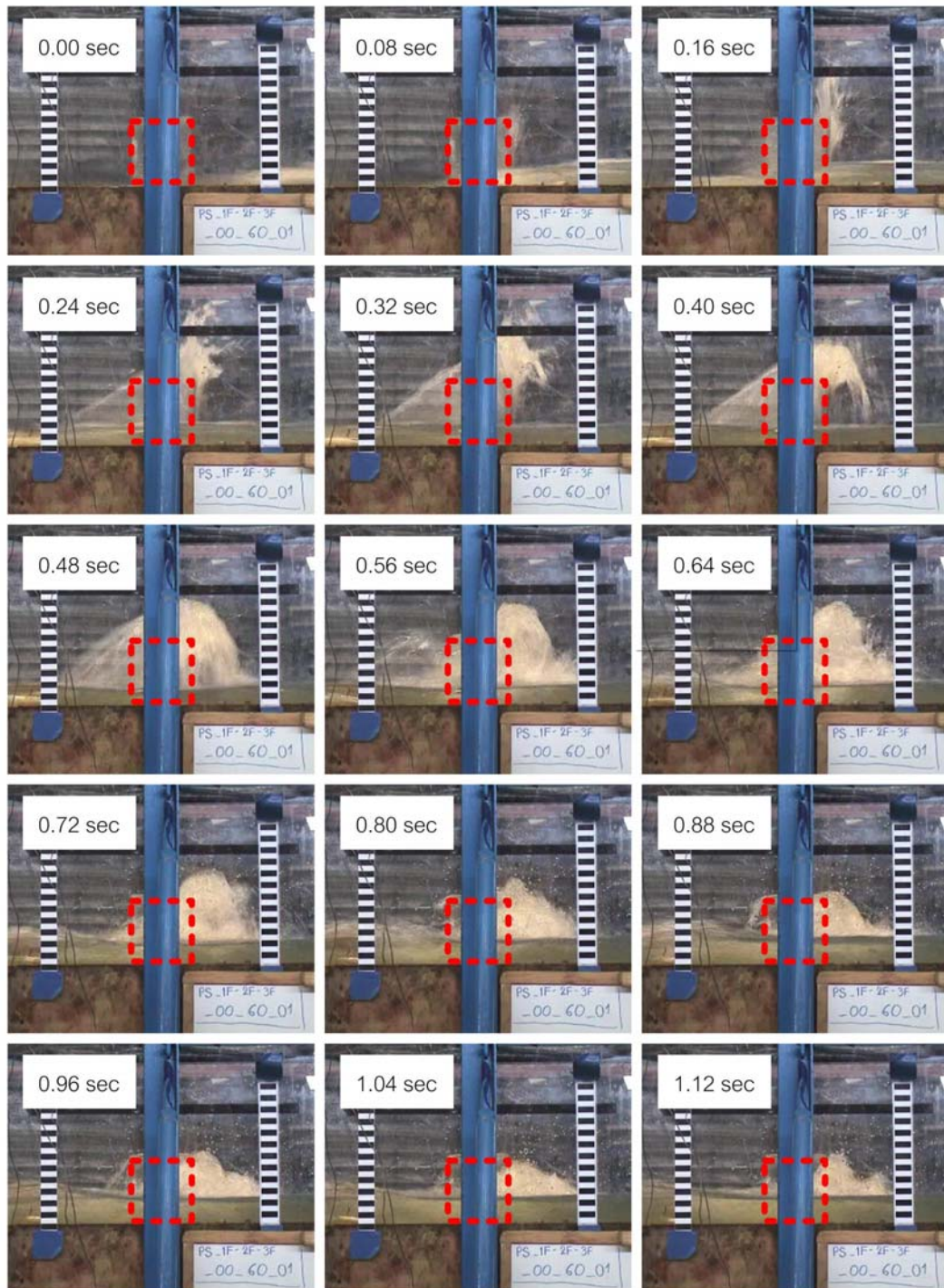


Figure 3-23. Sequence of the wave attack on the building model in the side view with nominal wave height of 60 mm

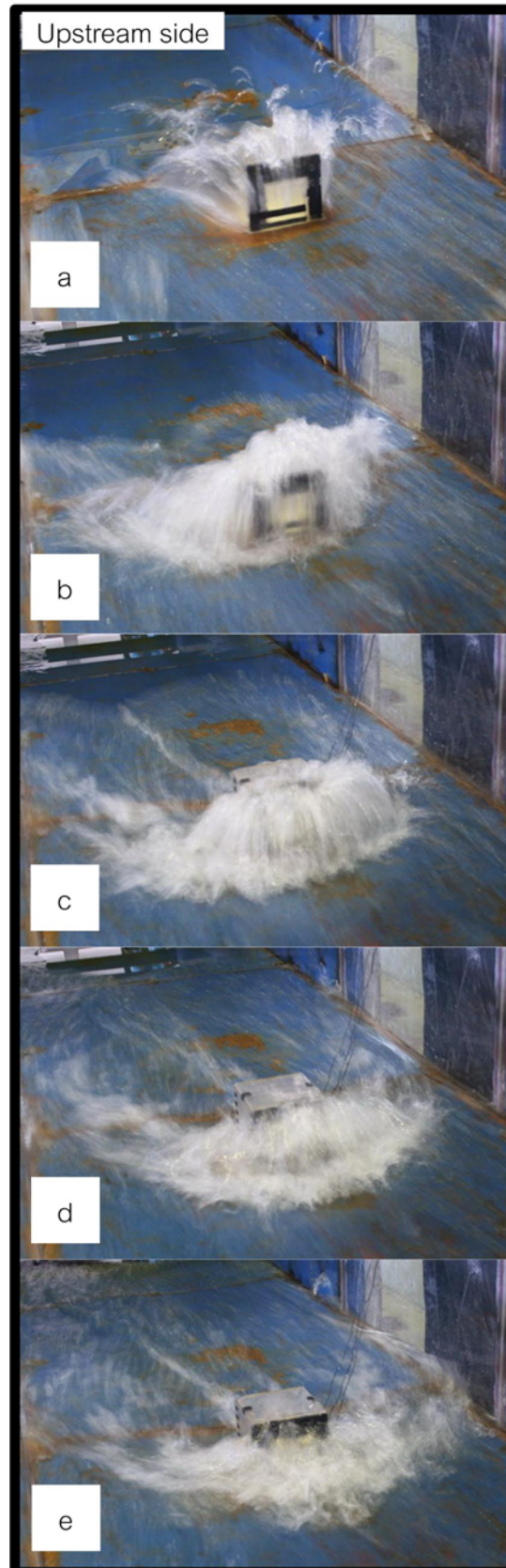


Figure 3-24. Sequence of the wave attack on the square model at upstream side with nominal wave height of 60 mm

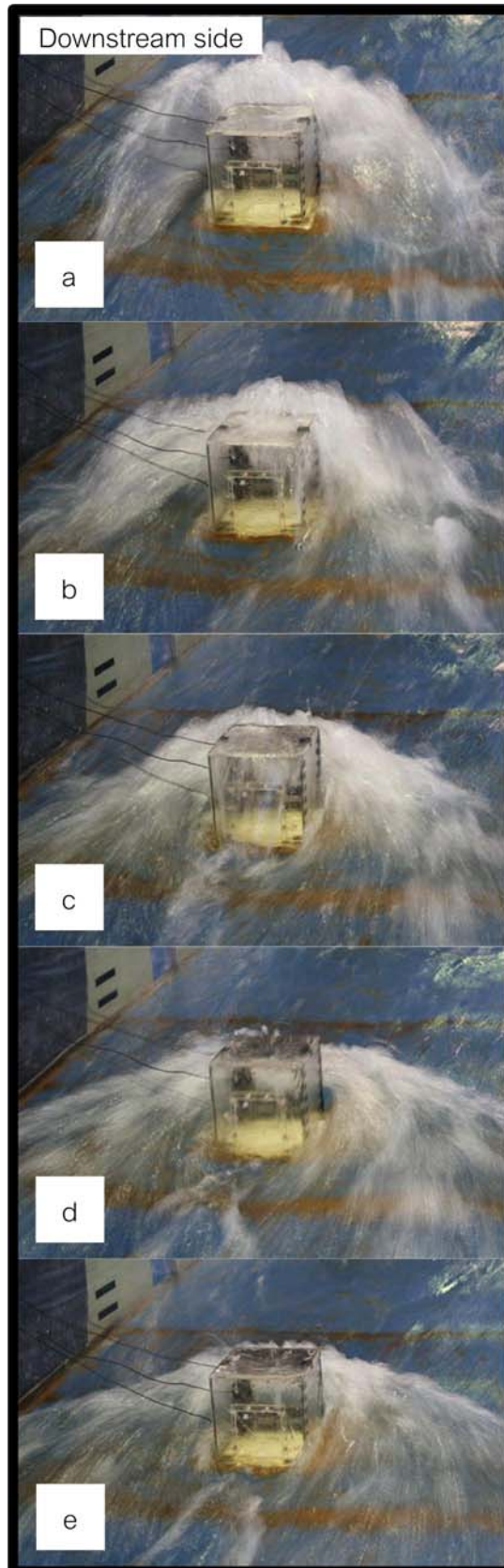


Figure 3-25. Sequence of the wave attack on the square model at downstream side with nominal wave height of 60 mm

3.7.4 Time history of force on models with and without openings

The time histories of the force on models for various nominal heights and openings are shown in Figure 3-26 for Khaolak slope profile and in Figure 3-27 for Kamala slope profile. In each figure, the forces on the model without openings are shown with solid line while the models with 25% and 50% openings are shown with gray line and dotted line, respectively. Results from three experimental runs are shown for each case. The experimental results from different runs in each case are quite well replicated.

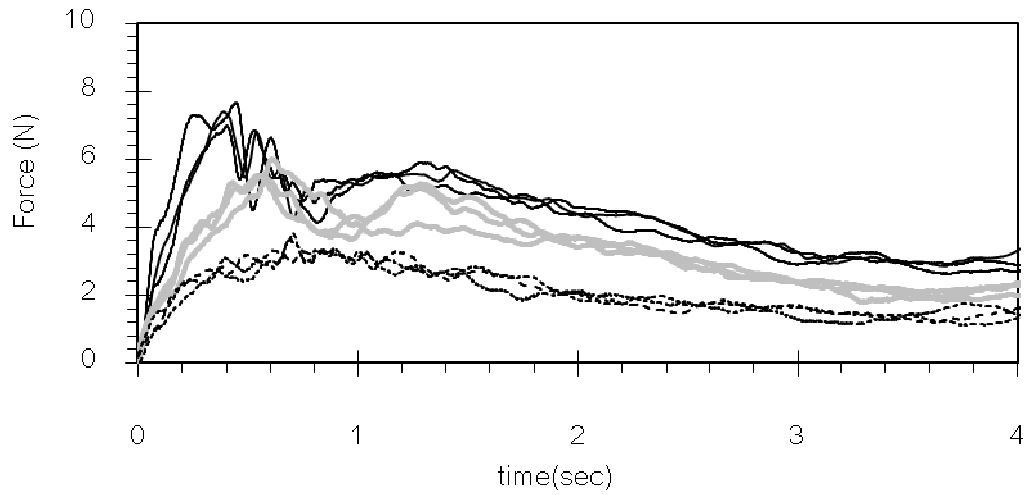
In each case, the flow in the first second or so is highly unsteady and turbulent. After that, the flow is much more smooth. The loading on models is observed to be dependent on the condition of slope profile, opening area and nominal wave height. The peak forces at different levels in each case occur at different times. However, no clear peaks are exhibited in some cases. In this study, the maximum force in the first four seconds is considered and analyzed.

3.7.5 Effect of openings

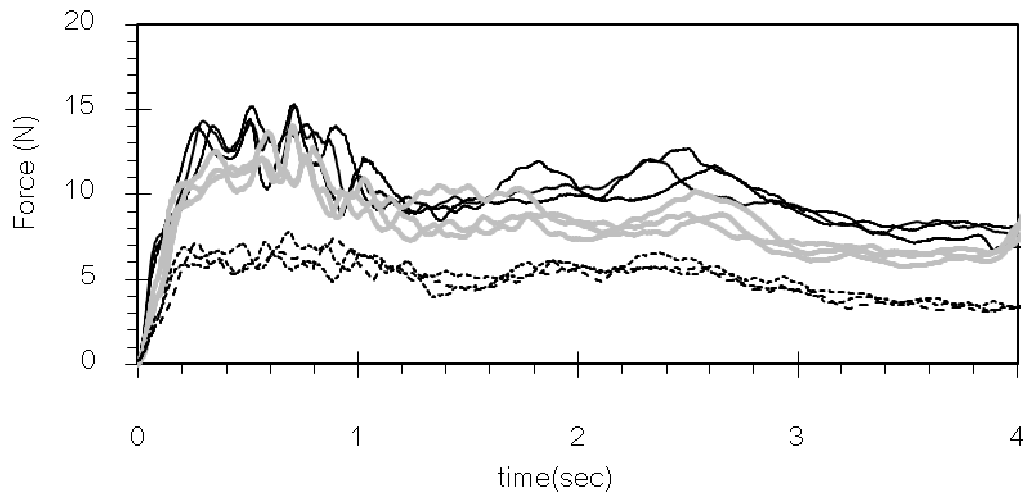
Table 3-4 and Table 3-5 show the maximum forces on square models with various nominal wave heights and opening configurations for Khaolak and Kamala slope profiles, respectively. The values are calculated from the average of maximum forces in three experimental runs of each case. The percentage in parentheses shows the ratio of force on the model with openings to that without openings.

For the models with openings, the force recorded by the load cell registers that acting over the whole model. The wave exerts loading not only the front panel, but also on the back panel facing upstream, and on the faces inside the model. More details will be covered in section 3.7.10

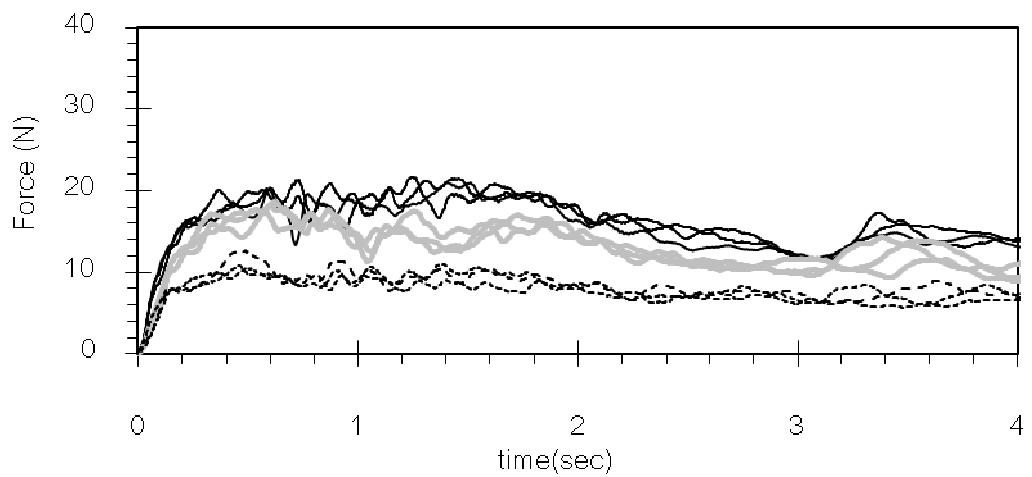
The results show that there is a reduction in the forces acting on the whole building in the order of 15% - 25% for the 25% opening configuration, and 35% - 50% for case of 50% opening configuration, except the case of 25% opening configuration with 40 mm nominal wave height on Kamala slope profile for which the reduction is only 5%.



(a) Nominal wave height 30 mm

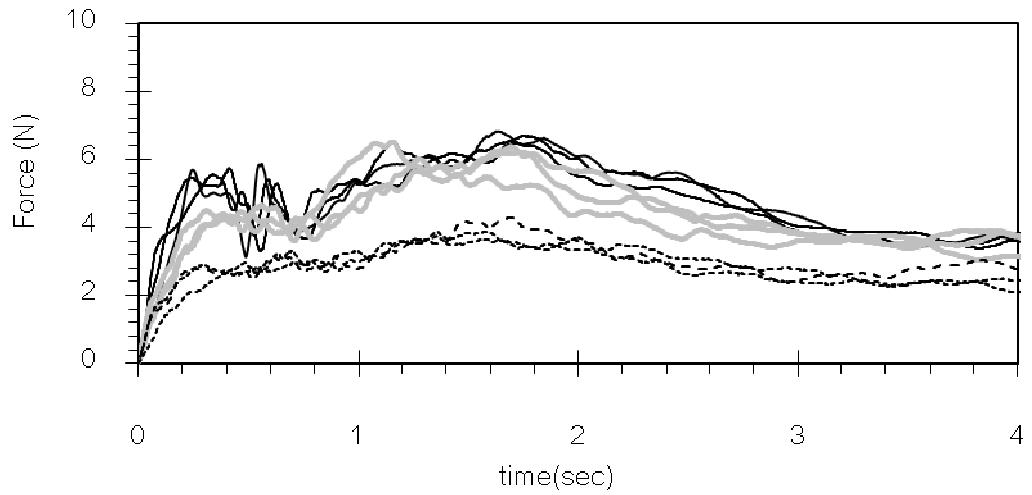


(b) Nominal wave height 60 mm

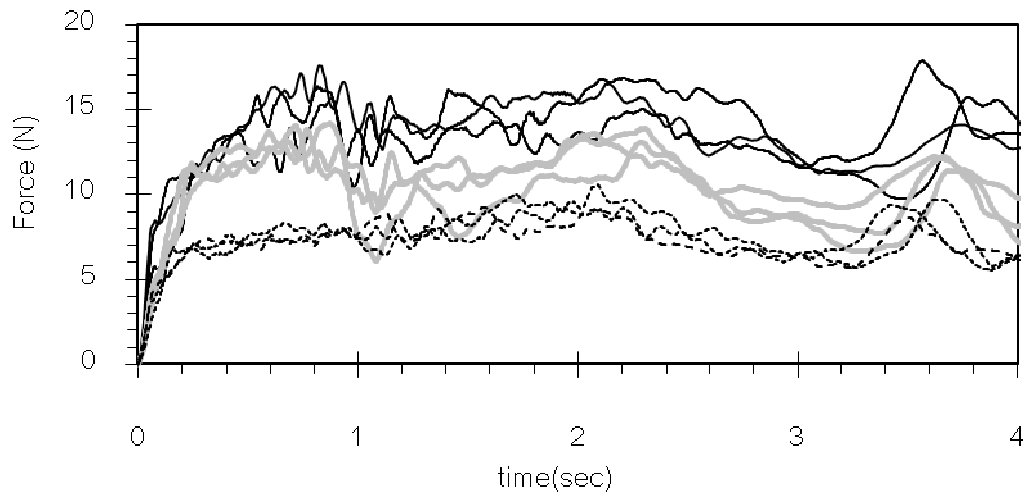


(c) Nominal wave height 80 mm

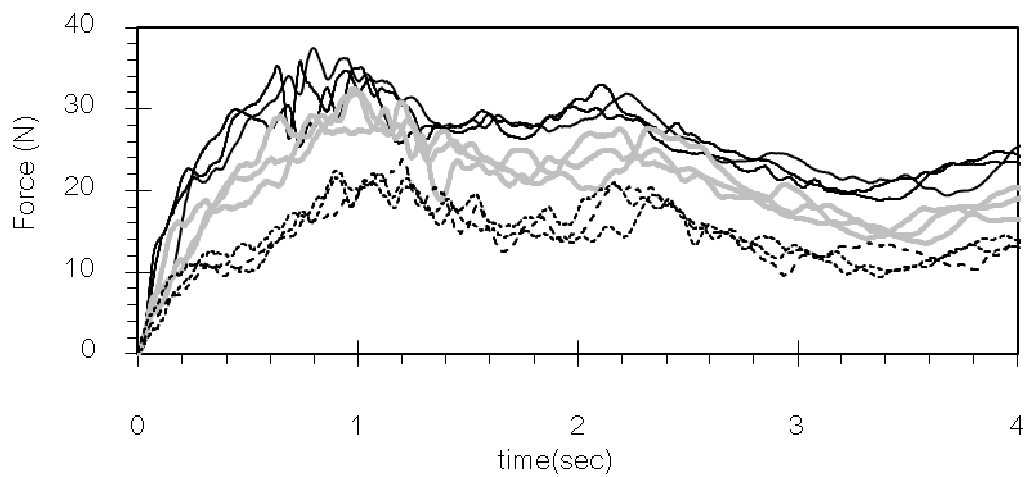
Figure 3-26. Typical time history of force for Khaolak slope profile with 0% opening (solid line), 25% openings (gray line) and 50% openings (dotted line)



(a) Nominal wave height 40 mm



(b) Nominal wave height 60 mm



(c) Nominal wave height 80 mm

Figure 3-27. Typical time history of force for Kamala slope profile with 0% opening (solid line), 25% openings (gray line) and 50% openings (dotted line)

Table 3-4. Maximum forces (N) on square model for Khaolak slope profile.

Opening (%)	Nominal wave height	Nominal wave height	Nominal wave height
	30 mm	60 mm	80 mm
00	7.35 (100%)	15.22 (100%)	21.38 (100%)
25	5.68 (77%)	12.87 (85%)	18.17 (85%)
50	3.60 (49%)	7.50 (49%)	11.51 (54%)

Note: Values in parentheses are percentage of the model without openings

Table 3-5. Maximum forces (N) on square model for Kamala slope profile.

Opening (%)	Nominal wave height	Nominal wave height	Nominal wave height
	40 mm	60 mm	80 mm
00	6.68 (100%)	16.70 (100%)	36.13 (100%)
25	6.38 (95%)	14.04 (84%)	31.25 (86%)
50	3.97 (59%)	9.69 (58%)	22.84 (63%)

Note: Values in parentheses are percentage of the model without openings

3.7.6 Time histories of pressure on upstream front panel

Figure 3-28 illustrates the typical time histories of normalized pressures at the upstream face and the resultant force on the square shape model without openings under a nominal wave height of 80 mm on the Khaolak slope. The normalized pressure is normalized with the hydrostatic pressure based on the maximum flow depth. The force is shown in gray line while the pressures at the locations 1F, 3F, 4F and 5F are shown in black solid line, long dashed line, dashed line and dotted line, respectively. The pressure location designations are shown in Figure 3-19.

At the initial wave attack, there is initial impulse pressure at 1F while no pressure is measured at other locations. The maximum pressure at 1F is approximately 4 times the hydrostatic pressure and subsequently decreases to slightly less than 2 times the hydrostatic pressure with small fluctuations. It is interesting to note that the effect of splash up is picked up at locations higher up on the model with some time lag from the initial impact. For the pressure at 3F, it increases with time to a quasi-steady state at

about 1.25 times the hydrostatic pressure. At the top level 5F, the maximum normalized pressure is less than 0.5.

The maximum force and maximum pressure at each level occur at different times as evident in Figure 3-28. Also the vertical pressure distribution changes over time, with peak value occurring near the base at initial impact of the leading front of the wave and it propagates upward as inundation rises.

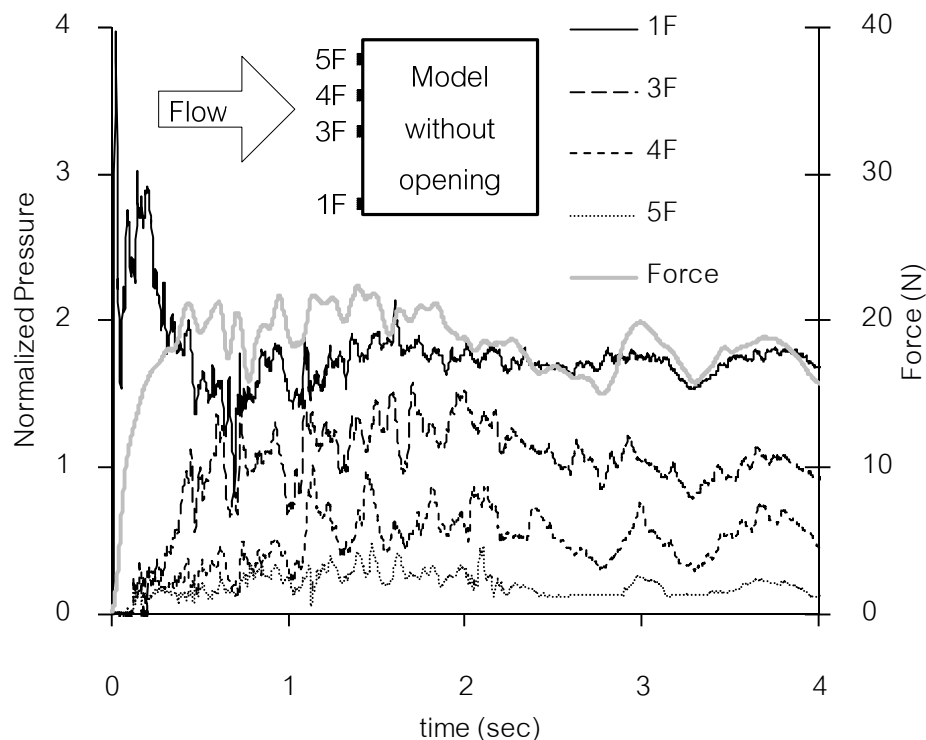


Figure 3-28. Typical time histories of normalized pressures and forces for square shape model without openings and nominal wave height 80 mm

3.7.7 Vertical pressure profile

Existing design guidelines recommend that the hydrodynamic forces be applied to structures as a uniform load. However, the experimental results show that the pressures vary with height as depicted in Figure 3-28. It is important to observe from the figure that the maximum pressures at different levels occur at different instants of time. Furthermore, the maximum pressures and maximum force occur at different instants of time. In practical design for overall stability, the maximum resultant force on the whole

structure is to be considered. For this reason, the vertical pressure distribution is considered at the instant of time when the maximum force occurs.

Figure 3-29 demonstrates the relationship between the normalized pressure and normalized height on the front face of the square shape model in the case of Kamala slope at the instant the resultant force acting on the model is maximum. The normalized pressure is the pressure, P divided by hydrostatic pressure, ρgh_m , where ρ is fluid density, g is gravitational acceleration and h_m is maximum flow depth at the location of interest when there is no flow obstruction. The normalized height is the height from the base, Z divided by h_m . The normalized pressures on the models with different opening configurations are presented in the same plot.

An observation of Figure 3-29 indicates clearly that the vertical pressure profile is not uniform. The pressures are larger in the lower part of the model with the maximum value about three times the hydrostatic pressure. Due to restriction in instrumentation, there is no pressure data above the normalized height of two. Nevertheless, the measured pressure near this height is already very small, so the lack of pressure data in the top part is not so significant.

It has been proposed by Asakura et al. (2002), based on 3D hydraulic model tests with flow not overtopping the model, a vertical distribution of maximum pressure with a maximum value of 3 times hydrostatic pressure. Lukkunaprasit et al. (2009a) conducted model tests with both topping and no topping conditions and proposed a simplified vertical pressure distribution at the instant of maximum force by a bi-linear distribution. The uniform distribution over one wave height reflects the hydrodynamic characteristics.

The proposed vertical pressure distributions by Lukkunaprasit et al. (2009a) and Asakura et al. (2002) are also shown in Figure 3-29 with solid and dashed lines, respectively. Clearly, the two lines provide a reasonable good upper bound for the experimental data, except for a few cases of models with openings.

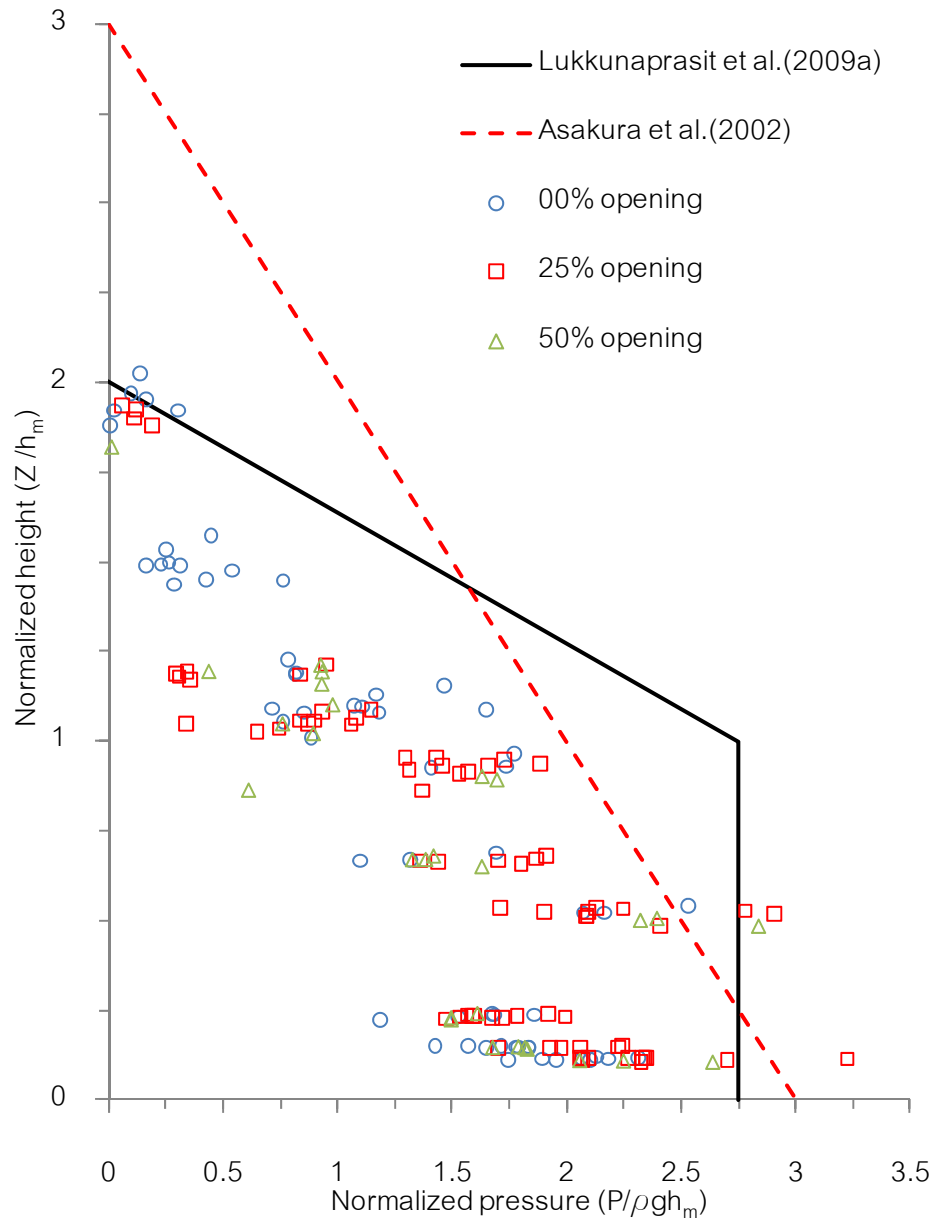


Figure 3-29. Variation of normalized pressure with height at the instant of maximum force - Kamala slope and square shape

3.7.8 Time histories of pressure variation across the frontal face at the same level

Figure 3-30 through Figure 3-33 illustrate the typical time histories of normalized pressures on models with and without openings at the same level. The pressure location designations are shown in Figure 3-19. The pressure values at the same level and configuration of openings are averaged and depicted in Figure 3-34 and Figure 3-35. It should be observed that the normalized pressures do not vary much across the width at the same level and hence can be regarded as the same in practice.

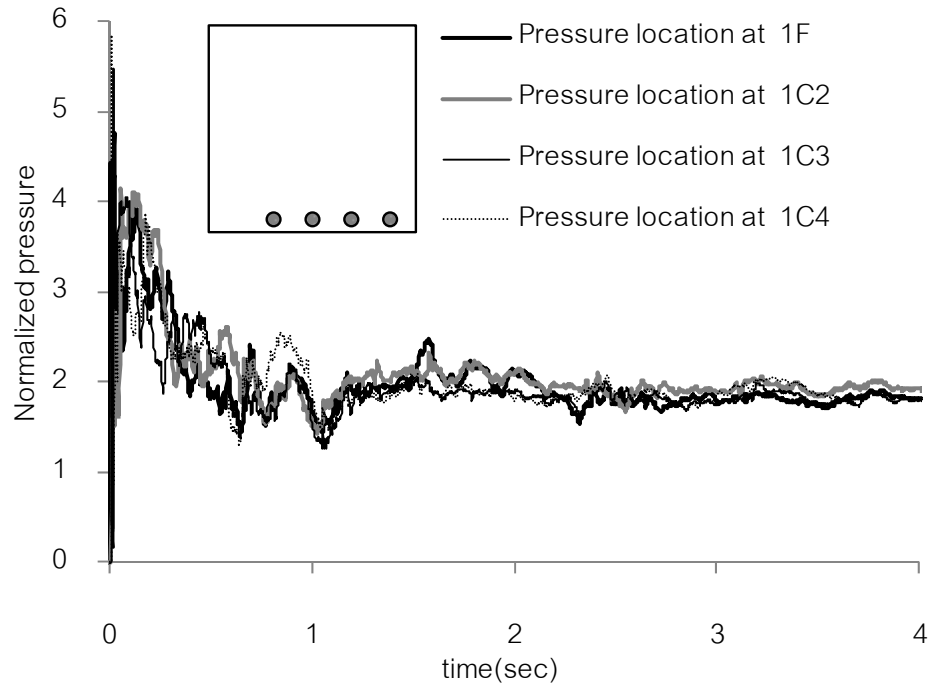


Figure 3-30. Time history of pressure in case: KS1F-1C2-1C3-1C4_00_90_01
(Khaolak slope, Square shape, No opening, Nominal wave height 80 mm)

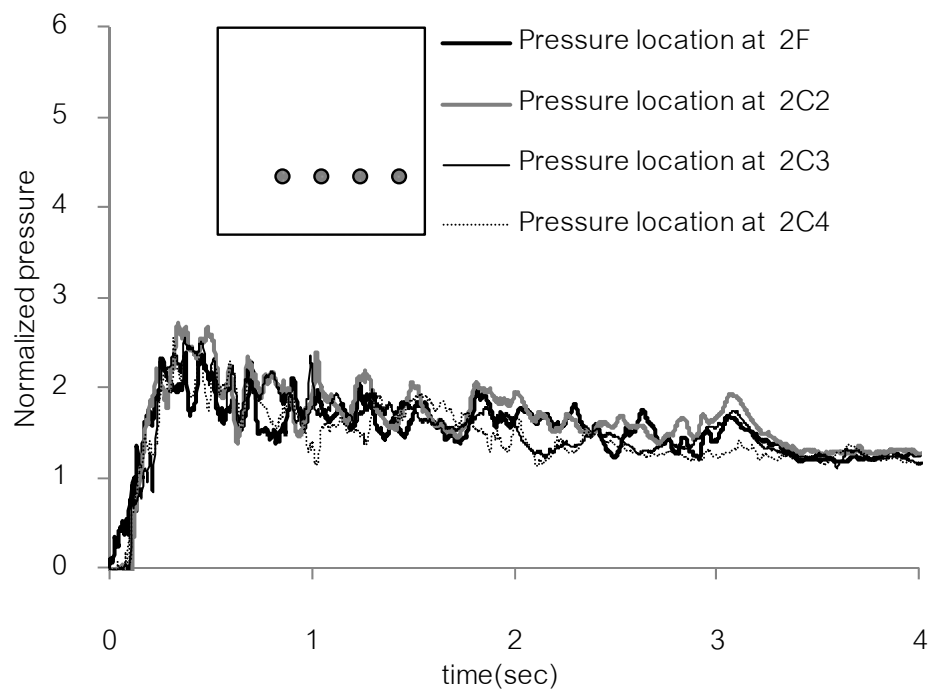


Figure 3-31. Time history of pressure in case: KS2F-2C2-2C3-2C4_00_90_03
(Khaolak slope, Square shape, No opening, Nominal wave height 80 mm)

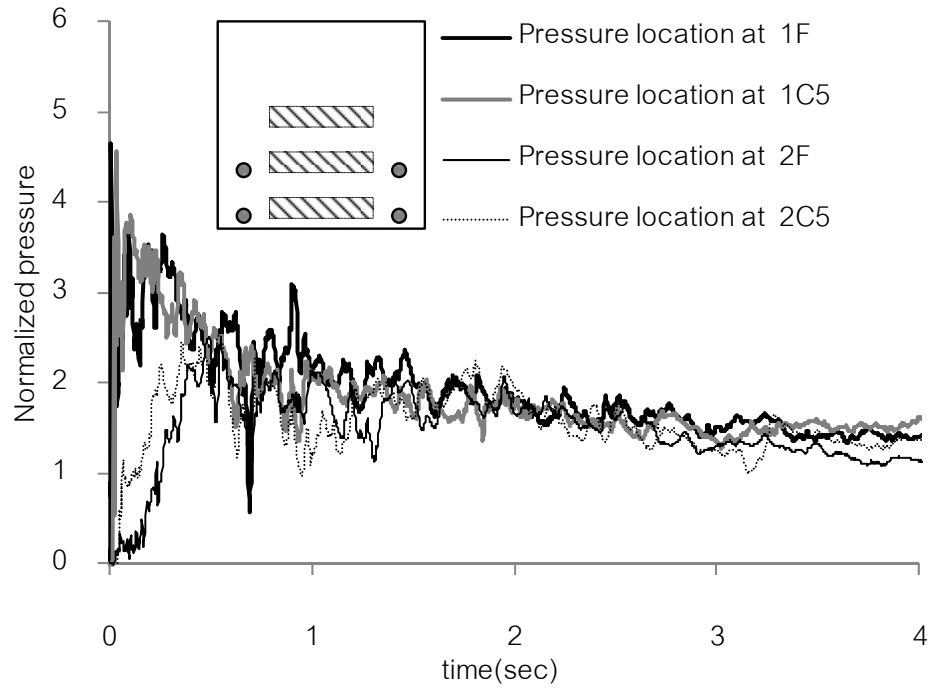


Figure 3-32. Time history of pressure in case: KS2F-2C5-1F-1C5_25_90_03
(Khaolak slope, Square shape, 25% opening, Nominal wave height 80 mm)

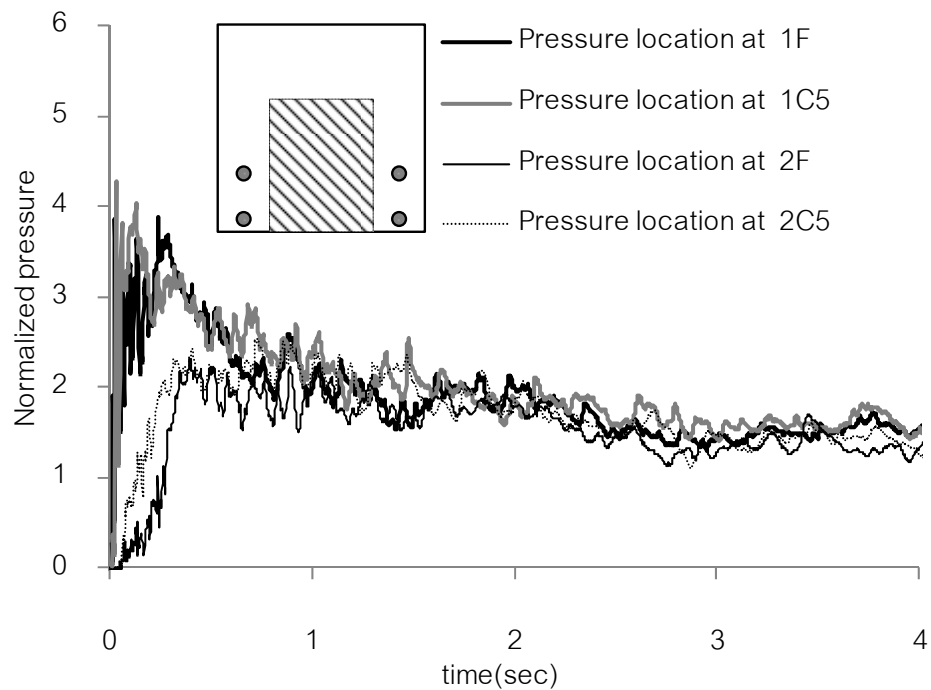


Figure 3-33. Time history of pressure in case: KS2F-2C5-1F-1C5_50_90_05
(Khaolak slope, Square shape, 50% opening, Nominal wave height 80 mm)

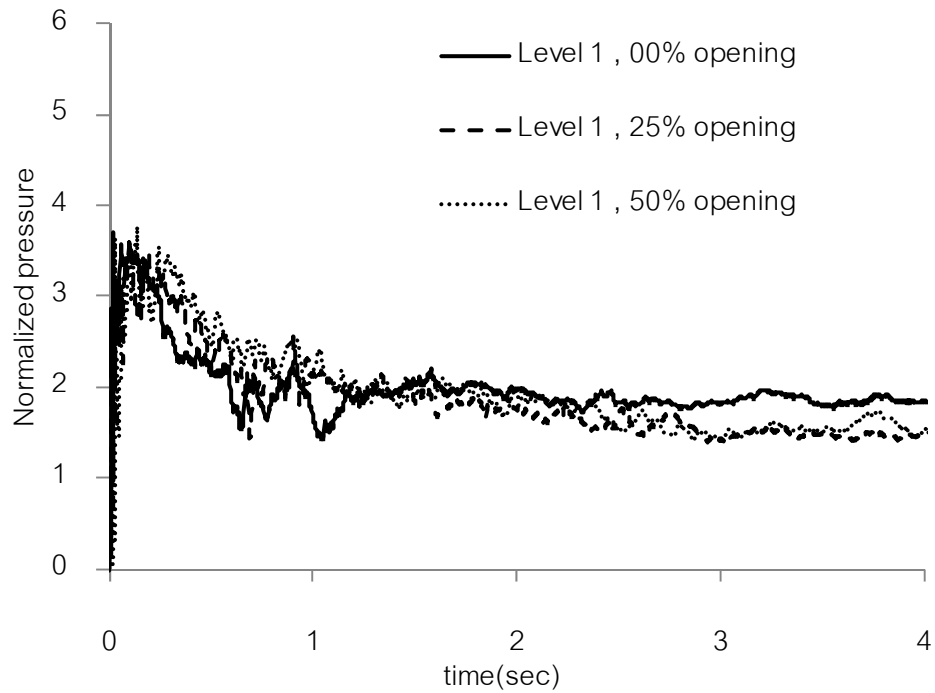


Figure 3-34. Time history of average pressure at level 1 with different configuration of openings on the square shape and nominal wave height 80 mm at the Khaolak slope

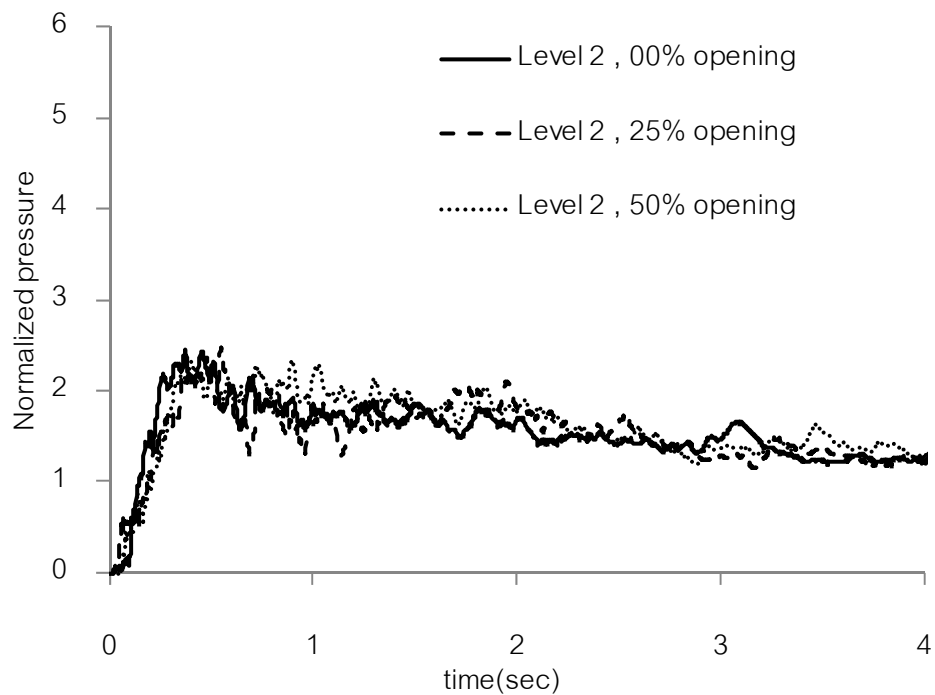


Figure 3-35. Time history of average pressure at level 2 with different configuration of openings on the square shape and nominal wave height 80 mm at the Khaolak slope

3.7.9 Time histories of pressure on the back panel

Figure 3-36 illustrates the typical time histories of normalized pressures on the front and back panels of the model without openings at levels 1 and 2. The locations of the pressure gauges are also shown in the figure.

As expected, the normalized pressures at the back panel of the model are very small (in the order of 20%) compared with the pressures on the front panel of the model at the same level. Furthermore, there is a time lag about 1 second before the pressure at back panel starts to pick up.

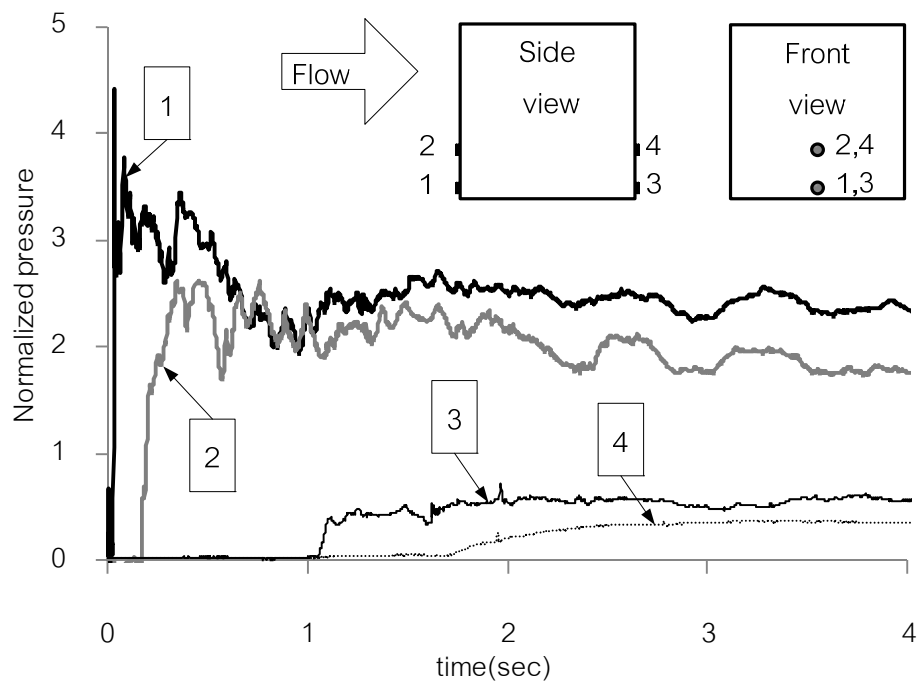


Figure 3-36. Time history of pressure on the front and back of model
(Khaolak slope, Square shape, No opening, Nominal wave height 80 mm)

3.7.10 Time histories of pressure inside the model with opening

To investigate the pressure induced inside the model once the wave flows through the openings, pressure gauges were installed inside the model on the back of the front panel, and on the front face of the back panel as shown in Figure 3-37 and Figure 3-38. The typical time histories of normalized pressures for the model with 25% openings are depicted in the figures. For the small nominal height of 40 mm, the pressures inside the model do not occur at time of wave impingement on the model. There is a time lag of about 0.25 second before the pressure on back panel starts to pick up. Also the front face of the back panel felt the effect of the flow passing through the openings slightly sooner than the back face of the front panel. Nevertheless, after about one second, the inside pressures of the model are not quite different. For the faster flow with nominal height of 80 mm, the inside pressures at the front and back panels match each other quite well in general, except some minor discrepancy at the beginning (Figure 3-38).

From the above findings the following can be inferred. Since the pressure on the back panel at the downstream end of the model is relatively small, and the pressures on the panels inside the model are more or less balanced, the resultant force (i.e. base shear) on the model should be approximately equal to the force exerted on the front panel only. The force calculated from the integration of the pressure values on the front face using the time histories in Figure 3-28 is plotted in Figure 3-39 together with the time history of the measured force from the load cell. Evidently, they are in good agreement. This also verifies that the experiments were executed to a reasonably good quality.

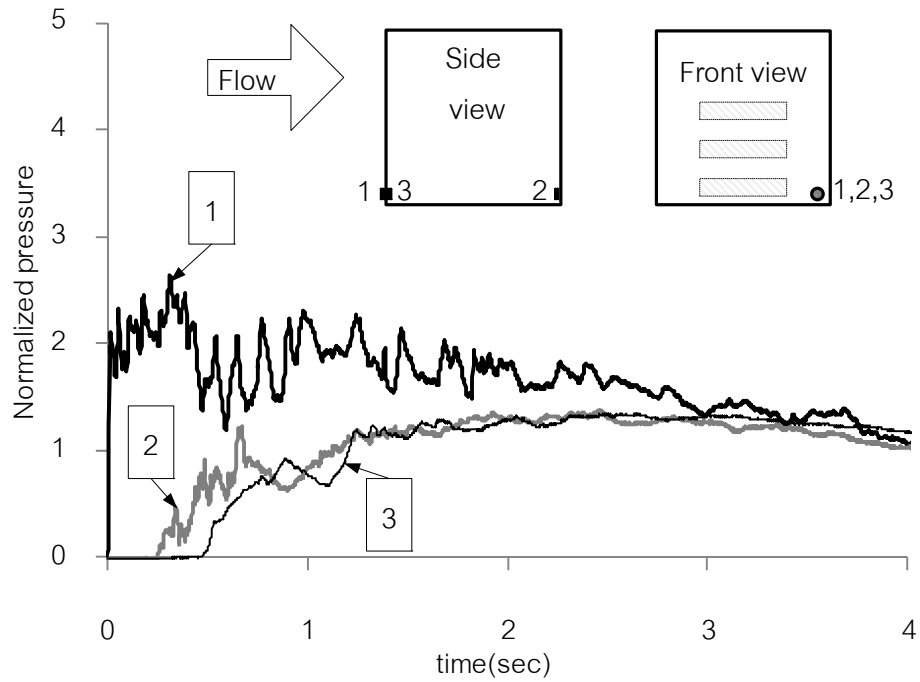


Figure 3-37. Time history of pressure inside of model

(Kamala slope, Square shape, 25% opening, Nominal wave height 40 mm)

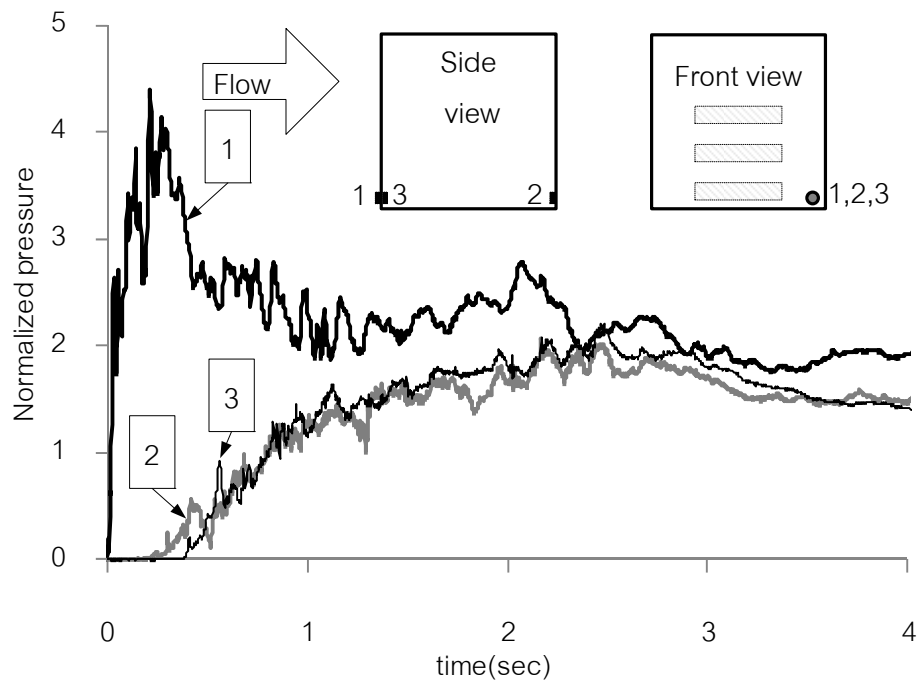


Figure 3-38. Time history of pressure inside of model

(Kamala slope, Square shape, 25% opening, Nominal wave height 80 mm)

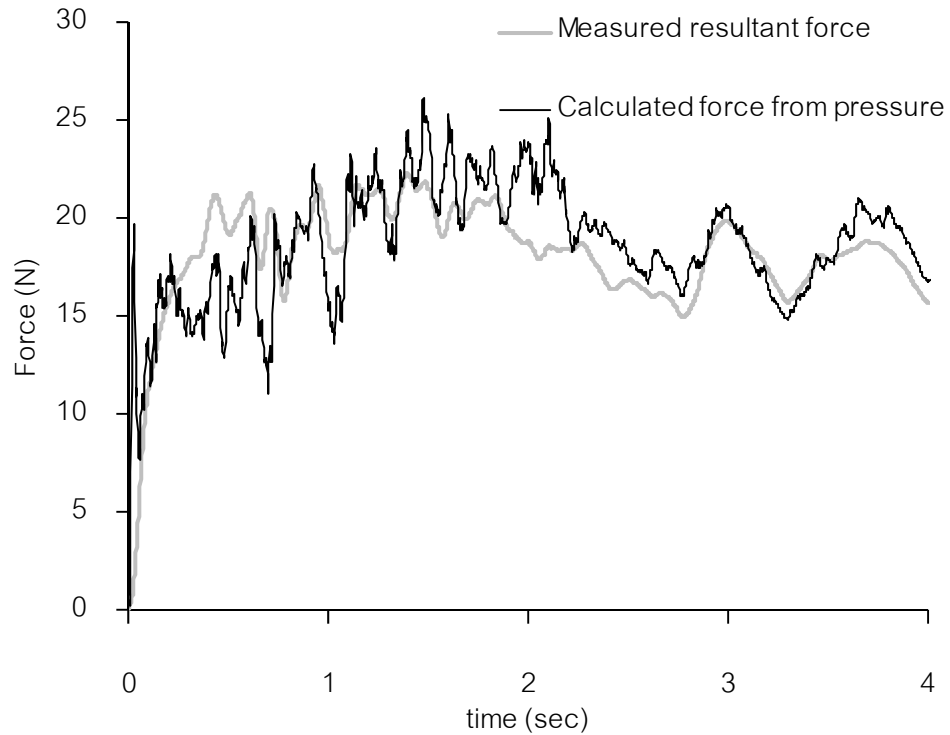


Figure 3-39. Comparison of measured resultant force with calculated force from pressure

3.7.11 Effect of shapes

Besides the square shape, solid models (without openings) with rectangular and octagonal shapes in plan were also investigated for tsunami loading. The cross sections of the models are shown in Figure 3-6. The width of the projected frontal area of each shape is 0.15 m, except for the rectangular shape model which is 0.24 m wide. Therefore, the measured force from the rectangular shape model is scaled by 0.625 (which is $0.15/0.24$) so that it is the force on a rectangular model of equivalent width of 0.15 m, and thus it can be compared with other shapes.

The maximum forces for different model shapes versus the maximum flow depth are plotted in Figure 3-40. Table 3-6 shows the maximum forces on various models with various nominal wave heights for Kamala slope profile. The values are calculated from the average of maximum forces in several experimental runs of each case. The percentage in parentheses shows the ratio of the force for each shape to that of the square shape. The experimental results show that, for the configurations considered, there is not much discrepancy in the drag coefficient for the square and rectangular

shapes. For the octagonal shape, the reduction of force is about 10, 20 and 25% for the nominal height of 40, 60 and 80 mm, respectively.

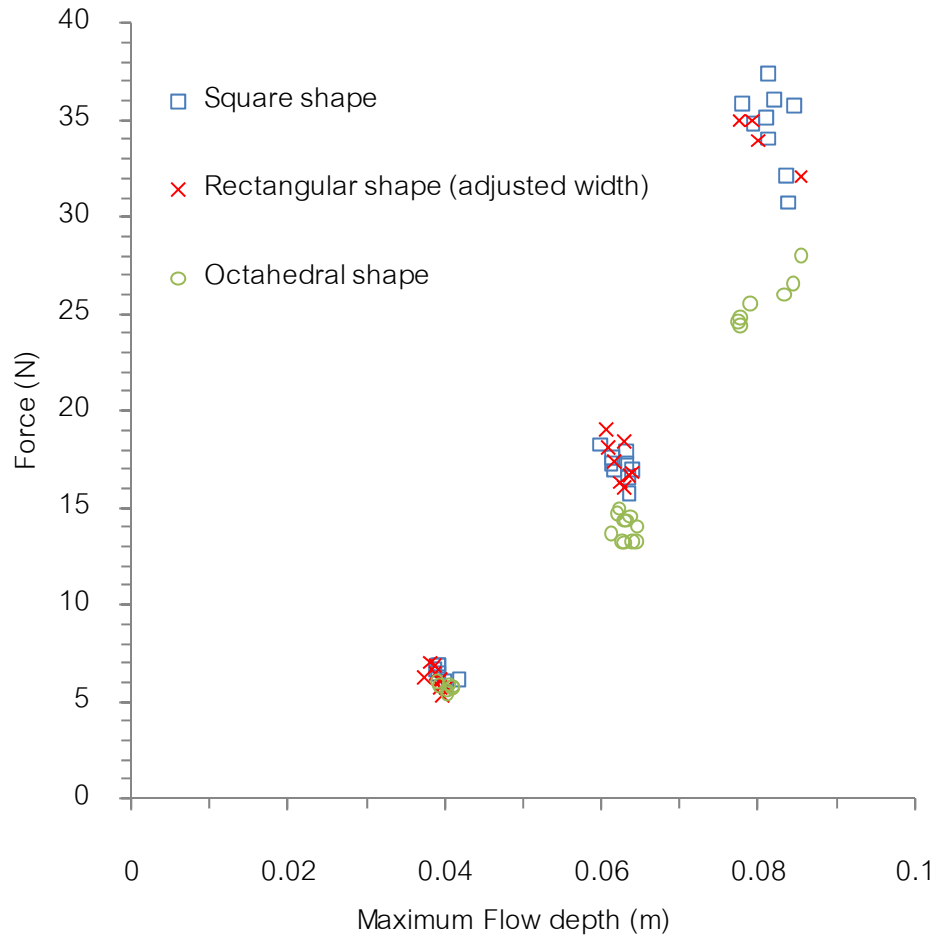


Figure 3-40. Comparison of measured maximum forces with different shapes

Table 3-6. Maximum forces (N) on model without openings for Kamala slope profile.

Shape	Nominal wave height		
	40 mm	60 mm	80 mm
Square	6.52 (100%)	17.17 (100%)	34.67 (100%)
Rectangular (Adjusted width)	6.19 (95%)	17.35 (101%)	33.99 (98%)
Octahedral	5.76 (88%)	13.97 (81%)	25.70 (74%)

Note: Values in parentheses are percentage of the model in square shape

3.7.12 Confirmation of experimental results with Fujima et al. (2009)

From the literature, several researchers have proposed expressions for estimating tsunami loading in terms of hydrostatic pressure with different horizontal wave pressure index. The general form of hydrostatic formula has been proposed to estimate tsunami loading as follows:

$$F_{sta} = \beta \times \rho g h_{im}^2 \quad (3-2)$$

where F_{sta} is the hydrostatic force per unit width of a structure, β is the horizontal wave pressure index, ρ is the water density, g is the gravitational acceleration, h_{im} is maximum inundation depth at the location of model without the presence of the model. The horizontal wave pressure indexes proposed are 4.5 and 3.3 for Asakura's equation and Tanimoto's equation, respectively.

Fujima et al. (2009) compiled experimental data from various researchers in Japan. These results are presented in Figure 3-41. The ordinate (y axis) is the value of horizontal wave pressure index and the abscissa (x axis) is the ratio of h_{im} to the distance from shoreline to structure, D . For $\frac{h_{im}}{D} < 0.05$, the data show large scatter. Fujima et al. concluded that the hydrostatic form was not appropriate for structures located far from the shoreline, and the mean value of β over the range investigated is about 1.90. Clearly, Asakura's equation ($\beta = 4.5$) excessively overestimates the force whereas Tanimoto's equation ($\beta = 3.3$) is more appropriate for safety estimation (Fujima et al., 2009).

For our experiment, the measured forces on models of square shape without openings for Kamala slope profile are also shown in Figure 3-41 as hollow circles. It may be observed that the experimental results in this study cluster around Tanimoto's curve and are quite consistent with other experiments.

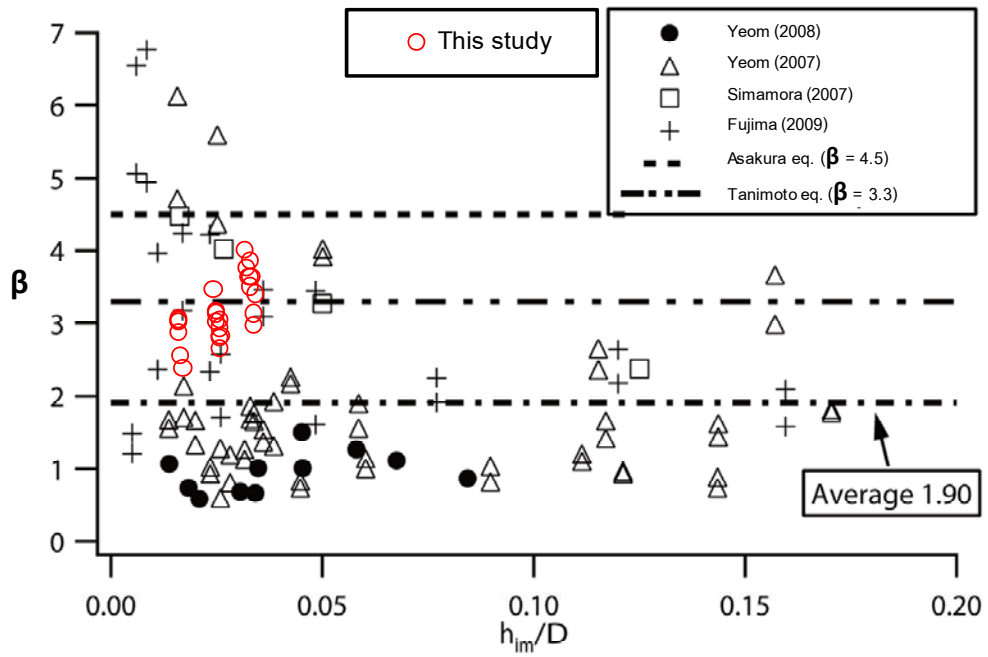


Figure 3-41. Comparison of measured maximum forces with results in literature (Fujima et al., 2009)

CHAPTER 4

EXPERIMENTAL VERIFICATION OF FEMA P646

This chapter presents the experimental verification of FEMA P646 (FEMA, 2008). To this end, it is necessary to estimate runup heights from data of flow depths and velocities. A method to obtain such relationship is proposed.

4.1 Hydrodynamic Forces in FEMA P646

The FEMA P646 - Guidelines for Design of Structures for Vertical Evacuation from Tsunamis (FEMA, 2008) - provides guidance on estimating the extreme forces caused by tsunamis. There are many types of tsunami load effects such as hydrostatic forces, hydrodynamic forces, buoyant forces, debris impact forces, etc. For the breaking wave, it is not of concern in design of vertical evacuation buildings due to the breaking of waves offshore, which does not affect buildings onshore. Therefore only the hydrodynamic, debris impact and buoyant forces are of primary concern. However, the debris impact force is beyond the scope of our study, which the buoyant force is well understood. Thus, only the hydrodynamic force in FEMA P646 will be verified.

The hydrodynamic forces result from the lateral pressures (or suction) on front and back panels and the friction forces along the sides of the structure. The hydrodynamic force, F_d , is expressed as

$$F_d = \frac{1}{2} \rho_s C_D B (hu^2)_{max} \quad (4-1)$$

where ρ_s is the fluid density including sediment (1200 kg/m^3), C_D is the drag coefficient, B is the breadth of the structure in the plane normal to the flow direction, h is the flow depth, u is the flow velocity at the location of structure and hu^2 is the momentum flux per unit mass per unit breadth. The hydrodynamic forces distribute as a uniform load and the resultant acts approximately at the center of the wetted surface area. The recommended value of drag coefficient is 2.0 for a square shape.

When the flow propagates onshore, a bore is formed if the flow propagates over still water of a finite depth. On the other hand, if the flow rushes up on a dry bed, a “dry-bed surge” takes place. Ramsden (1993) found that the initial impulsive force was detected in a bore but was not found in the dry-bed surge. According to Arnason (2005), the value of the impulsive force is approximately 1.5 times of the hydrodynamic force as depicted in Figure 4-1.

In a real situation, the tsunamis attack as a train of 2 or more waves. The subsequent waves could generate bores over the terrain flooded by a previous tsunami. Therefore, FEMA P646 recommends the impulsive force be taken as 1.5 times of the hydrodynamic force for conservatism.

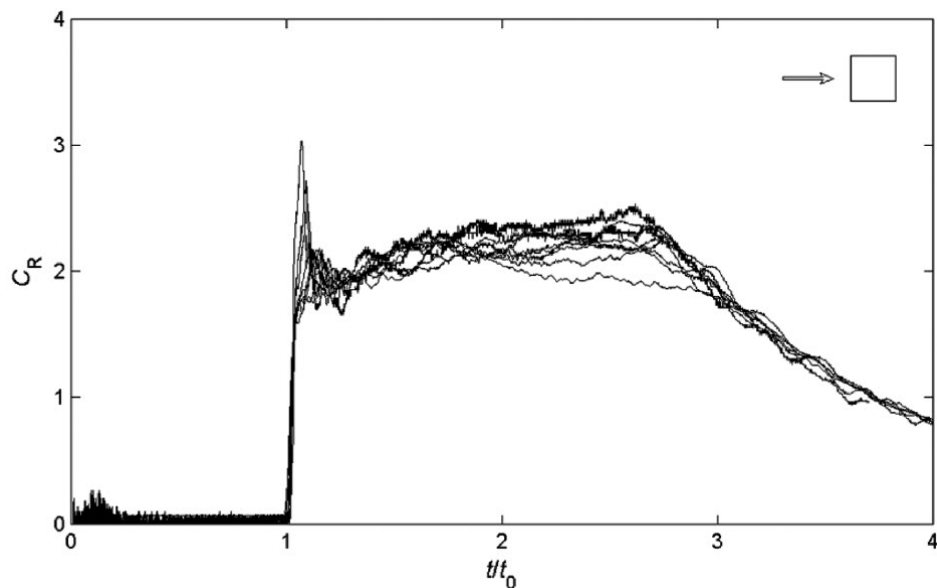


Figure 4-1. Horizontal force-time histories in dimensionless quantity on the square column with various bore conditions (Arnason, 2005)

The term $(hu^2)_{max}$ represents the momentum flux per unit mass. As pointed out by several researchers (e.g. Yeh (2007)), $(hu^2)_{max}$ is not equal to $h_m * u_m^2$, since the maximum flow depth, h_m , and maximum flow velocity, u_m , at a particular site may not occur at the same instant of time. Yeh (2007) has proposed that the hydrodynamic force be determined from $(hu^2)_{max}$, which is the maximum momentum flux per unit mass occurring at the site during the tsunami attack. This can be evaluated from a detailed numerical simulation using a very small grid size. To avoid such a complicated

simulation, Yeh (2007) developed an exact analytical solution for two-dimensional flow based on a nonlinear shallow-water wave theory with some simplifications and assumptions. The simplification is that the beach has a uniform slope. The fluid is assumed to be incompressible and inviscid, and the velocity is uniform over the depth. The envelope curve of the maximum momentum flux is related to the maximum runup height, R . The envelope curve can be expressed by

$$\frac{(hu^2)_{max}}{gR^2} = 0.125 - 0.235 \frac{z}{R} + 0.11 \left(\frac{z}{R}\right)^2 \quad (4-2)$$

where z is the ground elevation at the location of building from the initial shoreline.

4.2 Estimation of Runup Height from Flow Depth and Velocity

To compare experimental results with design guidelines in FEMA P646 (FEMA, 2008), the runup height is needed so that the maximum momentum flux in Eq. 4-2 can be calculated, subsequently the hydrodynamic force or the drag force can be estimated from Eq. 4-1.

The runup height cannot be directly measured because the wave flume is of open channel type with the open end. Therefore, it is necessary to estimate the runup height from data of flow depths and velocities, which were measured in the experiments. The procedures described herein have been proposed by Lukkunaprasit et al. (2009b).

Peregrine and Williams (2001) have proposed equations, which predict flow depths and velocities for a bore advancing onto a uniformly sloping beach. These analytical formulas are based on the nonlinear shallow-water theory with the assumption of incompressible and inviscid fluids (no friction).

With slightly different scaling (Yeh, 2007), Peregrine and Williams' formulas can be expressed as follows:

$$\delta = \frac{1}{36\tau^2} (2\sqrt{2}\tau - \tau^2 - 2\zeta)^2 \quad (4-3)$$

$$v = \frac{1}{3\tau} (\tau - \sqrt{2}\tau^2 - \sqrt{2}\zeta) \quad (4-4)$$

where $\delta = d/R$, $v = u/\sqrt{2gR}$, $\tau = t \tan \alpha \sqrt{g/R}$, $\zeta = z/R$, d is the flow depth, α is the bottom slope and t is the time (time starts when the bore passes the initial shoreline).

The maximum runup height is estimated by using method of least squares fit to Eq. 4-3 and Eq. 4-4 for the experimental data of flow depths and velocities. The main assumption underlying these equations is that the shear in the water is insignificant, whereas the profiles of flow depths in experiments as shown in Figure 3-21 and Figure 3-22 demonstrate the friction effect at the leading tongue of the flow. Lukkunaprasit et al. (2009b) assume that the friction effect is limited to the tongue region; therefore, curve fitting is executed for the specific region next to the domain affected by friction. From this hypothesis, the experimental data range in time from 0.2 to 0.8 second is fitted with a smooth curve by means of the least squares procedure for estimation of the maximum runup height.

Figure 4-2 shows an example of curve fitting results based on the above reasoning. This example is the case of Kamala slope profile and nominal wave height 60 mm. The method for estimating the runup height involves trial and error of two variables, which are runup height and time, and then they are substituted into Eq. 4-3 and Eq. 4-4. The appropriate runup height is selected using the least squares method for minimum error, which is defined as the sum of square of the difference between the measured data and the values predicted by the equation. As shown in Figure 4-2, the circle marks present the time history of flow depth and velocity recorded in the experiments, and the gray line presents the predicted relation from Peregrine and Williams' formulas.

In each case, the data of flow depth and velocity are processed in the same manner to predict the runup height. Figure 4-3 shows the maximum runup height with maximum flow depth. The relation between maximum runup height and maximum flow depth is almost linear.

The calculated forces by Eq. 4-1 and 4-2 are compared with the experimental values, and the results are presented in the next section.

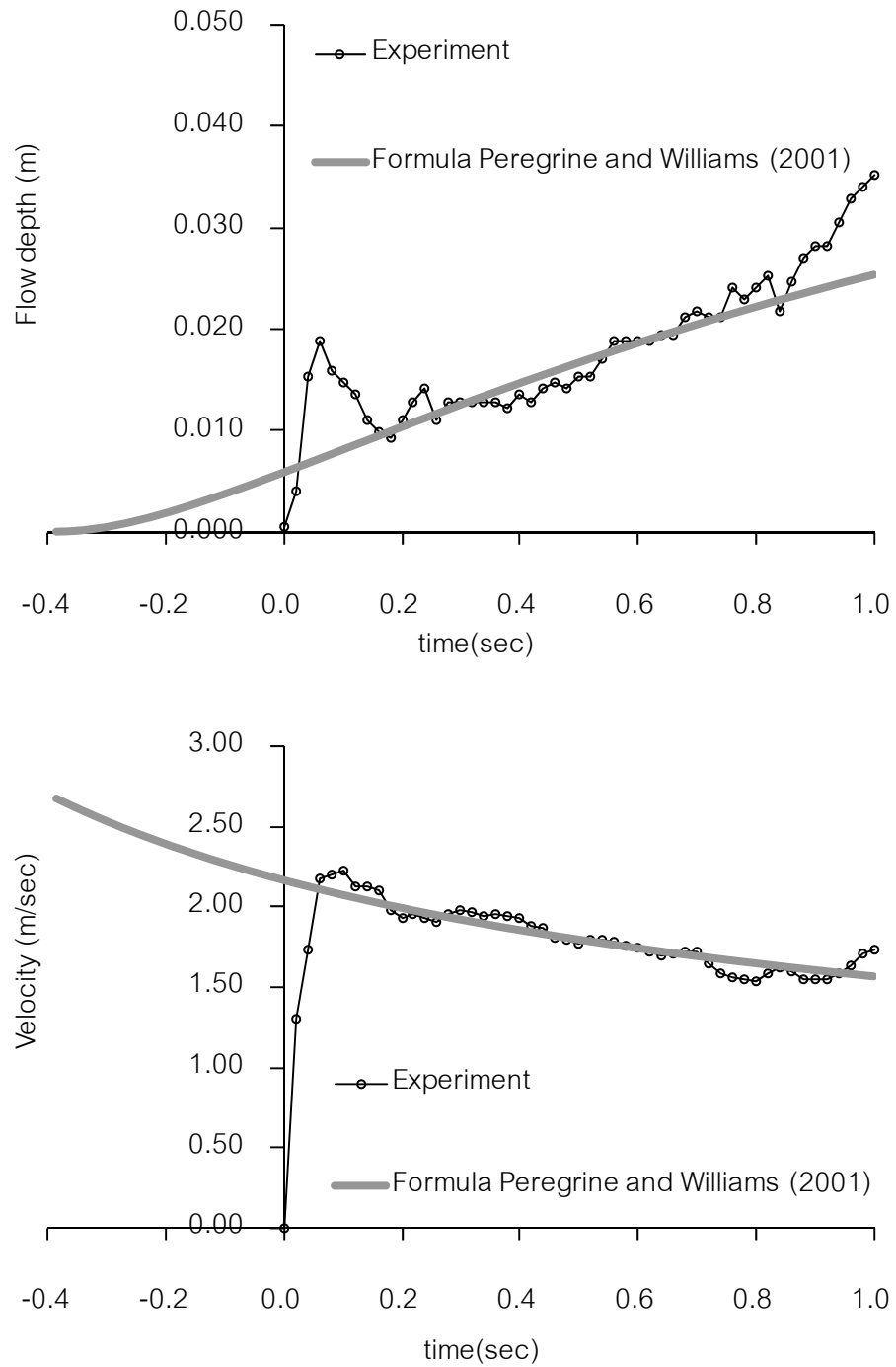


Figure 4-2. Example of curve fitting on the measured depths and velocities by using the formula of Peregrine and Williams (2001)

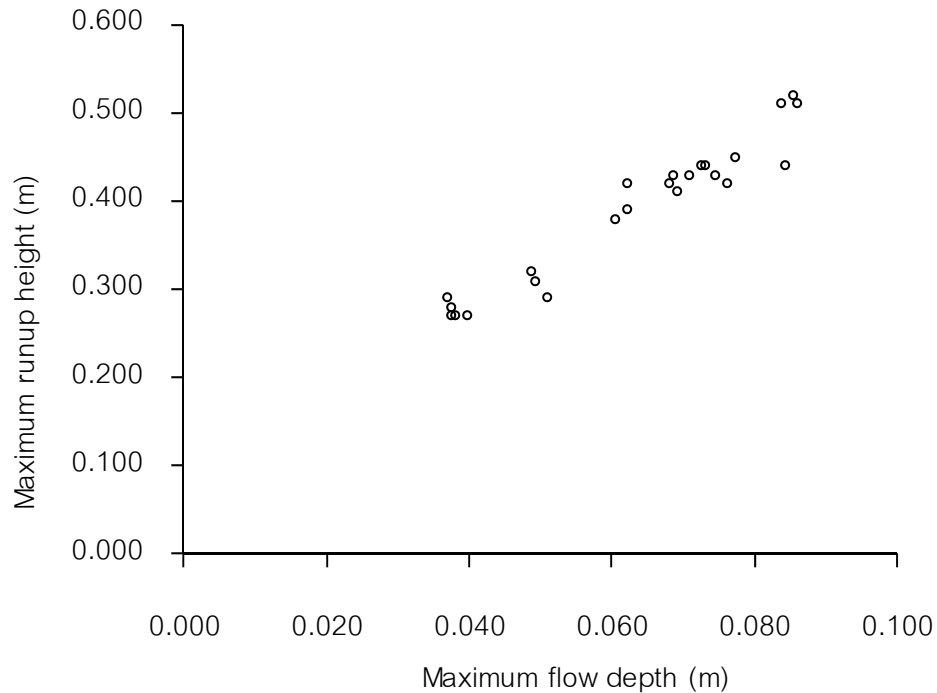


Figure 4-3. Relationship of maximum runup height and maximum flow depth

4.3 Comparison of Experimental Results with FEMA P646

The configurations to be compared are the slope profile at Kamala, Phuket and the square shape model without openings. Three types of forces are compared, viz., the experimental forces, the hydrodynamic forces based on experimental momentum flux, and the calculated forces based on the maximum runup height determined according to the procedure described in the previous section.

The hydrodynamic forces based on experimental momentum flux are computed from Eq. 4-1, where the drag coefficient is 2.0 and the maximum momentum flux is determined from the time history of the momentum flux based on the experimental results of flow depth and velocity (in the absence of model).

The calculated forces based on the computed maximum runup height are computed from Eq. 4-1, where the drag coefficient is 2.0 and maximum momentum flux is computed from Eq. 4-2.

4.3.1 Building without openings

The maximum measured and calculated forces versus the maximum flow depth are plotted in Figure 4-4. The measured forces are shown with circle symbols for which there are about eight data points for each nominal wave height, while the hydrodynamic forces based on experimental momentum flux are indicated by the square symbols and the computed values based on adjusted maximum runup heights are indicated by the triangular symbols.

Interestingly, the hydrodynamic force computed by using the experimental flow depth and velocity agrees quite well with the measured force from experiments. This indicates that the hydrodynamic force represents well the real force resulting from tsunamis.

The computed values based on the adjusted maximum runup heights are upper bound for the measured forces, in general. Thus, Eq. 4-2 provides a conservative estimate of tsunami loading for practical purposes.

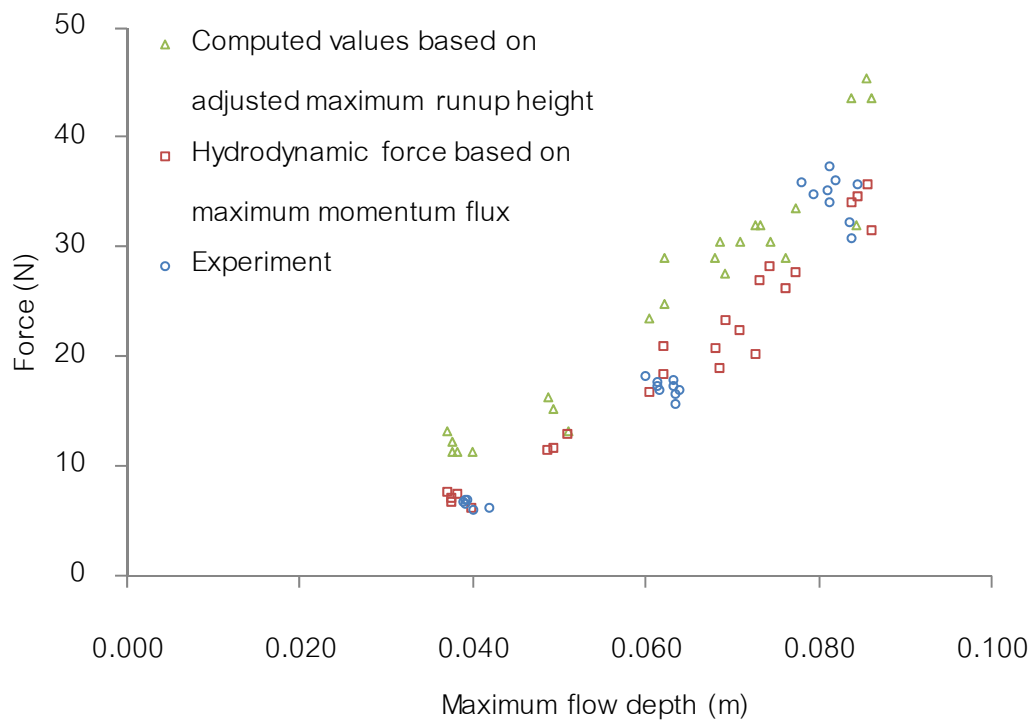


Figure 4-4. Comparison of measured maximum forces with predicted forces based on momentum flux and runup for model without openings

4.3.2 Buildings with openings

For buildings with openings, there is no recommendation for calculating tsunami force in FEMA P646. In actual buildings, there are windows or doors or other open space; therefore, this standard has limitation in application in practice. This issue will be treated in Chapter 5 where a simple procedure is suggested for determining tsunami loading on buildings with openings.

CHAPTER 5

THE ADAPTED FEMA P646 AND ITS VERIFICATION WITH EXPERIMENTS AND FIELD LOAD TEST

FEMA P646 does not provide any recommendation for buildings with openings which presents some limitation in application of the guidelines in practice. This chapter extends the applicability of FEMA P646. A simple approach is proposed to adapt it for buildings with openings. The approach is verified with experimental results of a physical model of a damaged building in the 2004 Indian Ocean tsunami, and a field load test.

5.1 Detail of Case Study Building

The building tested in this study is the weather monitoring building (WMB) of the Meteorological Department station in Takua Pa, Phang-Nga Province, Thailand. The building is located at 8° 41.444" N, 98° 14.489" E in Khaolak, Phang-Nga which was severely hit in southern Thailand in the 2004 Indian Ocean tsunami. Figure 5-1 shows the building which was slightly damaged by the tsunami. The building is about 220 m from the shoreline and the building front faces the sea. The ground level of building was about 5 m above the sea level when tsunami hit. The flow depth at the building was about 4.4 m. The runup heights were 6-10 m on the coast of Khaolak and the maximum value in this area was about 12 m (Matsutomi et al., 2006). Figure 5-2 shows the plan and elevation of this building, which is one story in height with two bays. The ground floor is raised above the ground level by about 0.9 m. The framing consists of non-ductile reinforced concrete components (beams, columns, and slabs) with un-reinforced brick masonry infill panels. The foundation is of shallow type. The details of the building are reported in Lukkunaprasit et al. (2010).

As for building damage, primary members except perimeter beams for architectural purposes suffered minor damage (Lukkunaprasit et al., 2010). Hairline cracks occurred in beams and columns. The brick walls in the plane perpendicular to tsunami flow were completely destroyed except the ones below the ground floor level as shown in Figure 5-1. A major brick wall in the plane parallel to tsunami flow (designated

as BW in Figure 5-3), which is 2.6 m wide and spans the full height, survived with some residual cracks as shown in Figure 5-3. The other major brick walls close to BW were totally damaged. It is speculated that these brick walls were damaged from the action of the tsunami in the perpendicular direction. The reason is that if they were damaged by in-plane action, the tremendous force they resisted at impending failure would have been transferred to the bounding columns, which would have suffered severe damage since they were not designed to resist such force. Instead, the observed damage in the columns is minor as described earlier.



Figure 5-1. Photograph of case study building (front view)

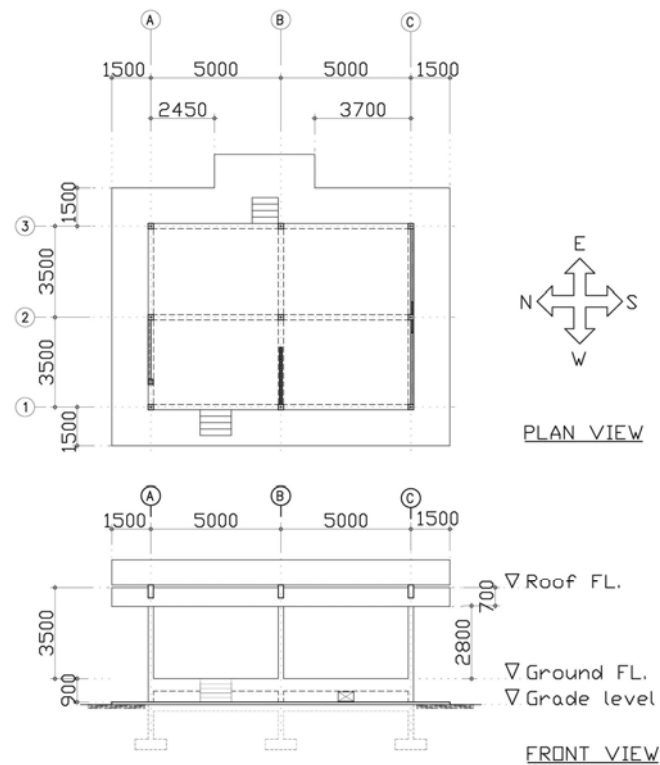


Figure 5-2. Case study building plan and elevation (unit: mm)



Figure 5-3. The inside view of the building shows the remaining structure and major brick wall (BW)

5.2 Field Load Test

The purpose of field load test is to infer the tsunami loading that actually occurred in the 2004 Indian Ocean tsunami event from test results on the damaged building. As depicted in Figure 5-4, the past history of the loading curve as shown by the dashed line is unknown. For structure suffering only minor damage (such as the case of WMB building as described in the last section), the re-loading curve will approximately pass through the previously loaded state as shown in solid line. Thus, in the field load test, the building was re-loaded past the state of the previous loading, which was identified by the more severe level of damage induced in the building compared with that before re-loading. Consequently, the maximum load attained in the field load test can be regarded as an upper bound of the tsunami loading exerted on the damaged building in past event (Lukkunaprasit et al., 2010).

The overview of the test set up in field load test is shown in Figure 5-5 and Figure 5-6. The details of test setup and results of the field load test have been reported by Lukkunaprasit et al. (2010) and Ruangrassamee et al. (2008). The test was terminated at 381 kN (total load on the whole building) for safety reason. The average displacement at the roof level was about 10 mm. It should be noted that this is very small, in the order of

0.3% of the story-height. Story-drift in this range is normally on the ascending branch of the load deflection curve unless brittle failure has taken place.

The level of damage in the building was observed from the crack widths in the columns, beams and BW. At termination of the test, the cracks in the columns and beams were still small. However, the crack width can be clearly observed in BW. The major diagonal crack in BW with a residual crack width of 0.5 mm at the initial stage widened to a crack width of 2.5 mm at the final stage of loading. After unloading, the residual crack width reduced to 1.5 mm, well larger than the initial crack width of 0.5 mm. This indicates that the tsunami loading on the “damaged” building in past event was more likely not larger than 381 kN. In other words, this load from the field load test is considered an upper bound of the tsunami loading exerted on the damaged building.

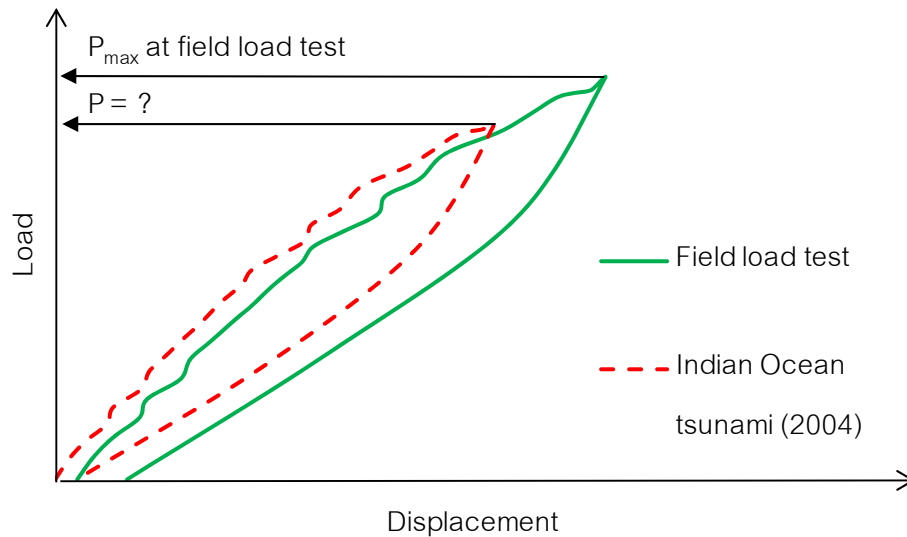


Figure 5-4. Schematic diagram of the re-loading curve in the push-over of the damaged building



Figure 5-5. Overview of test setup in field load test (front view).



Figure 5-6. Overview of test setup in field load test (side view).



Figure 5-7. Major brick wall with cracks before and after testing

5.3 Wave Flume Experiment

5.3.1 Experimental setup

The experimental setup in the wave flume was the same as that described in section 3.3 except for the scaling which was selected as one-to-fifty. The model shown in Figure 5-8, was to simulate the damaged WMB building on Kamala slope profile. The model dimensions at the ground floor level were 200 mm in width, 140 mm in depth. For the roof floor level, the width was 260 mm and the depth was 200 mm as shown in Figure 5-8 and Figure 5-9. The total height of the model was 103 mm.

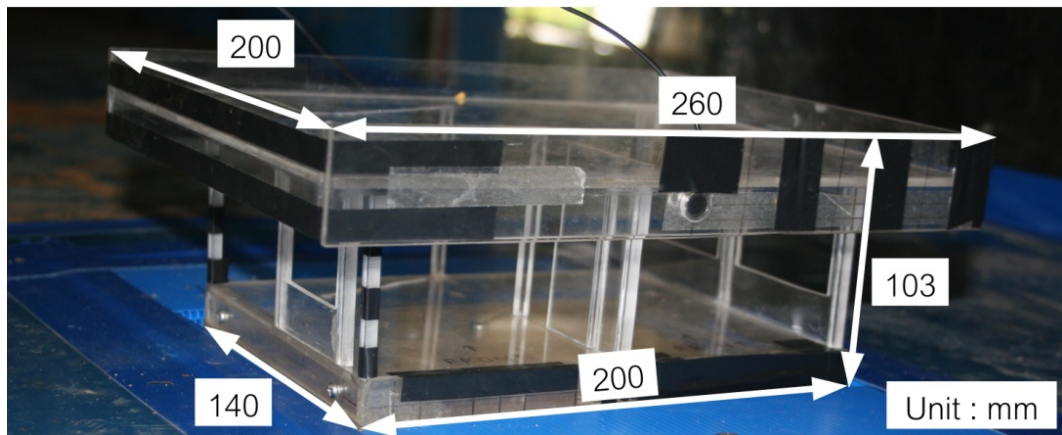


Figure 5-8. Model of WMB in wave flume

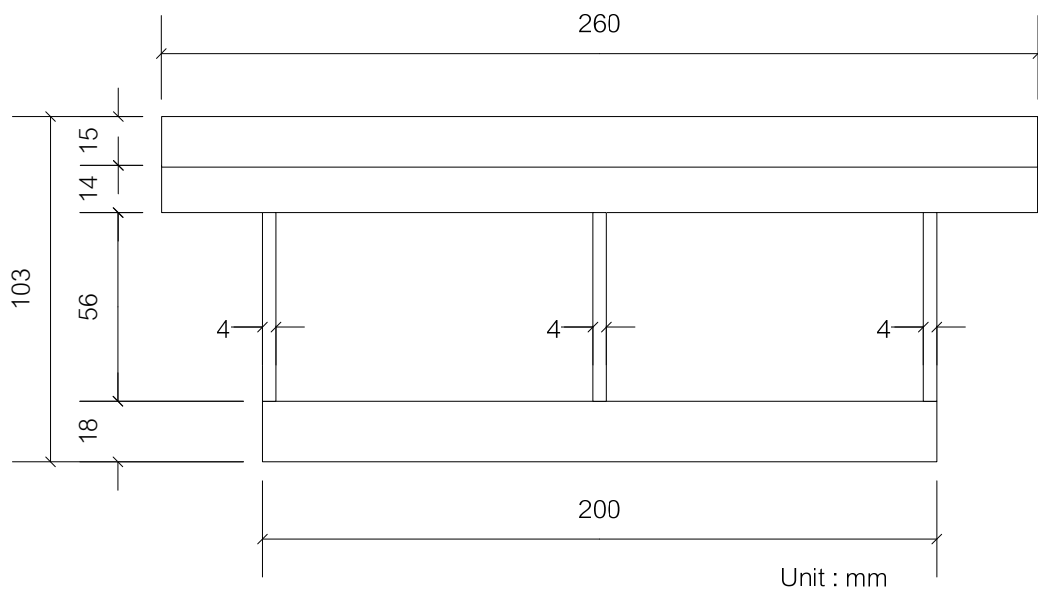


Figure 5-9. Model dimensions of WMB in wave flume

5.3.2 Experimental results

The characteristics of flow past the model is shown in Figure 5-10 at the upstream side for nominal wave height of 60 mm. Each capture of the video image is marked with the time that has elapsed since the wave impinges on the model. The flow approximately reached the level of the fin (4.4 m in prototype) where the watermark was observed in the damaged building.

The time histories of the force on the WMB model are shown in Figure 5-11. The force history for each case is shown with dashed line and the averaged curve is shown in solid line. Judging from the turbulence nature of the flow, the replication of experimental runs is seen to be reasonably good.

When the leading front of the wave hit the model at the bottom wall, the wave splashed up on the upstream side as shown in Figure 5-10 at $t = 0.5$ sec after initial impact on the bottom wall. At this instant, the force records the first peak value of about 11 N in average. Thereafter, the flow depth increases but the flow velocity decreases as described in section 3.7.2. Furthermore, the increase in frontal exposure area is very small (until the wave reaches the fin). The result is that the force exerted on the building decreases after the first peak until the inundation reaches the fin at about 2 seconds, when the force starts to increase again.

It should be noted that the maximum force at the first peak does not affect the building as a whole because this force acts on the box-like portion of the building below the ground floor. Therefore, the local peak forces after 2 seconds are considered since they attack on the superstructure, which is vulnerable to damage. The maximum drag forces after first peak are summarized in Table 5-1 with the prototype scale determined by using the Froude similitude. The maximum runup heights are estimated using the same procedure in section 4.2. It should be observed that the maximum runup heights of 0.39 - 0.40 m, which are generated in the wave flume and correspond to 19.3 – 19.9 m in the prototype, do not represent the actual condition in this area since the maximum runup heights in the vicinity of the building location were reported to be around 12 m (Matsutomi et al., 2006). However, the loads obtained from the wave flume experiments can be used to verify the adapted FEMA P646 in the next section.

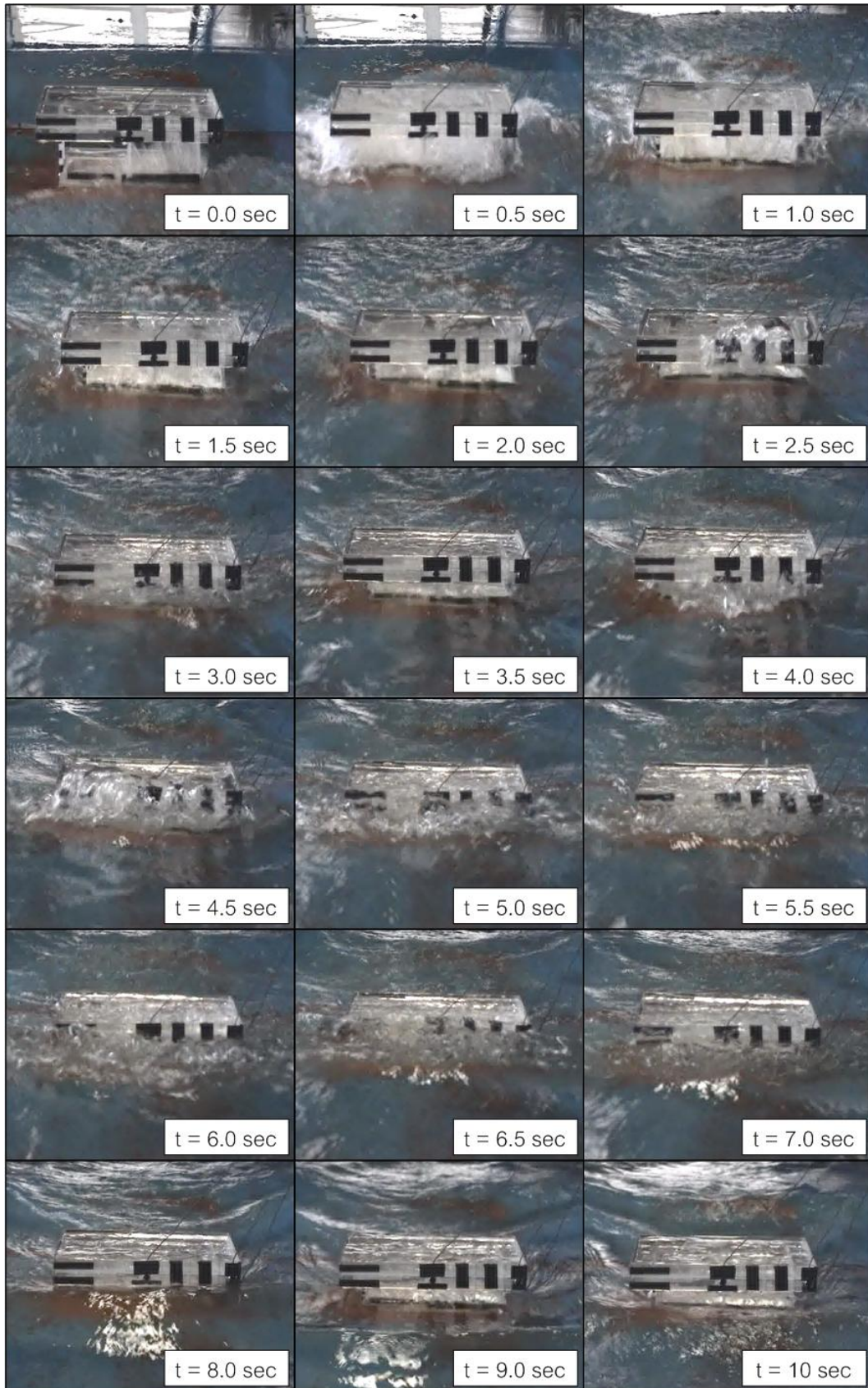


Figure 5-10. Sequences of the wave attack on WMB model at upstream side
with nominal wave height 60 mm

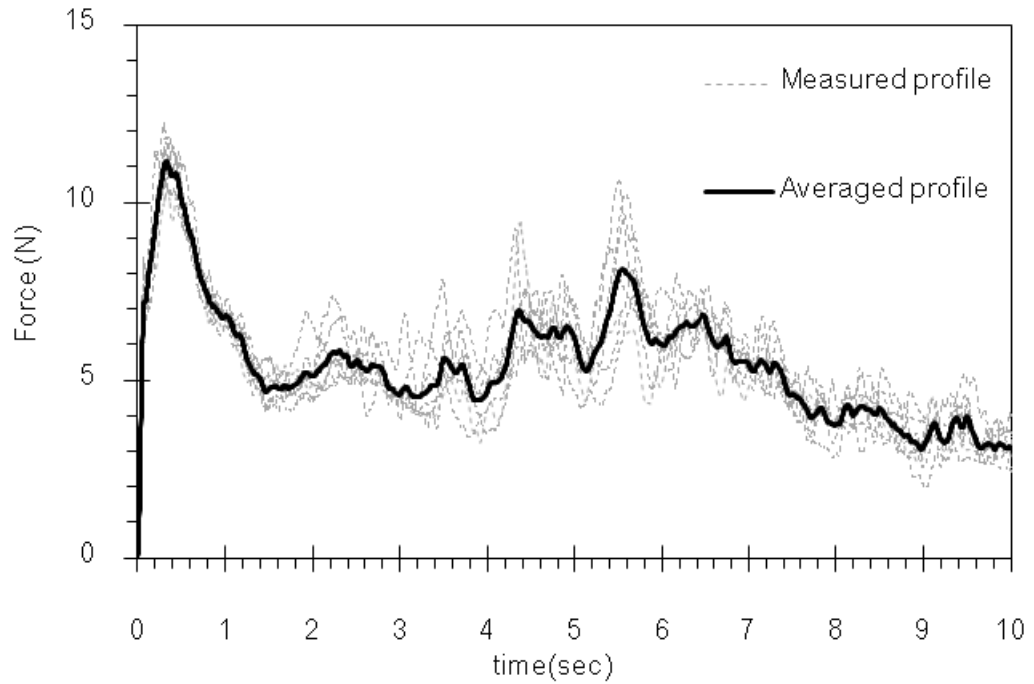


Figure 5-11. Typical time history of force for WMB model

Table 5-1. Experimental results of maximum drag forces (after first peak) and estimated maximum runup heights

Case	Model (1:50 scale)			Prototype	
	Maximum flow depth (m)	Maximum runup height (m)	Maximum drag force (N)	Maximum runup height (m)	Maximum drag force (kN)
1	0.065	0.40	7.6	19.94	951
2	0.065	0.40	9.5	19.94	1182
3	0.064	0.39	10.2	19.62	1275
4	0.063	0.39	10.6	19.31	1330
5	0.063	0.39	9.7	19.36	1207
6	0.064	0.39	8.1	19.67	1010
7	0.064	0.39	8.8	19.67	1095

5.4 Adapted FEMA P646

As concluded in section 3.7.8 to 3.7.10, the pressures exerted across the width of models at the same level are practically the same, even though the opening configurations are different. Furthermore, the net contributions of the pressures other than those acting on frontal panel are negligible. Figure 5-12 illustrates the models with and without openings. The drag force per unit width is given by Eq. 5-1:

$$\frac{F_d}{B} = \frac{1}{2} \rho C_D (hu^2)_{max} \quad (5-1)$$

For the model without openings, the drag force F_d is given by Eq. 5-2.

$$F_d = \frac{1}{2} \rho C_D (hu^2)_{max} * B \quad (5-2)$$

For the model with openings, the drag force F'_d is given by Eq. 5-3.

$$F'_d = \frac{1}{2} \rho C_D (hu^2)_{max} * B_{eff} \quad (5-3)$$

in which the effective width B_{eff} is $B * \frac{A_{eff}}{A}$ (see Figure 5-12). Thus,

$$F'_d = \frac{1}{2} \rho C_D (hu^2)_{max} * B * \frac{A_{eff}}{A} \quad (5-4)$$

i.e.,

$$F'_d = F_d * \frac{A_{eff}}{A} \quad (5-5)$$

where A is the gross area, and A_{eff} is the effective area, which is the attacked area on the front panel with the reduced area of openings. This equation is suitable for models which have a uniform vertical distribution of openings.

Since the gross area is $B * h_{in}$, Eq. 5-4 can be put in another form:

$$F'_d = \frac{1}{2} \rho C_D (hu^2)_{max} * \frac{A_{eff}}{h_{in}} \quad (5-6)$$

in which h_{in} is the maximum inundation height on the building.

Now, a question arises as to what effective area should be used. As mentioned in section 3.7.7, the bilinear vertical pressure profile proposed by Lukkunaprasit et al. (2009a) indicates that pressure is registered up to a height of $2h$. For simplicity, the pressure effect on the front panel is simplified (for computation of A_{eff}) to be constant over a height of 1.5 times the maximum flow depth as shown in Figure 5-13. The effective area exposed to tsunami attack is then determined based on the effective height of $1.5h$.

The measured maximum forces from experiments versus the computed forces based on the adapted FEMA P646 in Eq. 5-6 are presented in Figure 5-14. For nominal wave heights of 40 and 60 mm, the adapted FEMA P646 gives a rather conservative estimate of the maximum force. For the highest flow depth with nominal height of 80 mm, the adapted FEMA P646 underestimates the measured force by about 15%. Therefore, the proposed equation yields a reasonable conservative estimate of the experimental results, in general.

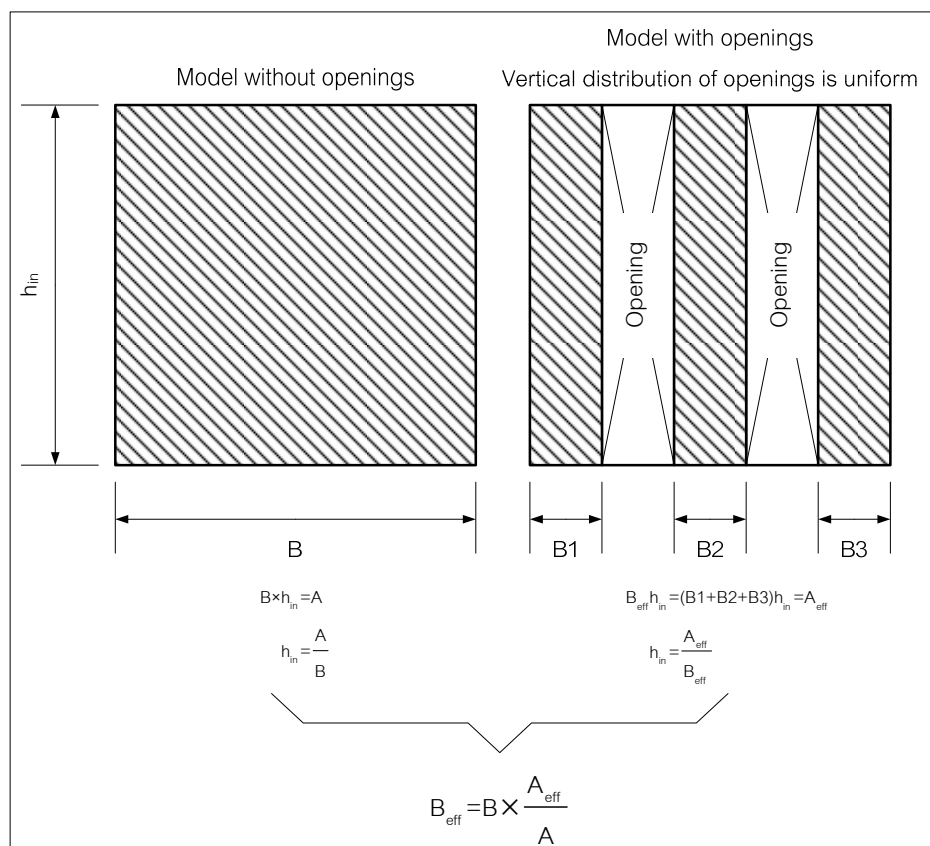


Figure 5-12. Effective area of model with opening

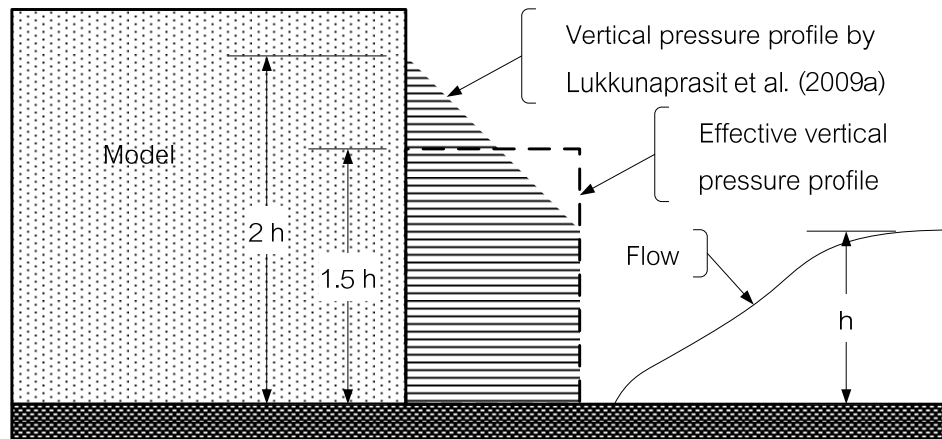


Figure 5-13. Simplification of vertical pressure profile

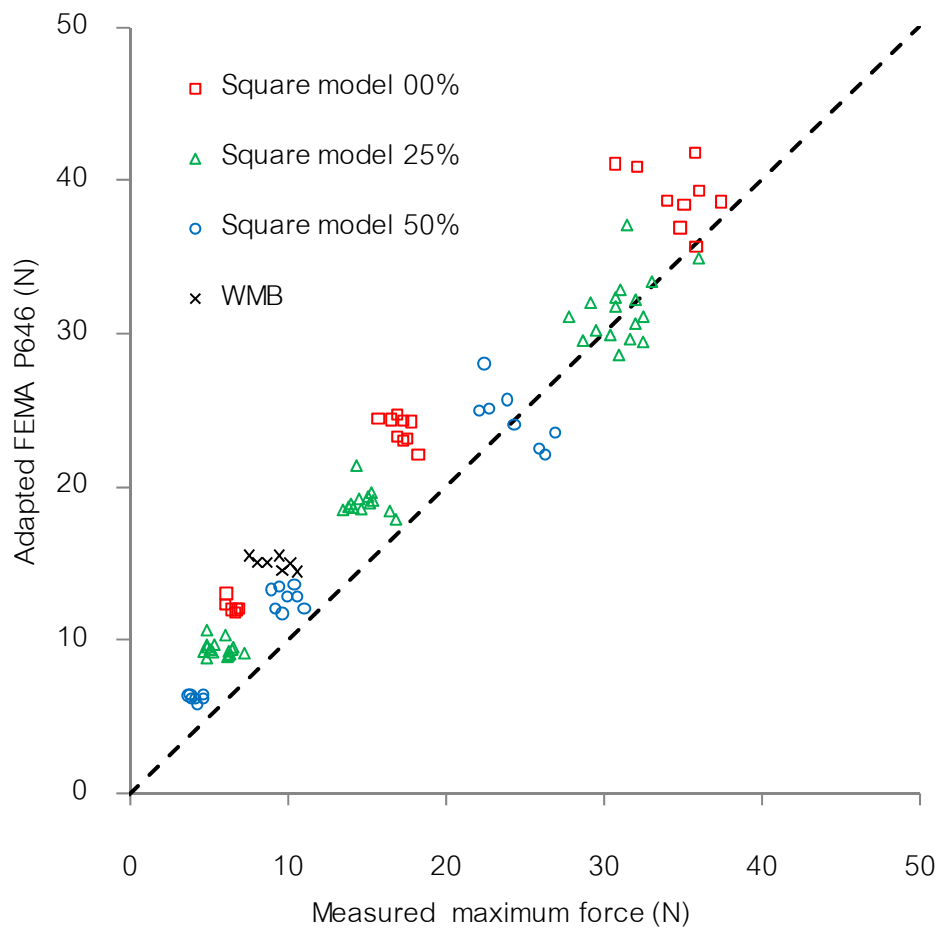


Figure 5-14. Measured maximum force in wave flume experiments versus computed forces from Adapted FEMA P646

5.5 Comparison of Field Tested Load with Computed Load from Adapted FEMA P646

The drag force calculated from the adapted FEMA P646 is verified with the load from the field load test of WMB. In the comparison, the attacked area is based on the increase in area exposed to tsunami attack before the nonstructural components were washed away. There was a water mark at the level of the fin at 4.4 m which is assumed to the maximum flow depth. From previous section, the effective height is 1.5 times the maximum flow depth, or 6.6 m whereas the height of WMB is 5.1 m. Thus, the effective height of 5.1 m is used resulting in the effective area (shown shaded in Figure 5-15) and the gross area of 33.08 sq m. and 55.2 sq m., respectively.

As mentioned in section 5.1, the maximum runup heights were about 10 -12 m in Khaolak area. The drag forces on the building computed based on the adapted FEMA P646 are 260 and 498 kN corresponding to the maximum runup heights of 10 and 12 m, respectively. Appendix B shows an example computation of hydrodynamic force using the adapted FEMA P646. The range of these computed forces is shown shaded in Figure 5-16. It should be noted that the drag forces are quite sensitive to change in the runup height.

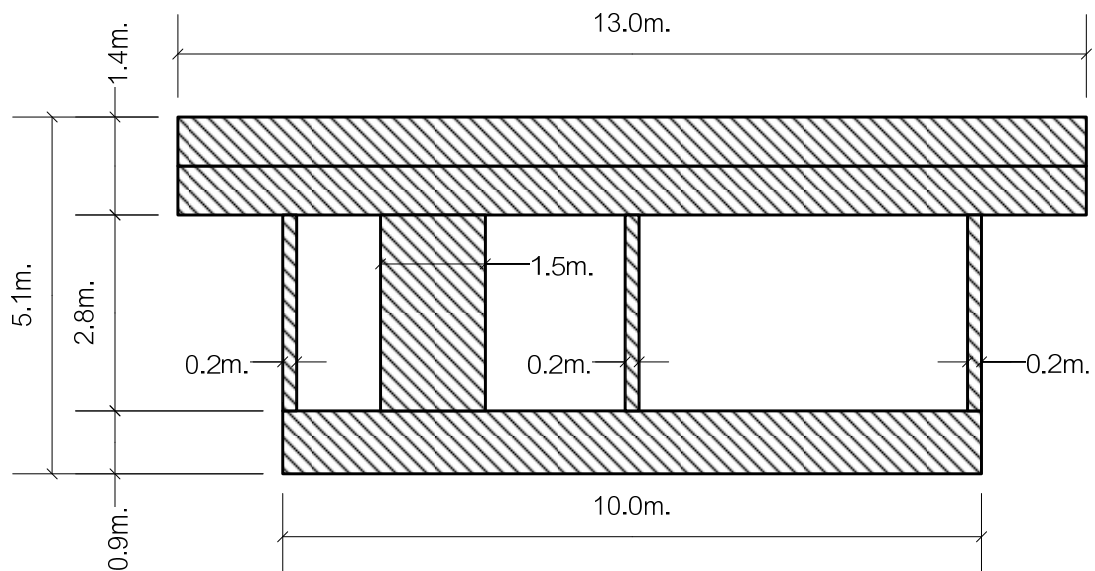


Figure 5-15. Frontal area of building submerged in flow

Figure 5-16 presents the comparison of forces from the adapted FEMA P646, FEMA 55 and field load test. The estimated drag force from FEMA 55 is computed from Eq. 2-5 using the drag coefficient of 1.25 for the wall at grade level and the fin as specified by FEMA 55 for large obstruction with ratio of width to water height of 2.95. For each column, 0.2m in width by 2.8 m in height, and for nonstructural walls, the drag coefficient of 2 is employed. The velocity is computed from Eq. 2-6 and the flow depth is 4.4 m. The predicted maximum load of 498 kN (at maximum runup height of 12 m) from the proposed procedure compares well with the pushover load of 381 kN from field load test. However, the FEMA 55 loading is much higher than the pushover load. Thus, the adapted FEMA P646 is in reasonable agreement (to within 30%) with the pushover load from the field load test.

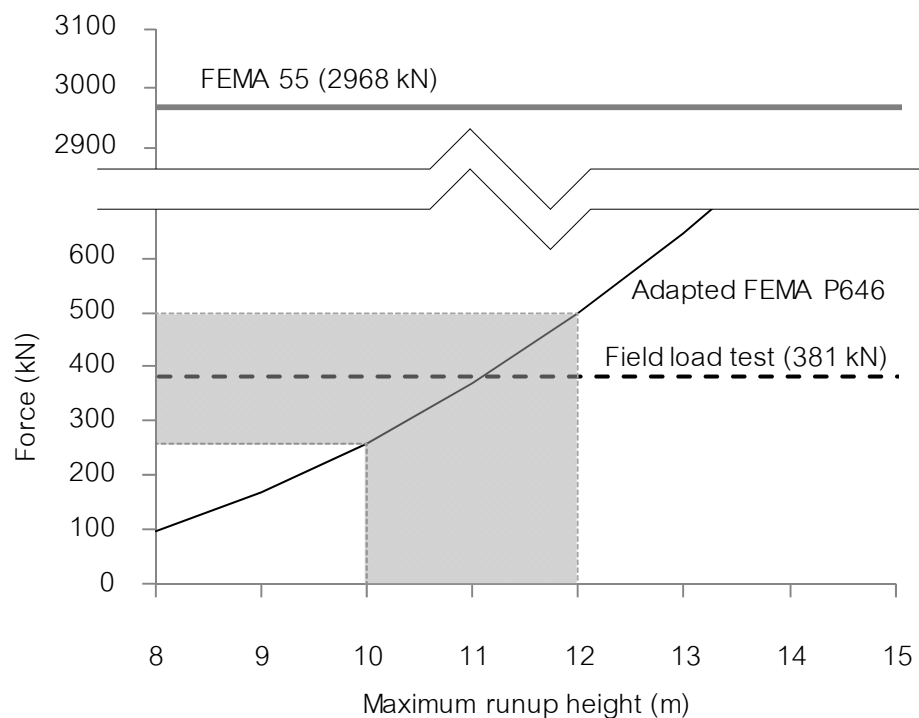


Figure 5-16. Comparison of computed forces from adapted FEMA P646 and FEMA 55 with measured force from field load test

CHAPTER 6

CONCLUSIONS AND RECOMMENDATIONS

6.1 Conclusions

For the configurations of models investigated in this study, the following conclusions can be drawn:

- a) The experiments show that for the same nominal wave height, different flow velocities are obtained for different slope profiles. Thus, formulas for calculating tsunami loading should include both flow depth and flow velocity as parameters.
- b) There is a reduction in the wave force acting on the whole building in the order of 15%-25% for the case of 25% opening configuration, and 35%-50% for the case of 50% opening configuration.
- c) The pressure values at the same level can be regarded as identical for square shape models with different configurations of openings.
- d) The pressure on the back panel at the downstream end of the model is relatively small, and the pressures on the panels inside the model are more or less balanced; therefore, the net contributions of the pressures other than those acting on the frontal panel are negligible.
- e) The maximum forces on the octagonal shape model are 88%, 81% and 74% of those on the square shape of the same width for nominal wave heights of 40, 60 and 80 mm, respectively.
- f) The adapted FEMA P646 is proposed for the building with openings and verified by experiments as well as field load test of the damaged weather monitoring building in the 2004 Indian Ocean tsunami. In general, the proposed equation yields a reasonable conservative estimate of the experimental results and the pushover load from the field load test.

6.2 Recommendations for Future Studies

The following recommendations are suggested to improve the study in the future:

- a) The experiments in a wave flume should be designed to produce the tsunami runup and drawdown processes on the beach in order that the maximum runup height can be measured directly.
- b) The flow depth, flow velocity, force and pressure should be measured in the same experimental run for better accuracy in analyses. The flow velocity should be measured by using the Laser Doppler Velocimetry (LDV), which can be placed outside the flow being measured; thereby it does not affect the flow.

REFERENCES

- Arnason, H. (2005). *Interactions between an incident bore and a free-standing coastal structure*, Doctoral dissertation, Department of Civil and Environmental Engineering, University of Washington, Seattle, Washington.
- Arnason, H., Petroff, C. and Yeh, H. (2009). Tsunami bore impingement onto a vertical column. *Journal of Disaster Research* 4(6): 391-403.
- Asakura, R., Iwase, K., Ikeya, T., Takao, M., Kaneto, T., Fujii, N. and Ohmori, M. (2002). The tsunami wave force acting on land structures. *Proceedings of the 28th International Conference on Coastal Engineering*, Cardiff, Wales, pp. 1191-1202.
- CCH. (2000). *City and County of Honolulu Building Code*, Department of Planning and Permitting of Honolulu Hawaii, Honolulu, Hawaii.
- Cross, RH. (1967). Tsunami surge forces. *Journal of the Waterways and Harbors Division, Proceedings of the American Society of Civil Engineers* 93(WW4): 201-231.
- FEMA. (2000). *Coastal Construction Manual*, FEMA 55 report, Edition 3, Federal Emergency Management Agency, Washington, D.C.
- FEMA. (2008). *Guidelines for design of structures for vertical evacuation from tsunamis*, FEMA P646 report, Federal Emergency Management Agency, Washington, D.C.
- Fujima, K., Achmad, F., Shigihara, Y. and Mizutani, N. (2009). Estimation of tsunami force acting on rectangular structures. *Journal of Disaster Research* 4(6): 404-409.
- Fukui, Y., Nakamura, M., Shiraishi, H. and Sasaki, Y. (1963). Hydraulic study on tsunami. *Coastal Engineering in Japan* 6: 67-82.
- Hamzah, MA., Mase, H. and Takayama, T. (2000). Simulation and experiment of hydrodynamic pressure on a tsunami barrier. *Proceedings of the 27th International Conference on Coastal Engineering*, Sydney, Australia, pp. 1501-1507.

- Hughes, SA. (2005). *Physical models and laboratory techniques in coastal engineering (Advanced series on ocean engineering - Volume 7)*, World Scientific, Singapore.
- Lukkunaprasit, P., Chinnarasri, C., Ruangrassamee, A., Weesakul, S. and Thanasisathit, N. (2008). Experimental investigation of tsunami wave forces on buildings with openings. *Solutions to Coastal Disasters Congress 2008: Tsunamis*, ASCE, Oahu, Hawaii, pp. 82-93.
- Lukkunaprasit, P. and Ruangrassamee, A. (2008). Building damage in Thailand in the 2004 Indian Ocean tsunami and clues for tsunami-resistant design. *The IES Journal Part A: Civil & Structural Engineering* 1(1): 17-30.
- Lukkunaprasit, P., Ruangrassamee, A., Stitmannathum, B., Chintanapakdee, C. and Thanasisathit, N. (2010). Calibration of tsunami loading on a damaged building. *Journal of Earthquake and Tsunami* 4(2): 105-114.
- Lukkunaprasit, P., Ruangrassamee, A. and Thanasisathit, N. (2009a). Tsunami loading on buildings with openings. *The International Journal of The Tsunami Society* 28(5): 303-310.
- Lukkunaprasit, P., Thanasisathit, N. and Yeh, H. (2009b). Experimental verification of FEMA P646 tsunami loading. *Journal of Disaster Research* 4(6): 410-418.
- Matsutomi, H., Sakakiyama, T., Nugroho, S. and Matsuyama, M. (2006). Aspects of inundated flow due to the 2004 Indian Ocean tsunami. *Coastal Engineering Journal* 48(2): 167-195.
- Okada, T., Sugano, T., Ishikawa, T., Takai, S. and Tateno, T. (2005). *Tsunami loads and structural design of tsunami refuge buildings*, The Building Centre of Japan.
- Peregrine, DH. and Williams, SM. (2001). Swash overtopping a truncated plane beach. *Journal of Fluid Mech* 440: 391-399.
- Ramsden, JD. (1993). *Tsunamis: Forces on a vertical wall caused by long waves, bores, and surges on a dry bed*, Report No. KH-R-54, W. M. Keck Laboratory of Hydraulics and Water Resources, California Institute of Technology, Pasadena, California.

- Ramsden, JD. (1996). Tsunamis forces on a vertical wall caused by long waves, bores, and surge on a dry bed. *Journal of Waterway, Port, Coastal, and Ocean Engineering* 122(3): 134-141.
- Ramsden, JD. and Raichlen, F. (1990). Forces on vertical wall caused by incident bores. *Journal of Waterway, Port, Coastal, and Ocean Engineering* 116(5): 592-613.
- Ruangrassamee, A., Thanasisathit, N., Stitmannaitum, B. and Lukkunaprasit, P. (2008). Behavior of a reinforced-concrete building under tsunami loading patterns by full-scale pushover test. *Proceedings of the 5th International Conference on Urban Earthquake Engineering, Center for Urban Earthquake Engineering (CUEE)*, Tokyo Institute of Technology, Japan.
- Ruangrassamee, A., Yanagisawa, H., Foytong, P., Lukkunaprasit, P., Koshimura, S. and Imamura, F. (2006). Investigation of tsunami-induced damage and fragility of buildings in Thailand after the december 2004 Indian Ocean tsunami. *Earthquake Spectra* 22(S3): S377–S401.
- Yeh, H. (2006). Maximum fluid forces in the tsunami runup zone. *Journal of Waterway, Port, Coastal, and Ocean Engineering* 132(6): 496-500.
- Yeh, H. (2007). Design tsunami forces for onshore structures. *Journal of Disaster Research* 2(6): 531-536.

APPENDICES

Appendix A

Similitude Ratio for Froude Similarity

Froude number is a dimensionless number defined as the ratio of inertial force to gravity force as shown below.

$$Fr = \frac{u}{\sqrt{gL}} \quad (\text{A-1})$$

where Fr is Froude number, L is the length dimension, u is the flow velocity and g is the gravitational acceleration. In Froude similarity, the Froude number is required to be the same in model scale as in the prototype scale, i.e.

$$\left(\frac{u}{\sqrt{gL}}\right)_m = \left(\frac{u}{\sqrt{gL}}\right)_p \quad (\text{A-2})$$

where the subscripts m and p represent the model scale and prototype scale, respectively. Equation A-2 can be re-written as:

$$\frac{u_p}{u_m} = \sqrt{\left(\frac{g_p}{g_m}\right)\left(\frac{L_p}{L_m}\right)} \quad (\text{A-3})$$

Rearranging and substituting the scale ratios yield

$$\frac{u_r}{\sqrt{g_r L_r}} = 1 \quad (\text{A-4})$$

where the subscripts of r represent the ratio of prototype scale to model scale.

Equation A-4 is the Froude similarity criterion. Since the gravitational acceleration scale is unity; therefore, this equation is simplified to

$$u_r = \sqrt{L_r} \quad (\text{A-5})$$

Thus, the velocity scale (u_r) is equal to the square root of length scale (L_r).

To determine the time scale (T_r), we note that the velocity scale is dimensionless equivalent to divide the length scale to time scale, and then substituting into Froude similarity criterion as shown in below.

$$u = \frac{L}{T}$$

Therefore,

$$u_r = \frac{L_r}{T_r} \quad (\text{A-6})$$

From Eq. A-5 and A-6:

$$\frac{L_r}{T_r} = \sqrt{L_r}$$

Therefore,

$$T_r = \sqrt{L_r} \quad (\text{A-7})$$

From equation A-7, the time scale is equal to the square root of length scale.

For the force scale (F_r), the dimension of force is, by definition

$$F_r = \frac{M_r \times L_r}{T_r^2} \quad (\text{A-8})$$

Substituting the mass scale and the time scale in terms of the length scale into the above equation and rearranging yields

$$F_r = \frac{L_r^3 \times L_r}{(\sqrt{L_r})^2} = L_r^3 \quad (\text{A-9})$$

From equation A-9, the force scale is equal to the third power of the length scale.

For the other physical flow parameters, the similitude ratios for Froude similarity can be derived in a similar manner.

Appendix B

Example Computations of Force using Adapted FEMA P646 on WMB

For WMB, The building is located at onshore where the elevation is 5.075 m above the mean sea level. For our example calculation, the maximum runup height is specified as 12 m.

For the hydrodynamic force in adapted FEMA P646, The maximum momentum flux is estimated from equation 4-2 with $R = 12$ m and $z = 5.075$ m.

$$(hu^2)_{max} = gR^2 \left[0.125 - 0.235 \frac{z}{R} + 0.11 \left(\frac{z}{R} \right)^2 \right] = 63.977 \frac{m^3}{sec^2} \quad (B-1)$$

Hence, from equation 5-4 the hydrodynamic force is found to be:

$$\begin{aligned} F'_d &= \frac{1}{2} \rho C_D (hu^2)_{max} * B * \frac{A_{eff}}{A} \\ &= \frac{1}{2} \left(1000 \frac{kg}{m^3} \right) (2.0) \left(63.977 \frac{m^3}{sec^2} \right) * (13 m) * \frac{(33.08 m^2)}{(55.20 m^2)} \\ &= 498.42 kN \end{aligned} \quad (B-2)$$

CURRICULUM VITAE

Nuttawut Thanasisathit was born in Bangkok, Thailand on January 27, 1982. He received a Bachelor of Engineering degree with the second-class honors from the Department of Civil Engineering, Chulalongkorn University, Thailand in 2002. After he graduated, he worked at Thai Engineering Consultants Co.,Ltd. in the position of Structural Engineer for two years. In 2005, he received a scholarship from The Royal Golden Jubilee Ph.D. Program in Thailand Research Fund to continue his studies in a doctoral program at the Department of Civil Engineering, Chulalongkorn University. While studying, he worked as a research assistant under the supervision of Professor Panitan Lukkunaprasit. During his study, he was a visiting research student with Professor Harry Yeh at Oregon State University, USA from August, 2008 until July, 2009. His research concerns tsunami loading on building.